Technische Universität München

TUM School of Life Sciences

Uniform and homogenous hot-melt coating in a Wurster fluidized bed

Bernd Mario Wörthmann

Vollständiger Abdruck der von der TUM School of Life Sciences der Technischen Universität München zur Erlangung des akademischen Grades eines

Doktors der Ingenieurwissenschaften (Dr.-Ing.)

genehmigten Dissertation.

Vorsitz: Prof. Dr. rer. nat. Ute Weisz

Prüfende der Dissertation:
1. Prof. Dr.-Ing. Heiko Briesen
2. Prof. Dr.-Ing. Petra Först

Die Dissertation wurde am 19.02.2024 bei der Technischen Universität München eingereicht und durch die TUM School of Life Sciences am 13.05.2024 angenommen.

Acknowledgments

During my PhD at the chair of process system engineering at the Technical University of Munich, I received great support from various people.

First, I would like to thank my supervisor Prof. Dr.-Ing. Heiko Briesen for the opportunity to do my PhD thesis at his chair. At the same time, I am very grateful for the continuous motivation, the freedom to pursue new ideas, the always open ear, and the guidance through my work and science.

Besides my supervisor, I am grateful to Prof. Dr.-Ing. Petra Först for reviewing and checking my thesis. Furthermore, I would like to thank Prof. Dr. rer. nat. Ute Weisz, for chairing the examination of my thesis.

I want to express my special appreciation to Prof. Dr. Ing. Johannes Lindner for his specialist support and outstanding guidance.

I would also like to express my gratitude to the following persons and involved parties:

Mentor	Many thanks to my mentor Dr.-Ing. Hans-Jürgen Heidebrecht for his always motivating manner and guidance since I met him during my bachelor's degree.
Project committee	For funding the AiF project 19970N "Homogenes Schmelzcoating" and the expert support I would like to thank the following companies and associations: Forschungskreis der Ernährungsindustrie e.V. (FEI), Verband Deutscher Maschinen- und Anlagenbau e. V. (VDMA), Bundesverband der Deutschen Süßwarenindustrie e.V. (BDSI), Südzucker AG, Kuchenmeister GmbH, Raps GmbH & Co. KG, Romaco Innojet GmbH, Symrise AG, Kahl GmbH & Co. KG, Dr. Paul Lohmann GmbH, Evonik Operations GmbH, BASF SE, Lödige Maschinenbau GmbH, Krüss GmbH, Jungbunzlauer Ladenburg GmbH, Driam Anlagenbau GmbH, Givaudan Schweiz AG, Neuhaus Neotec GmbH, Juchem Food Ingredients GmbH, and Hanns G. Werner GmbH + Co. KG.
TUM colleagues	Unfortunately, not all measuring instruments are freely available at TUM. It is, therefore, even nicer when the informal channels

still work occasionally. Special thanks to Dr. rer. nat. Caren Sönnichsen as well as to Christina Häußinger and Cara Kolb.

SVT I am very grateful to all former and current members of the chair of process system engineering. Thanks a lot for the collegial relationship and the always pleasant working atmosphere.

Lab staff Heartfelt thanks to Gabi, Alex, and especially to Michaela, who keeps the lab, particularly the µCT running!

Workshop staff Walter, Sepp, Alexander, Hannes, Johannes, and Johann: A big thank you for the numerous custom-made components and repairs.

Office Much gratitude to Beate, Karin, and Friederike for the always open door and your support in organizing and managing.

IT Thomas, thank you for your IT support during and after my time at the chair.

EG Null Zwo Hans, Christoph, Mathias, Outi, and Ramona: Many thanks for the time spent together, the funny moments, and the inspiring technical discussions.

Friends Martin, Lakshmi, and Sebastian, you are the best! Without you, my time in Freising and life besides the chair would have been different.

Students I was allowed to supervise 12 students during my doctoral studies in the context of research internships, bachelor, and master theses. Therefore, I would like to thank Michael B., Alexander L., Johann W., Matthias O., Martha F., Markus E., Christian S., Nina B., Theresa W., Lisa T., Jodok G. and Andreas H.. Without you, the number and variety of experiments and studies would not have been possible - thank you very much!!!

In a special way, however, I would like to thank my family, without whom I would never have made it this far. I am incredibly grateful to my parents for the educational opportunities. Veri, Mom, and Dad: Thank you for always standing behind, supporting, and believing in me.

Finally, I would like to thank my wife, Veronika, for her patience, understanding, support, and her love.

„Das Ganze ist mehr als die Summe seiner Teile.“

Aristoteles

Abstract

The hot-melt coating process is used in various industries such as the food, pharmaceutical, agricultural, and chemical industries. The applications are various but have many influencing factors and dependencies in common. Particularly in the case of natural hot-melt coating, the relationships between process parameters and material properties are very complex and still need to be thoroughly investigated and understood.

Therefore, this work deals with the detailed investigation of the coating layer thickness uniformity and batch homogeneity of natural hot-melt coatings.

The work included imaging and developing a three-dimensional image evaluation method for detailed coating layer thickness analysis. The results showed that natural hot-melt coatings exhibit irregular layer thicknesses and structures. A correlation between the process temperature and the uniformity of the coating, as well as a coating material dependence, was shown. In addition, layer phenomena such as delamination could be demonstrated for hot-melt coatings. However, further investigations are required to clarify the phenomenon. One hypothesis derived for the irregular coating thicknesses and the occurrence of delamination was the different wetting behavior of the materials.

This hypothesis motivated a second study investigating the relationship between wetting and delamination behavior. The study showed good wetting behavior for all tested coating materials, whereas the delamination behavior differed strongly. Instead, the process temperature and the coating material were identified as influencing factors on the delamination probability. In current scientific literature, a correlation between the crystallization behavior and the crystal stability of the coating material components is more likely.

Based on the findings of the first two studies, fluorescence spectroscopy was used to investigate the batch homogeneity of hot-melt coatings. The intention was to be able to use a supplementary and statistically robust method for interpreting results since not only can non-uniform coatings influence batch homogeneity, but also subsequent delamination or chipping-off of the coating layer could affect batch homogeneity.

Overall, the methods developed by several studies have shown that coating quality strongly depends on material selection and process parameter setting. The process temperature, for example, influences the batch homogeneity and layer thickness

uniformity of hot-melt coatings, enabling precise coating quality and functionality adjustment.

Kurzzusammenfassung

Das Schmelzcoating-Verfahren findet in verschiedenen Industrien wie der Lebensmittel-, Pharma-, Agrar- oder in der chemischen Industrie Anwendung. Die Anwendungen sind dabei sehr unterschiedlich haben aber viele Einflussfaktoren und Abhängigkeiten gemein. Besonders beim natürlichen Schmelzcoating sind die Zusammenhänge aus Prozesseinflussgrößen und Materialeigenschaften sehr komplex und noch nicht vollständig aufgeklärt und verstanden.

Diese Arbeit beschäftigt sich deshalb mit der detaillierten Untersuchung der Schichtdickenhomogenität und Batchhomogenität natürlicher Schmelzcoatings.

Im Rahmen der Arbeit wurde die Bildgebung und Entwicklung eines dreidimensionalen Bildauswertungsverfahrens für die detaillierte Schichtdickenanalyse fortgeführt. Die Ergebnisse zeigten, dass natürliche Schmelzcoatings unregelmäßige Schichtdicken und Schichtstrukturen aufweisen. Ein Zusammenhang zwischen der Prozesstemperatur und der Homogenität der Beschichtung genauso wie eine Coatingmaterialabhängigkeit konnte gezeigt werden. Zusätzlich konnten Schichtphänomene wie Delamination für Schmelzcoatings nachgewiesen werden. Die Untersuchungen ermöglichten aber noch keine Aufklärung der Phänomene. Eine Hypothese, die für die unregelmäßigen Schichtdicken und für das Auftreten von Delamination abgeleitet wurde, war unterschiedliches Benetzungsverhalten der Materialien.

Diese Hypothese motivierte eine zweite Studie zur Untersuchung des Zusammenhangs zwischen dem Benetzungs- und Delaminationsverhaltens. Im Rahmen der Studie zeigte sich für alle getesteten Coatingmaterialien ein sehr gutes Benetzungsverhalten, wohingegen sich das Delamiantionsverhalten stark voneinander unterschieden hat. Als Einflussfaktoren auf die Delamiantionswahrscheinlichkeit konnte stattdessen die Prozesstemperatur sowie das Coatingmaterial selbst identifiziert werden. Im Kontext aktueller wissenschaftlicher Literatur liegt zudem vielmehr ein Zusammenhang zwischen dem Kristallisationsverhalten bzw. der Kristallstabilität der jeweiligen Coatingmaterialbestandteile nahe.

Basierend aus den Erkenntnissen aus den ersten beiden Studien sollte es mittels Fluoreszenzspektroskopie ermöglicht werden die Batchhomogenität von Schmelzcoatings zu untersuchen. Die Motivation dahinter war eine ergänzende und statistisch robuste Methode zu Ergebnisinterpretation heranziehen zu können, da nicht nur ungleichmäßiges Beschichten die Batchhomogenität beeinflussen kann, sondern

auch nachträgliche Delamination oder ein Abplatzen der Coatingschicht die Batchhomogenität beeinflussen könnte.

Insgesamt haben die in mehreren Studien entwickelten Methoden gezeigt, dass die Beschichtungsqualität stark von der Materialauswahl und der Einstellung der Prozessparameter abhängig ist. Die Prozesstemperatur beeinflusst beispielsweise die Batchhomogenität und Schichtdickenhomogenität von Schmelzcoatings, ermöglicht dadurch aber auch eine präzise Einstellung der Coatingqualität und Funktionalität.

Contents

List of Figures

List of Tables

List of Abbreviations

µCT ..... *micro-computed tomography*

2D ..... *two-dimensional*

3D ..... *three-dimensional*

CLSM ..... *confocal laser scanning microscopy*

GRAS ..... *Generally Accepted as Safe*

HLB ..... *hydrophilic-lipophilic balance*

HMC ..... *Hot-melt Coating*

OCT ..... *optical coherence tomography*

PSD ..... *particle size distribution*

TAG ..... *triacylglyceride*

TPI ..... *terahertz pulse imaging*

Chapter 1

Introduction

Fluidized bed hot-melt coating (*HMC*) is widely used in the agricultural, chemical, food and pharmaceutical industries. Coatings can have a wide variety of application purposes due to the specific modification of the surface properties. They can, for example, protect sensitive ingredients from reactive environmental factors such as moisture, light, or oxygen. However, the process is also used in the pharmaceutical and food industries for controlled release, taste masking, or improved handling by changing the flow behavior and preventing dust formation (Achanta et al., 2008; Mörl et al., 2007).

The continuous growth in demand for solids with functional properties and the growing quality requirements are increasing the importance of coating applications. In addition, the growing demands for environmental sustainability and energy efficiency are pushing the so-called hot-melt coating process with natural coating materials into the focus of industry and research.

Coating materials such as hydrogenated vegetable oils, like hydrogenated palm oil, or waxes like carnauba wax and rice bran wax offer high innovation potential (Achanta et al., 2008) due to benefits such as sound moisture barrier (Gontard et al., 1995), environmental compatibility and, cost-efficient availability (Jannin and Cuppok, 2013). In addition, a time- and energy-intensive drying step is not required compared to solvent-based coating since the coating material crystallizes after wetting the particle surface, allowing high spray rates and a rapid layer build-up.

However, the great potential of natural HMC is limited by various influencing factors and complex interrelationships. The main reason is the need for a more fundamental understanding of the complex relationships between material properties and process parameters on the final product. The functionality is directly related to the coating layer structure, which is supposed to be of uniform thickness and free of pores and cracks (Markl et al., 2015). In particular, the benchmarks of intraparticle coating uniformity and interparticle coating homogeneity are decisive for the quality and functionality of the coating (Dong et al., 2017).

The high-quality requirements for natural HMC are a great challenge and require a high degree of knowledge about the interaction of process parameters and the properties of the coating material, especially for HMC of fine particles (> 100 µm). Therefore,

understanding the influences of different parameters on product quality is essential. Although HMC is already a standard process in industrial applications, it is not yet well understood. Basic phenomena like agglomeration, delamination, or abrasion are still hard to predict and control, making HMC a subject of recent research.

Many recent studies focus on process-influencing parameters and novel analytical methods to analyze the coating layer structure in order to better understand and predict the complex relationships between coating quality and process conditions. Among the most critical process-influencing factors are atomization pressure, spray rate, fluidization velocity, process temperature, and plant design (Achanta et al., 2008; Jannin and Cuppok, 2013; Sudke and Sakarakar, 2013).

The essential quality criteria for high-functional coatings are dissolution kinetic, mean coating layer thickness, fraction of non-coated surface, coating layer thickness distribution of a single particle, coating structures, and interparticle batch homogeneity.

Recently, studies are increasingly focused on the systematic understanding of the coating process, e.g., through modeling and numerical simulations. The potential of numerical simulations for an improved process understanding is enormous. However, the validity of modeling and numerical simulations depends on the accuracy of the input experimental data (van Kampen and Kohlus, 2018; Wang et al., 2016).

Dissolution tests and particle size analyses are commonly used and relatively simple methods for evaluating the coating result. Dissolution kinetics are particularly suitable for determining the protective effect. However, the dissolution kinetics of a particle collective do not allow direct conclusions to be drawn about the homogeneity between particles since the functionality and protective effect in each case depend on both the intraparticle layer thickness uniformity and the interparticle homogeneity (Dong et al., 2017; van Kampen et al., 2015).

This is also valid for particle size measurements, commonly used as a standard method to prove the coating's success. However, the validity and information content of particle size analyses are severely limited due to several assumptions (all particles are spherical, each size class grows uniformly, ideal layer without inclusions, pores, or delamination). Consequently, no complete conclusions can be drawn concerning intraparticle uniformity and batch homogeneity (Bachmann et al., 2019; Heinicke and Schwartz, 2004).

In contrast, modern methods such as confocal laser scanning microscopy (CLSM) (Laksmana et al., 2009; Sondej et al., 2016), optical coherence tomography (OCT) (Markl et al., 2014; Markl et al., 2015; Pietsch et al., 2019), terahertz pulse imaging (TPI) (Lin

et al., 2015) or micro-computed tomography (µCT) (Müller et al., 2018; Perfetti et al., 2010) allow more detailed investigations of the coating layer structure.

These include key features such as layer thickness, layer thickness distribution, layer porosity, occurrence of crack formations, or delamination. In particular, µCT measurements enable a detailed, high-resolution, non-destructive analysis of the surface, bulk, and internal structures of materials in the field of particle technology (Schiele et al., 2021; Schmideder et al., 2019; Schoeman et al., 2016) and can contribute to a better systematic understanding of the process.

Despite their high information density, these measurement methods have yet to lead to a complete understanding of the process. Long measurement times, large amounts of data, high analysis costs, and complex and complicated measurement and analysis procedures are substantial limitations. In addition, there needs to be more data and analytical methods for investigating layer structures for natural HMC in literature.

Other studies focus on characterizing the properties of coating materials, which can influence coating and product quality. Goslinska and Heinrich investigated the coating properties of natural waxes by studying their material properties, such as water vapor permeability, and thermal properties, such as minimum film formation temperature or surface roughness. In particular, beeswax and rice bran wax proved advantageous natural coating agents (Goslinska and Heinrich, 2019).

Lopes et al. (2015) investigated the crystallization behavior as a function of process temperature control of triacylglycerides, specifically tristearin. It was shown that the process temperature control can notably influence the crystal form. Low process temperatures lead to unstable α-crystals, which tend to recrystallize. This results in a structural change of the coating layer morphology, which can subsequently reduce the interparticle batch homogeneity (Lopes et al., 2015). Post-coating tempering or adding additives to the coating material can also help promote polymorphic stabilization at lower temperatures (Becker et al., 2015; Chansanroj et al., 2007; Lopes et al., 2017).

Although numerous studies have been carried out on processes and material properties, there are still fundamental gaps in literature with regard to methods, factors influencing intraparticle uniformity and interparticle homogeneity, and their correlation with material properties. In particular, there is still a lack of precise and reliable experimental data for accurate modeling and simulations.

Therefore, this thesis aims to establish novel techniques for detecting and examining influential factors during the HMC process. The goal is to facilitate the development of more conclusive interpretations of experimental data via significant findings.

Chapter 2

Theoretical background

2.1 Coating Basics

The coating of particles has a long tradition and dates back to ancient times. At that time, it was used to conserve foods such as nuts or dried fruits (Waßmann et al., 2011). However, the first heyday was much later, in the post-World War II period, when film coating entered the pharmaceutical industry. During this time, coating technology developed rapidly, and the industrial use of coating processes became increasingly popular. Thus, it is no coincidence that it was precisely during this period, in 1959, that Prof. Dale Wurster developed the Wurster coating process, which is still widely used today (Hampel, 2015; Waßmann et al., 2011; Wurster, 1953)

Nowadays, it is hard to imagine everyday life and industrial applications without coating products and coating applications. The coating of particulate materials has become a fundamental operation and is used in various industries such as pharmaceutical, food, chemical, cosmetics, biomedical industry and, nuclear fertilizer agriculture, etc. The process influences the surface properties and, thus, the functionality. The objectives include the following (Bose and Bogner, 2007; Saleh and Guigon, 2007)

- Protection from oxygen, humidity, light, or any other incompatible element,
- Controlled release of active agents
- To confer desired interfacial properties to the particles, making them more proper for the final target applications (e.g., dispersion in plastics, electrostatic pulverization, etc.),
- To reduce the affinity of powders concerning aqueous or organic solvents,
- To avoid caking phenomena during storage and transport,
- To improve the appearance, taste, or odors of products,
- To conserve nutrients contained in food products,
- To functionalize powders (catalysts, enzyme-coated detergents, etc.), and
- To increase the particle size.

There are barely any limits to adapting product properties and functionalities by applying a coating layer. Generally, the coating process can coat various materials, with particle sizes ranging from a few microns to centimeters. Different fully automated industrial coating systems are currently known for coating solids. Depending on the requirements

of the product, a wide variety of coating systems can be used. Figure 1 provides an overview of the most common coating processes (Saleh and Guigon, 2007).

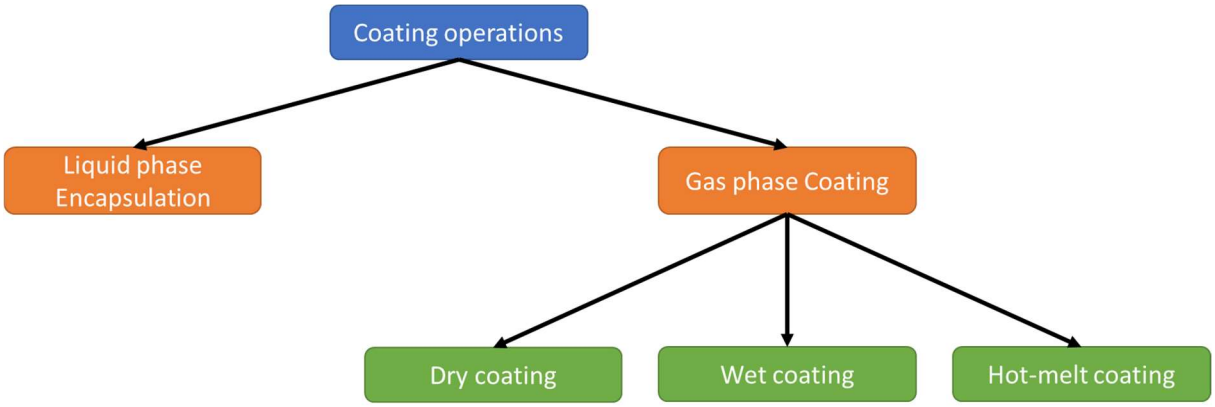

Figure 1: Classification of coating processes (adapted from (Saleh and Guigon, 2007)).

2.1.1 Liquid Phase Encapsulations

Liquid phase encapsulation was specially developed for active substances such as enzymes, living cells, and biocatalyst systems. In this encapsulation type, a liquid is dispersed in an immiscible liquid (continuous phase). This results in the formation of a microcapsule wall by an in-situ polymerization reaction surrounding the active liquid phase. The method comprises four techniques: interfacial polymerization, polymer-phase separation, polyelectrolyte complex formation, and solvent evaporation (Saleh and Guigon, 2007; Thies, 1989).

2.1.2 Wet Coating

Wet coating is the industrial coating process used most. The coating agent is first dissolved or suspended in a solvent. The coating liquid is then sprayed onto solid particles. The coating liquid is evaporated, forming a coating layer from the dissolved solid. Therefore, an essential process step in solvent-based coating is matching the spray rate versus the drying rate (Bose and Bogner, 2007). An additional drying step is performed at increased temperature for rapid evaporation of the solvent. In general, the solvent should be easily evaporable. This is why, on the one hand, highly volatile solvents are often used in wet coating, although they are often environmentally harmful. This is accompanied by an increased risk of explosion and potentially harmful solvent residues in the product. On the other hand, more ecologically friendly alternatives, such as water-based coatings, are significantly more energy-intensive and increase the microbial hazard to the product (Bose and Bogner, 2007). Therefore, the industry has a strong drive toward solventless coating.

2.1.3 Dry Coating

The handling difficulties associated with solvents do not exist with dry coating, as it is a solventless coating technique. In dry coating, the coating material consists of fine solid particles (> 1µm). The formation of a coating layer is obtained by the adhesion of the fine coating material particles to the carrier particle by van der Waals forces or by electrostatic forces. Consequently, the adhesive forces must overtake the disruptive forces (Saleh and Guigon, 2007). Driven by cost consideration and functionality, dry coating has evolved dramatically in recent years, resulting in several newly developed technology applications (Sauer et al., 2013). Dry coating is categorized into electrostatic dry coating, thermal adhesion dry coating, and liquid-assisted dry coating (Sauer et al., 2013). Dry coating has not yet found broad industrial applications and is limited to a few specialized products. These include electrode production for lithium-ion battery applications, which could be optimized using dry coating (Kawaguchi et al., 2018). For pharmaceutical applications, dry coating so far only represents an enormous potential. So, due to increasing demands on functionalities, dry coating technology can become one of the significant pharmaceutical coating technologies through further innovations (Sauer et al., 2013).

2.1.4 Hot-melt Coating

In the so-called hot-melt coating (HMC) process, a melt is applied as a coating material on a carrier material and is solidified by cooling. HMC is originated in the textile and paper industries in the 1940s (Rothrock and Cheetham, 1942) and entered the pharmaceutical industry in the 1980s (Dredán et al., 1999). Meanwhile, the HMC technique is widely used in various industries due to its cost-effective, efficient, precise, and solventless application. Besides thermoplastic resins, polyoxyethylene glycols, paraffins, silicones, and natural waxes or fats are suitable coating materials (Jannin and Cuppok, 2013; Müller et al., 2018; Sudke and Sakarakar, 2013).

In general, in HMC, the coating material can be melted either before or during the process. The layer formation is then induced by a cooldown of the melt, which results in the solidification of the coating material. Here, mixing and temperature control during the coating process are particularly important. HMC offers several advantages, especially compared to wet coating. In addition to eliminating organic solvents, the method provides significantly shorter process times, making the process cost-effective, environmentally friendly, and fast (Bodmeier, 2002). Furthermore, there is no risk of bacteriological contamination (Banker and Peck, 1981).

Product requirements such as controlled release (Mittal. B. et al., 2003), taste masking (Bold et al., 2012), and improving flowability or protection towards oxygen, water, and light (Achanta et al., 2001a, 2001b; Knezevic et al., 2009), can be provided by HMC (Sudke and Sakarakar, 2013). Due to an increased agglomeration tendency, the coating process is limited to a particle size > 100 µm (Bose and Bogner, 2007; Jannin and Cuppok, 2013), although more advanced apparatuses such as ploughshare mixers or vibrated fluidized beds already manage to coat particles < 100µm (Woerthmann and Briesen, 2022a, 2022b).

Since HMC in a fluidized bed is the focus of this thesis, the process will be discussed in more detail below.

2.2 Natural hot-melt coating in food and pharmaceutical industries

2.2.1 Hot-melt coating using fluidized bed technology

As already mentioned above, natural HMCs can be manufactured in a variety of plants. The most used systems are drum coaters, fluidized bed coaters, or, for particularly fine material (< 50µm), sometimes also in mixers such as the Ploughshare mixer (Woerthmann and Briesen, 2022a).

Fluidized bed technology is characterized by fluidizing particles with a gas against the gravitational force. In this process, a bed of particles is brought into a fluidized state. Static characteristics of the particle bed change due to the upstream flow. With increasing gas flow volume, the bed expands, the particles loosen and begin to move, and are converted into a fluid-like state. The gas flow causes intensive mixing of the particle bed. Due to the high gas velocities, heat, mass, and momentum transport in fluidized beds are intense and efficient (Kumpugdee-Vollrath and Krause, 2011). The fluidized state of the particle bed is reached as soon as the pressure difference between the up-bed and down-bed zone remains constant with a further increase in the gas volume. If gas velocity increases, particles are carried along the gas flow and ejected from the system.

Due to the many influencing variables, fluid bed processes are very complex to design and difficult to describe and predict mathematically (Jones and Percel, 1994). Therefore, since the particle size, density, and surface properties of the particle bed change considerably in coating processes, they are still designed using trial-and-error experiments and adjusted by empirical values (Kulah and Kaya, 2011).

Furthermore, fluidized beds are usually equipped with nozzles for coating processes, which can be placed at different positions in the system, influencing the airflow by additional turbulence.

Figure 2 shows five different apparatus implementations of fluidized bed systems.

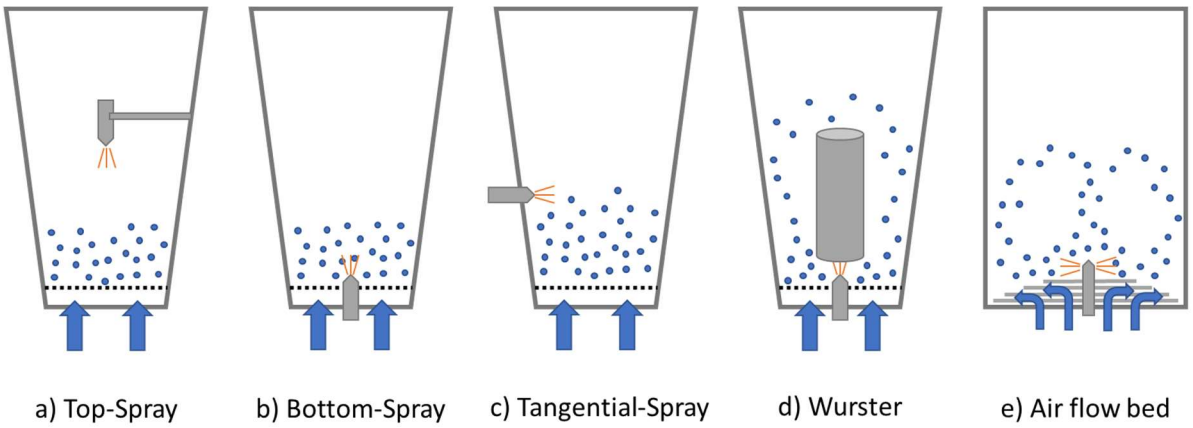

Figure 2: Schematic illustrations of different types of fluidized bed reactors.

Figures a) to d) show a classic conical fluidized bed design, while e) shows an Air flow bed, which is a further development of the traditional conical fluidized bed reactors. The particles can be sprayed with coating material through attached nozzles. The aim is to supply the coating material in a controlled manner by regulating the spray rate to apply it uniformly and homogeneously on the particle bed. With the so-called Top-Spray (see Fig. 2 a), the injection takes place from above, whereby the height of the nozzle device can be above or in the particle bed. The gas flow is opposite to the direction of spraying. On the one hand, Top-Spray is preferred for granulation and particle agglomeration (Heinrich, 2015). On the other hand, Jones and Percel (1994) consider the Top-Spray fluidized bed to be the system of choice for HMC.

Alternatively, a coating can be supplied tangentially (see Fig. 2 c).

In the Bottom-Spray configuration (see Fig. 2 b), however, the coating material is sprayed into the particle bed in the direction of gas flow. A unique development of the Bottom-Spray is the Wurster configuration (see Fig. 2 d). The Wurster process is characterized by an additional tube in the center of the fluidized bed. The concentric nozzle and the sectional perforated sieve bottom force the particles to circulate during the coating process, resulting in a uniform coating (Grave and Pöllinger, 2011). For HMC of pellets, granules, and fine material, Wurster coating in bottom spray configuration has established itself as the standard process (Grave and Pöllinger, 2011).

The Air flow bed (see Fig. 2 e) is characterized by its cylindrical design and orbiter inflow bottom. This gives the gas flow a directed flow profile, which allows the particle bed to be circulated similarly to the Wurster process and ensures good particle singulation. Due to the controlled flow, the Air flow bed is suitable for coating of fine solids (<20µm) (Hüttlin, 2011; Woerthmann and Briesen, 2022a).

In general, an additional differentiation can be made between discontinuous and continuous modes of operation. Heinrich (2015) summarizes extensive apparatus options of continuous fluidized beds.

To achieve a successful HMC for all process variants, it is essential to ensure that the coating material feed, nozzle, process air, and atomization air are temperature-con to prevent premature solidification of the coating material and to be able to guarantee a stable process. In the present work, the HMC was carried out batch-wise in a fluidized bed in the Wurster configuration.

2.2.2 Layer formation in the Wurster fluidized bed

As mentioned, the Wurster configuration is characterized by its uniform coating (Vollrath and Krause 2011), making it particularly suitable for products with high-quality requirements. The Wurster technology was developed in the 1950s by the American pharmacist Dale Wurster (Wurster, 1953). The process is particularly suitable for the coating of small particles, micro pellets, or mini tablets (Grave and Pöllinger, 2011), as a strong particle singulation is made possible by a controlled fluidization pattern.

Particles coated in a Wurster fluidized bed pass through four zones during the process (Karlsson et al., 2006; Laicher and Fuchs, 1998; Shelukar et al., 2000). These are the up-bed zone, the relaxation zone, the down-bed zone, and the horizontal transport zone. Fig. 3 (left) shows the four zones schematically. Fig. 3 (right) illustrates the sequence of layer formation as a function of the four zones mentioned.

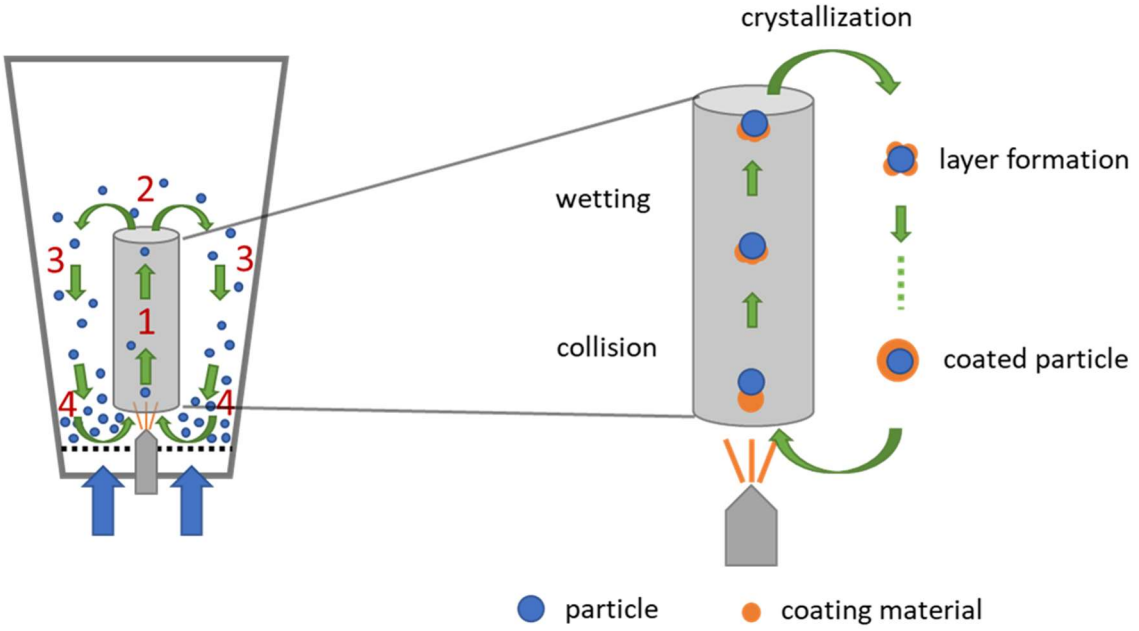

Figure 3: Schematic illustration of particle coating in a Wurster fluidized bed.

The up-bed zone is located inside the Wurster tube. The gas flow velocity is highest in this zone because the nozzle is located in the center of the Wurster tube, and the sieve bottom has larger perforated openings towards the center. After being sprayed with melted coating material, the particles in the up-bed zone are consequently conveyed pneumatically upwards into the relaxation zone. The particle surface is wetted by hot melt droplets during vertical transport, as shown in Fig. 3 (right). The relaxation zone is just above the Wurster tube and is characterized by an abrupt change of the gas velocity due to the sudden expansion of the diameter. The particle velocity drops, causing the particles to fall into the down-bed zone. In this zone, the hot coating material has time to solidify completely. If the residence time is too short or the temperature too high for material solidification, it will lead to undesirable agglomeration. If the particles arrive at the bottom of the particle bed, they are conveyed horizontally to the center due to local pressure differences, where they pass through the process again and pick up further coating material. The air gap of the Wurster tube is decisive for the movement profile in the Wurster fluidized bed coating. If the air gap is set too large, the desired movement profile cannot be achieved. Depending on the particle size, particle density, and the respective flow properties, the Wurster tube air gap needs to be adjusted (Grave and Pöllinger, 2011).

2.2.3 Key process parameters for hot-melt coating in a Wurster fluidized bed

As can already be deduced from previous chapters, the process parameters to be selected for a successful process differ from one another depending on the process and plant design. Furthermore, the physico-chemical properties of the coating material and the carrier particles must be considered for the appropriate process parameter selection in order to successfully carry out the process. This section will discuss and elucidate the main process parameters influencing HMC. To give an impression of the multitude of interrelationships and influencing factors impacting the functionality of the natural HMC, they are summarized in the following Ishikawa diagram (see Figure 4).

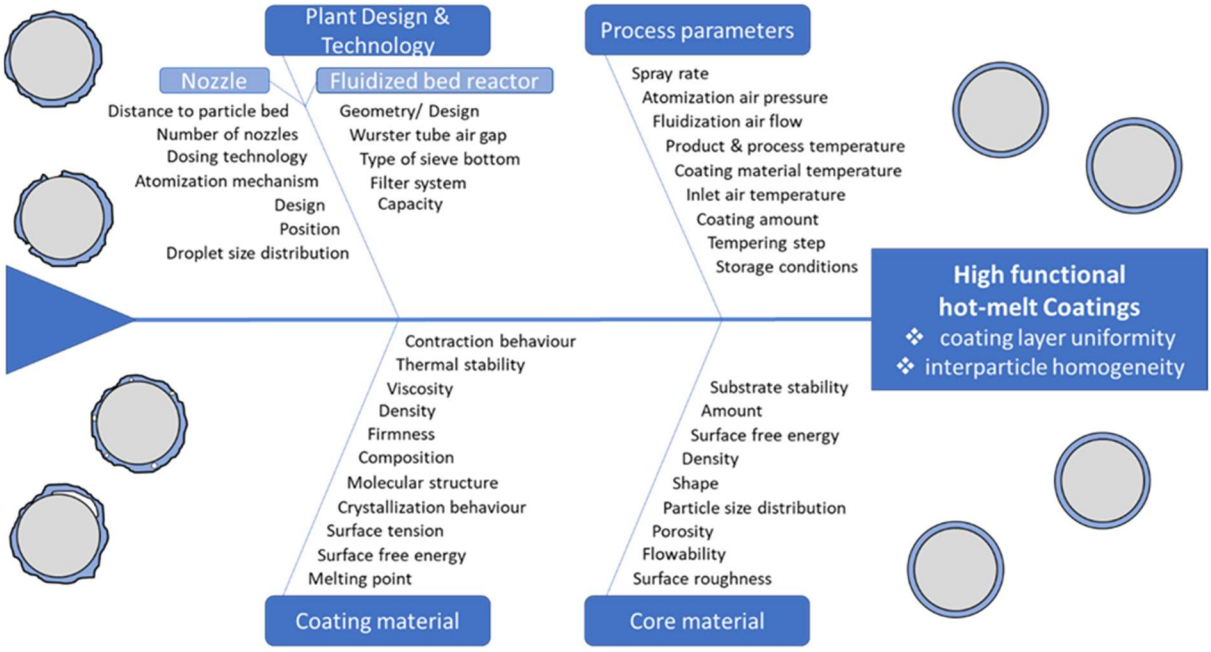

Figure 4: Overview of the multitude, interrelationships, and influencing factors on the functionality of natural hot-melt coatings.

Process temperature

Due to the temperature-dependent crystallization behavior, the coating quality depends decisively on the process temperature and the respective coating material. The significant influence of process temperature on the coating quality is due to the temperature dependence of the crystallization behavior of the coating material. The process temperature should generally be within a specific temperature range during the HMC process. To ensure the solidification of the coating material on the carrier particles, the range must be below the melting temperature and crystallization temperature of the coating material.

According to Acevedo and Marangoni (2015), three levels of influence on the coating structure can be distinguished (Acevedo and Marangoni, 2015):

- Macroscopic level (> 200 µm)

- Microscopic level (0.5 µm – 200 µm)

- Nanostructure (0.4 nm – 500 nm)

The influence of the process temperature is predominantly on the macroscopic and microscopic levels for hot-melt coating processes. This means that the product quality can be decisively affected by the parameter setting regarding mechanical stability or protective effect. For example, if the process temperature is too high, solidification will be delayed, resulting in agglomeration or, at worst, in the collapse of the fluidized bed (Jozwiakowski et al., 1990). However, if the temperature is too low, it does not guarantee a homogeneous coating as the material solidifies too quickly. Consequently, a crystallization effect and dust formation occur because the atomized coating material crystallizes before it can wet the particle surface and form a coating layer. The result will be a thinner coating layer thickness with a reduced protective effect. Jannin and Cuppok (2013) recommend a product temperature 10-15 K below the melting temperature of the coating material to ensure a homogeneous coating (Jannin and Cuppok, 2013). However, Müller et al. (2018) pointed out in their study that natural fats and waxes can exhibit broad melting and crystallization ranges (Müller et al., 2018). Therefore, for proper parameter setting, the respective crystallization behavior of the coating materials should be considered. Furthermore, the process temperature can affect the crystallization structure of the coating layer (Acevedo and Marangoni, 2015; Lopes et al., 2015).

Atomization conditions

The atomization conditions significantly influence the product quality and the coating layer structure. If the atomization conditions are not coordinated, agglomeration or dust formation, the so-called crystallization effect, can occur. Especially in interaction with the heat input and heat output, the droplet size is a decisive process variable that contributes to the success or failure of the coating process and is responsible for the product particle size (Wen, 2010). In general, the droplet size distribution depends on the atomization technology, atomization parameters, and coating material properties (Wong et al., 2013).

The nozzle type defines the atomization mechanism and mainly influences the droplet size distribution and the spray angle. In this work, a three-component nozzle was used, which allowed the spray angle to be controlled by the rinsing air and the droplet size to be controlled by the atomization air. Concerning the nozzle selection for a hot-melt

coating process, it is essential to ensure that the nozzle can be heated to prevent insufficient atomization and clogging of the nozzle due to a crystallization of the coating material. Furthermore, fluidized bed coating processes must consider the nozzle position, the number of nozzles, and the distance to the particle bed. The atomization pressure and the spray rate are among the main atomization process parameters for compressed air nozzles. The atomization pressure supplies the required energy for atomization and influences the droplet size distribution. Low pressures result in large droplets, which can lead to non-uniform coating, while high pressures result in tiny droplets (Wozniak, 2003). Therefore, the droplet size distribution is also critical for successful HMC.

The atomization of coating materials depends not only on the atomization pressure but also on other factors, such as the properties of the coating material, e.g., viscosity and surface tension. The viscosity and surface tension can be influenced in the process through the coating material temperature. Higher coating material temperatures lower viscosity and surface tension, facilitating atomization towards finer droplet sizes (Jannin and Cuppok, 2013).

However, other process variables must also be considered for a successful coating process to ensure a layer build-up. To generate a homogeneous coating layer, the droplets should be finely atomized and preferably of identical size. However, an increased surface-to-volume ratio leads to sufficient heat exchange between the droplet and the gas phase, resulting in an accelerated crystallization process (Shukla et al., 2001). Especially for fine and narrow droplet size distributions, the process temperature and the temperature difference between the coating material and the particle bed must be considered. The process temperature is composed of gas inlet temperature, atomization air temperature, coating material temperature, fluidization air flow, spray rate, and atomization air flow. The fluidization rate is mainly responsible for mixing, sufficient heat exchange, and cooling performance. The crystallization process can thus be influenced by several process parameters (Jannin and Cuppok, 2013; Qiyun, 2008)

As mentioned, tiny droplets with a narrow distribution are ideal for a uniform and homogeneous coating. This can be obtained by a low spray rate, high atomization air pressure, low coating material viscosity, and low surface tension (Wozniak, 2003). The droplets cool too fast, e.g., due to a too-high air flow rate or too-low coating material temperature or inlet gas temperature, dust formation, and the so-called crystallization effect, will occur instead of coating formation.

Droplet size distributions with too large droplets and a too wide distribution lead to slow or inhomogeneous solidification and layer formation. The result can be agglomerates or inhomogeneous layer structures with pore formation (Woerthmann et al., 2021). Thus, agglomeration occurs when heat removal and mixing via the fluidizing air is insufficient for a coating.

Consequently, detailed knowledge of the factors influencing atomization is crucial for coating success and functionality. However, few scientific studies on HMC with natural coating materials exist. On the one hand, more detailed knowledge about the physiochemical properties of natural fats and waxes must be provided. On the other hand, there is a lack of studies on atomization itself, although the measurement of droplet size distributions using laser diffraction or Phase Doppler anemometry depending on the atomization parameters is already possible (Indiana et al., 2015; Ludewig and Ganzelmeier, 1993).

A systematic nozzle selection and parametrization of the atomization conditions depending on the coating material properties must be improved for HMC. Literature can only be found regarding the influence of the spray rate on the dissolution kinetic (Jozwiakowski et al., 1990). Overall, there is a lack of literature on the atomization of liquids. However, it is a relevant influencing factor for HMC applications and solvent-based coatings and granulation processes.

Fluidization

Besides the process temperature and atomization conditions, the fluidization velocity also affects the coating quality. As described in Chapter 2.2.1, fluidization is responsible for particle dispersion and mixing. All particles must be fluidized without getting carried out of the fluidized bed. Insufficient fluidization can lead to inhomogeneous coating as heat is not dissipated quickly enough, possibly leading to agglomeration. The detailed interaction of various process parameters with fluidization conditions has already been explained under Atomization conditions. In contrast, excessive fluidization of the fluidized bed increases the coefficient of friction (Louge et al., 1991). The probability of collisions will increase, which may lead to particle breakage and increased abrasion of the coated particles (Kumpugdee-Vollrath et al., 2011). Product quality degradation will be the consequence. The proper setting of fluidization parameters during the coating process is complex because it depends on the particle size, density difference between solid and gas, and particle surface properties, which also change continuously during the coating process.

As mentioned above, the behavior of solid-gas fluidized bed coatings is strongly influenced by the particle properties. For an initial estimate of the fluidization parameters, the Ergun equation is suitable for determining the minimum fluidization. Additionally, the Geldart classification of powders can predict the solid particle fluidization behavior. The main influencing parameters of fluidization are particle diameter and density difference between gas, solid particles, and particle surface properties. According to Geldart (1973), particle-gas systems can be classified into four groups (A-D) depending on their behavior. Figure 5 shows the Geldart classification.

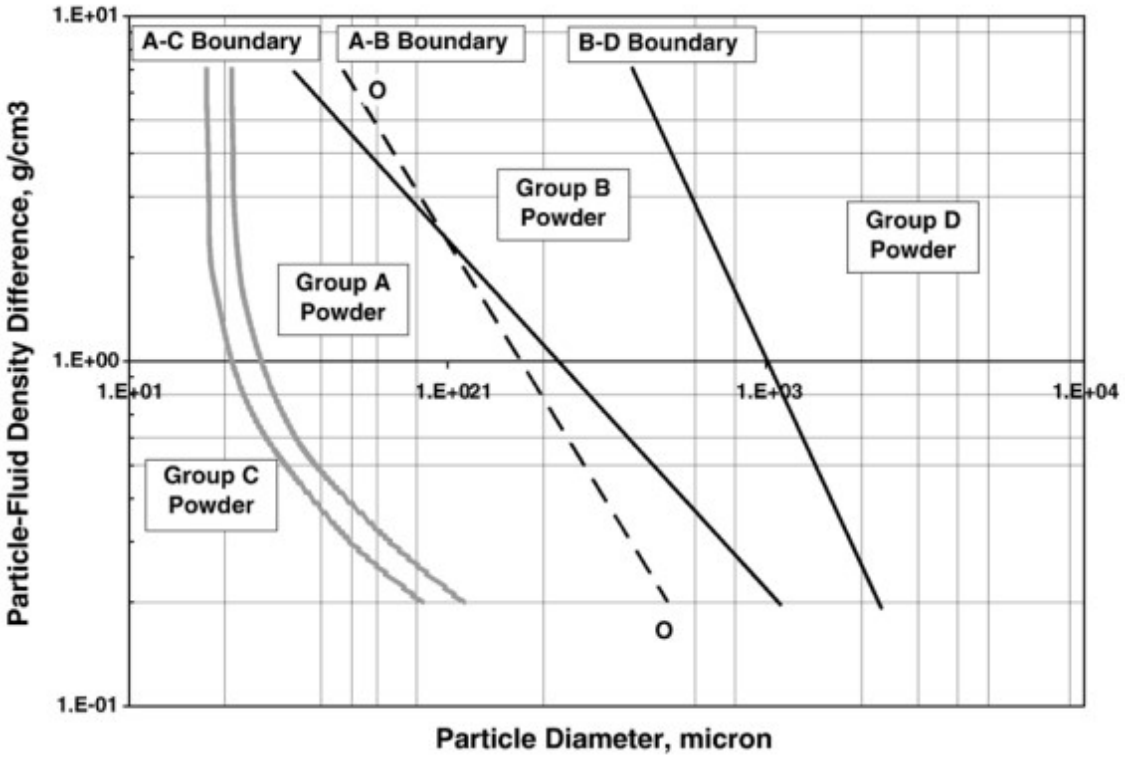

Figure 5: Geldart´s classification of powders (Yang, 2007). Reproduced with the permission from Elsevier B.V.

Group C, for example, are very cohesive fine-grained particles. Therefore, fluidization of group C particles is difficult due to strong cohesive and adhesive forces. Channel formation increases during fluidization. This makes particle singulation for coating processes difficult. For group C particles, additional mechanical agitators such as mixing geometries or vibration are suitable to overcome the adhesive forces and avoid channel formation. An example of Geldard Group C particles is icing sugar.

Group A particles are small (< 0.1 mm) with low solid density. A characteristic of Geldard Group A particles is that the fluidized bed expands, if the air flow rate is increased before air bubbles are formed. Formed air bubbles rise faster than the gas between the particles. If the gas flow is abruptly turned off, the bed collapses slowly.

Group B is described as "sand-like" and includes particles in the range of medium grain sizes and densities (40 µm ≤ d_p ≤ 500 µm and 1.4 * 10^3 kg/m^3 ≤ ρ_S ≤ 4 * 10^3 kg/m^3). The air bubble formation occurs right above the loosening velocity v_L. The bed expansion is small, and the bed collapses rapidly in case of a sudden gas stop. The coalescence of air bubbles during fluidization is also typical.

Group D contains large particles (> 0.5 mm) with a high density, which are usually easy to spout. Large gas bubbles rise faster than the gas between the particles, whereas smaller bubbles rise slower than the gas in the interspace, distinguishing gas exchange to groups A and B (Geldart, 1973; Kraume, 2004; Yang, 2007).

As already mentioned, the Geldart classification is only suitable for a rough classification of the particle system because, on the one hand, not all influencing factors are considered (e.g., surface properties), and, on the other hand, most particle systems are not ideal and are, for example, composed of different particle sizes (particle size distributions) or different particle shapes. Despite years of research into fluidized bed coating in the pharmaceutical and food industries, the preferred method for establishing new processes is still trial and error investigations (Kulah and Kaya, 2011).

2.3 Coating materials and their properties

The physico-chemical properties of coating materials are crucial for developing and designing an HMC process. This section, therefore, gives an overview of common natural coating materials, their requirements, and challenges regarding their properties and behavior.

2.3.1 Natural Coating Materials

A broad spectrum of coating materials is used for the HMC. These include, for example, hydrophobic waxes (e.g., carnauba wax), hydrogenated vegetable oils (e.g., hydrogenated palm oil), animal fats (e.g., cow ghee) or their derivatives such as polyoxylglycerides, fatty acids or partial glycerides.

The respective coating excipient is selected depending on the functional properties to achieve the product requirements. At the same time, specific process requirements need to be satisfied, for example, temperature stability. Achanta et al. (2008) summarized the ideal characteristics of a coating material for the HMC process as follows:

1) It should not undergo physical or chemical degradation at temperatures below 200°C.
2) It should have a melting point 75-80°C range.

3) Its melt transition should occur over a narrow temperature range and not soften before melting.
4) Its thermal behavior in the 30-200°C range should be independent of the preparation, storage conditions, and thermal history.
5) It should not undergo any thermal modifications when subject to temperatures as high as 200°C.
6) It should be available in varying hydrophilic-lipophilic balance (HLB) values.
7) Its melt viscosity should facilitate easy flow and spray.

In the food industry, low-cost and health-safe materials such as natural non-fossil lipids with GRAS (Generally Accepted as Safe) status are particularly preferred. Additionally, these offer good barrier properties to moisture due to their hydrophobic properties and are, thus, already in broad use in foods (Chansanroj et al., 2007; Gontard et al., 1995; Jannin and Cuppok, 2013; Sinchaipanid et al., 2004).

In general, lipid-based natural products can only partially satisfy the ideal criteria of Achanta et al. (2008). A challenge for a high-quality hot melt coating is the large variability and variation in the chemical composition of natural lipids due to geographic, climatic, or seasonal variations.

For this reason, synthetic coating agents with specifically adjusted properties are commonly used in the chemical or pharmaceutical industry (Becker, 2016). An undefined melting and crystallization point also increases the complexity of natural coating materials since broad temperature ranges are usually present (Achanta et al., 2008). The targeted blending of coating materials for easier processing is not recommended due to the associated expansion of the melting and crystallization ranges (Müller et al., 2018).

In addition, crystal modification below 200°C, as required by Achanta et al. (2008), cannot be excluded. Most vegetable and animal fats contain triacylglycerides (TAG), which show polymorphism (Idziak, 2018; Lopes et al., 2015). Figure 6 illustrates the different crystal forms and packing densities of TAGs.

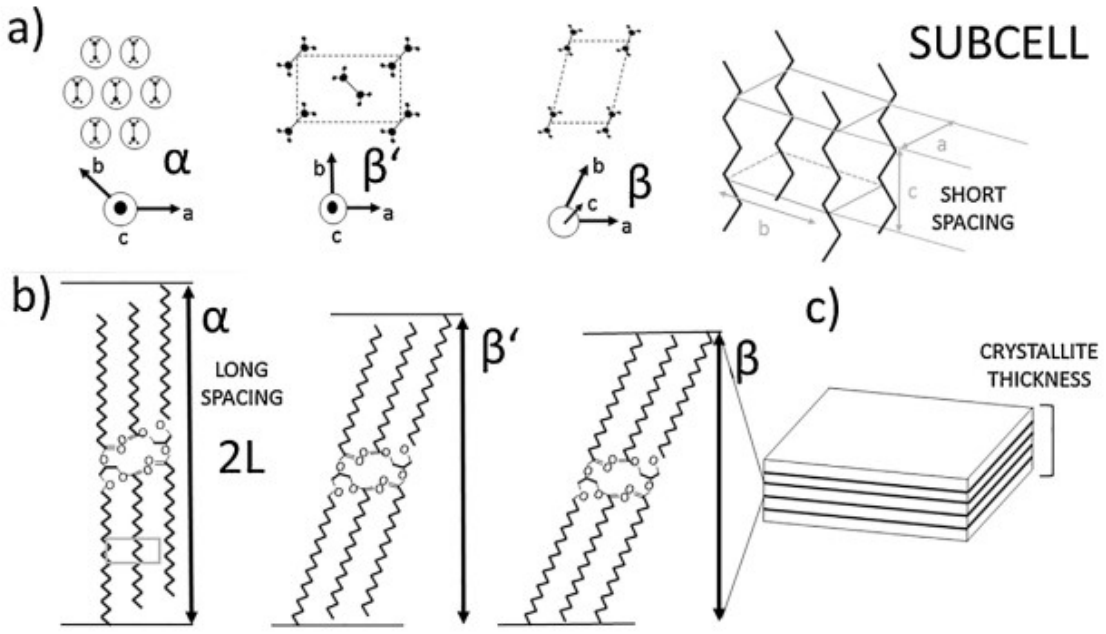

Figure 6: Schematic illustration of polymorphic shapes of TAG in a subcell (a) with vertical packing (b) and 3D representation of crystal thickness (c). Reproduced from Lopes et al. (2015) and Idziak (2018) with permission from Elsevier B.V. and AOCS Press.

Depending on the thermal history of the material, TAGs can exist as thermo-dynamically unstable hexagonal (α), metastable orthorhombic (β'), or stable triclinic (β) crystal structures (Lopes et al., 2015). The type of polymorphic crystallization structure determines both packing density and stability of the material as well as physicochemical factors such as melting point, recrystallization rate, and water solubility (Achanta et al., 2008; Sato et al., 2001; Sato et al., 2013).

Sato et al. (2013) state that a higher melting temperature results in more densely packed thermodynamically stable crystal forms. In general, using lipid-based coating materials always requires a specific adaptation and regulation of the manufacturing process to the given material properties to obtain a reproducible product quality. A fast-cooling process, for example, leads to more thermodynamically unstable α-crystals, which increases the probability of recrystallization and a transformation into more stable polymorphic forms (e.g., β', β). This subsequent transformation leads to a change in the molecular structure of the fat and to a different space requirement, resulting in a change of the coating layer structure and fluctuations in product quality (Minami et al., 2007). The spontaneous formation of flakes on the structure is also known as “lipid blooming”, generally known from bloomed chocolate (Lonchampt and Hartel, 2006; Mayama, 2009). Blooming can be avoided by directly crystallizing the stable β-forms due to an additional tempering step or, done in the pharmaceutical industry, by adding additional emulsifiers (Becker, 2016;

Lopes et al., 2015; Lopes et al., 2017). Structural correlations with delamination phenomena are not known in literature yet.

For this reason, it is even more important for food industry to know the properties of the coating materials used in detail to adapt the process in a targeted manner.

Complementary, Table 1 lists coating materials that are commonly used for HMC (adapted from Sudke and Sakarakar (2013)):

Table 1: Examples of coating materials for HMC (Sudke and Sakarakar, 2013).

Coating agent	**Chemical composition**	**Melting point/ range [°C]**	**Examples**
Animal fats	Clarified butter	80	Cow ghee
Fatty acids	Long-chain fatty acids	60-90	Behenic acid, stearic acid
Fatty alcohol	Long-chain fatty alcohol	50-55	Cetyl alcohol, wool alcohol
Partial glycerides	Mixture of mono-, di-, and triglycerides	54-74	Compritol® 888 ATO
Polyoxylglycerides	A mixture of glycerides and esters of fatty acid and PEG	50	Celucire® 50/02
Vegetable oils	A mixture of triglycerides, free fatty acids, phospholipids	60-71	Hydrogenated palm oil, hydrogenated soybean oil
Waxes	Esters of fatty acids and long-chain alcohols	62-86	Beeswax, Carnauba way, candelilla wax, rice bran wax

Chapter 3

Problem definition

The hot-melt coating process is widely used in food, chemical, and pharmaceutical industries. Its purpose of use is very diverse and includes, among other things, changing the functional properties of the particle surfaces, forming a protective layer, or influencing the release rate of the encapsulated substance. To achieve such purposes for each product particle, a high degree of uniformity of coating of the single particles and a high interparticle batch homogeneity are required.

However, a precise generation of the protective and barrier effect is challenging for hot-melt coatings due to various influencing factors and complex interrelationships. Furthermore, standard analytical methods, such as dissolution tests, scanning electron microscopy, or particle size analysis, do not allow a detailed layer structure analysis. The influence of material properties and process influencing factors on the resulting coating layer structure and interparticle batch homogeneity remained largely unexplored for HMC.

A precise method to analyze coating layer morphology is absent.

µCT measurements allow a detailed and non-destructive structural analysis of coated particles. The visualization and analysis of the coating morphology can contribute to a better understanding of the influencing factors and their complex interrelationships in HMC. Visualization of coated particles by µCT has already been demonstrated. However, no method exists to analyze and evaluate the three-dimensional layer structure. A new and precise method for measurement, including data evaluation, could fill this gap. Obtained findings can directly contribute to optimizing the functionality of HMC products. In addition, valuable and more detailed data can be obtained for modeling the layer structure formation and used for the prediction or targeted generation of a layer quality.

The literature lacks correlations between coating layer structure phenomena, process influencing factors, and coating material properties.

The occurrence of delamination of the coating layer is known. Still, it has rarely been investigated whether coating material properties or non-ideal process control are responsible. Nevertheless, delamination negatively affects the interparticle batch homogeneity and, thus, the functionality. Likewise, it is known that wetting and layer

formation are more limited in HMC compared to solvent-based coating. However, a correlation between delamination and wetting behavior has not been determined.

Although coating materials are generally well-studied, they should be studied more in relation to an HMC application and their resulting coating layer structure properties. A quantification of delamination in HMC combined with an investigation of the wetting behavior could, therefore, allow a correlation of structure phenomena with material properties and lead to a more targeted generation of functional HMC particles.

Easily applicable and accurate methods for investigating factors influencing the interparticle batch homogeneity of HMC are lacking.

The effectiveness and functionality of HMCs depend on the interparticle batch homogeneity. Nevertheless, only a few methods are suitable for investigating interparticle batch homogeneity. Methods such as particle size measurements cannot provide complete information on batch homogeneity without assumptions. In comparison, other methods like µCT allow only petite sample sizes. Apart from the large amount of data, a significant sample size would require an enormous effort in terms of time and costs. An inexpensive and accurate method for measuring the batch homogeneity of HMC sensitive enough to relate process parameters to batch homogeneity is lacking. In this context, studying batch homogeneity as a function of process parameters improves process understanding and contributes to the continuous improvement of the HMC application.

Chapter 4

Methodology

As mentioned in the problem definition, the number of methods available for detailed analysis of the coating structure of hot-melt coated particles is limited. 3D imaging using µCT has emerged as a suitable method for particle characterization and detailed layer structure analysis. However, 3D imaging for hot-melt coating applications is relatively new; thus, the present work was concerned with developing 3D imaging and analysis methods. Furthermore, the work developed complementary methods to contribute to further process understanding and data interpretation for developing high-quality hot-melt coatings regarding high intraparticle coating layer thickness uniformity and high interparticle batch homogeneity. In the following, the developed methods are briefly summarized. A detailed description of all methods can be found in the attached publications.

Method for analyzing interparticle coating layer thickness uniformity.

The method is based on 3D imaging using µCT measurement. In their publications, Müller et al. (2018) and Sondej et al. (2015) showed that µCT can image coated particles, and standardized and automated image analysis is possible. However, the methods published until then were limited to incomplete 2D image analysis. To fill this gap, this study aimed to develop a new, detailed, and standardized method for hot-melt coated particles, which uses all 3D information to determine the coating thickness uniformity. In addition to accurate 3D imaging of coated particles, a critical factor in developing the method for determining coating uniformity was selecting multiple representative measurement points on a spherical particle. Spherical pixelation using the HEALPix algorithm enables this representative sampling of measurement points on a sphere (Gorski et al., 2005). The proposed method allows determining the layer thickness distribution and the proportion of non-covered surface. Furthermore, the developed method can be used to identify and quantify factors influencing the coating layer uniformity.

Method for obtaining delamination frequency and wetting behavior.

Delamination of the coating layer is usually not visible from the outside and can only be detected using non-destructive µCT scans and subsequent image evaluation. A new µCT measurement procedure and 3D image evaluation were developed to obtain the

delamination frequency of hot-melt coating products. Up to 300 particles per batch were imaged and then examined and evaluated for delamination, cracking, and spalling to quantify the delamination frequency. Several material combinations concerning delamination and wetting behavior were investigated for a correlation of the delamination frequency with the wetting behavior of different coating materials. A drop shape analyzer was used to investigate the wetting behavior as a function of temperature.

Method for analyzing interparticle batch homogeneity.

Determining the interparticle batch homogeneity via the applied coating amount per particle is not trivial. µCT measurements are time-consuming and limited in sample size and, therefore, unsuitable for interparticle batch homogeneity analysis of hot-melt coatings. For this reason, a fluorescence method was developed, allowing the coating amount per particle to be determined for many particles. For this purpose, the coating material was dyed with a heat-stable fluorescent dye. A fluorescence photometric analysis of 384 particles per batch allowed the determination of the coating amount per particle and, thus, the interparticle batch homogeneity. With information from particle size measurements or µCT measurements such as layer thickness distributions or delamination tendencies, gaps in the process understanding can be closed further.

Chapter 5

Results

5.1 Paper I: A novel method for assessing the coating uniformity of hot-melt coated particles using micro-computed tomography (Woerthmann et al. 2020)

Summary

2D image analysis methods are commonly used to analyze coated particles and determine coating success. The benefits of the methods are, for instance, that they are not only fast but also can be applied in-line. However, the information content is significantly lower, especially compared to 3D methods such as µCT image analysis. Thus, a detailed evaluation of the coating layer thickness distribution, the coating layer structure, and the detection of the non-surface surface proportion is not possible with 2D image methods. Compared to solvent-based coating, wetting and spreading are more limited for hot-melt coatings; therefore, coating uniformity is more affected by process parameters, and more detailed analysis methods are needed. Since the effectiveness of hot-melt coating depends on its uniformity and the degree to which the surface is completely covered, the Briesen group focused on previous work on the feasibility of µCT imaging of hot-melt coated particles (Müller et al., 2018). 3D µCT images contain the most information about the coated particles' shape and structure. Consequently, a study was conducted to develop a 3D imaging and image analysis method to examine hot-melt coated particles.

This study presents a new method for identifying and quantifying factors affecting coating uniformity. The proposed method allows determining the layer thickness distribution and the proportion of non-covered surface. A crucial factor in developing the method for evaluating coating uniformity was sampling several measuring points on the sphere. The uniform sampling on a spherical surface is not trivial. However, it became possible using the so-called HEALPix algorithm (Gorski et al., 2005). The published method is based on particles coated in a Wurster fluidized bed. This study compares the results with commonly used methods for layer thickness determination. The results verify that the method presented is well-suited for the analysis of coating quality. The coating material properties show a significant influence, as stearin and palm fat form different coating layers. Furthermore, new influencing factors that affect the coating thickness distribution

and uniformity were identified and quantified. The influencing factors were quantified based on the dependence of the coating uniformity on the coating amount and the respective coating material. For example, the coating layer's relative uniformity was found to increase with the coating amount. Also, a complete and uniform coating with stearin was only achieved with a coating amount of 10% (w/w) and above.

Author contributions

J. Lindner and H. Briesen came up with the idea for this work. J. Lindner and F. Schmid performed the first experimental tests and µCT measurements. J. Lindner, T. Kovacevic, and P. Pergam developed an image analysis method with the help of M. Woerthmann. M. Woerthmann performed experimental tests and analyses and evaluated the obtained data. H. Briesen supervised all work. M. Woerthmann wrote the article. J. Lindner and H. Briesen corrected and proofread the article.

Copyright

Powder Technology 378 (2021) 51–59

Contents lists available at ScienceDirect

Powder Technology

journal homepage: www.elsevier.com/locate/powtec

A novel method for assessing the coating uniformity of hot-melt coated particles using micro-computed tomography

B.M. Woerthmann [a], J.A. Lindner [b], T. Kovacevic [a], P. Pergam [a], F. Schmid [a], H. Briesen [a,*]

[a] Process Systems Engineering, TUM School of Life Sciences Weihenstephan, Technical University of Munich, Germany
[b] Campus Burghausen, Rosenheim Technical University of Applied Sciences, Germany

ARTICLE INFO

Article history:
Received 24 March 2020
Received in revised form 16 September 2020
Accepted 26 September 2020
Available online 01 October 2020

Keywords:
Wurster fluidized bed
Hot-melt coating
Micro-computed tomography
Layer-thickness distribution
Coating uniformity

ABSTRACT

The effectiveness of hot-melt coating depends on its uniformity and the extent to which the surface is completely covered. Compared with solvent-based coating, spreading is more limited in hot-melt coating; thus, the coating uniformity is more affected by the process parameters. This study presents a new method for identifying and quantifying factors influencing coating uniformity. The proposed method facilitates the determination of coating-thickness distribution and non-covered surface proportion based on micro-computed tomography measurements. The proposed method is based on particles that have undergone hot-melt coating in a fluidized bed, and it is compared to common methods for layer-thickness determination. The influencing factors are quantified in terms of the dependency of coating uniformity on the coating amount and material. Material properties have a significant impact because stearin and palm fat create different coating layers. The proposed method is confirmed to be well suited for analyzing coating qualities.

1. Introduction

Coating in a fluidized bed has several applications in agriculture, chemical, food, and pharmaceutical industries with varying objectives. For example, it can be used for protection against a reactive environment, such as humidity, light, or oxygen. In food industry, coating protects fruit [1] and prevents flavor loss [2]. Another objective is the controlled release of pharmaceutical agents and food ingredients depending on temperature, acidity, pressure, or solubility conditions [3]. In food and pharmaceutical industries, it is also used to mask taste [4] and alter the surface properties, such as color or flowability, for better handling, e.g., to avoid dust and stickiness [2,5]. Depending on the application, the quality criteria of the respective coatings differ. An effective coating for taste masking must form a completely closed but thin layer, whereas the coating layer for time-controlled release must exhibit well-defined thickness and porosity [5]. In hot-melt coating, the coating material is melted and crystallized on the target particle. Important media for industrial use include hydrogenated palm oil, beeswax, and carnauba wax [3]. Coating materials of natural origin can be used and are advantageous as they pose a low microbiological danger. Moreover, hot-melt coatings are environmentally friendly because they do not require an evaporation step, which is required in solvent-based coating, resulting in faster process time. Furthermore, hot-melt coating processes can be applied to various plants. However, fulfilling these high-quality requirements for hot-melt coating is more challenging than for solvent-based coating. Another disadvantage of hot-melt coatings is their fast crystallization in a very limited period preventing even spreading on the particle surface. The low spray rates in hot-melt coating lead to a uniform distribution and low agglomeration [6]. In the case of wax mixtures, the melt crystallizes over a broad temperature range [7], rendering temperature control difficult because the melt temperature must be above the crystallization range before hitting the particle and spreading, with the bed temperature being below the crystallization range. Jones and Percel used an air temperature range of 10 °C–15 °C below the melting temperature and a spray temperature range of 40 °C–60 °C above the melting point [3,8]. In fat mixtures, a significant temperature difference is also necessary [7]. Another difficulty is the change in the coating layer during storage, which can be affected by heat changes and delamination. Consequently, understanding the influence of diverse parameters on the quality of the coated products is essential. The main factors influencing the coating process are atomization pressure, fluidization air velocity [9], spraying rate, temperature of fluidization air, and properties of the coating material, such as viscosity and thermal behavior [4,10]. The crucial quality characteristics of the coating layer include the mean layer-thickness, thickness distribution over the entire batch, thickness distribution on a single particle (uniformity), uncoated-surface proportion, and coating morphology.

To examine these quality characteristics, various methods are available. A very widespread, simple, robust, and fast method for estimating the increase in the layer-thickness of the coated particles is the

* Corresponding author at: Process Systems Engineering, Gregor-Mendel-Str. 4, 85354, Freising, Germany.
E-mail address: heiko.briesen@tum.de (H. Briesen).

https://doi.org/10.1016/j.powtec.2020.09.065
0032-5910/

measurement of the particle-size distribution using image analysis or laser diffraction measurements [11,12]. Both techniques require a narrow particle-size distribution and a large number of particles to accurately determine the mean-coating layer-thickness [13,14]. Nevertheless, this method provides a high statistical significance of the mean layer-thickness. Apart from the mean layer-thickness, no information regarding the growth of differently sized particles or coating layer uniformity has been obtained. Additional methods for determining layer-thickness include near-infrared (NIR) spectroscopy and Raman scattering [15]. However, further characterization of the coated particles is limited because these methods do not provide any information about the uniformity of the coating layer on a single particle. This information is necessary for the characterization of the process and the coating's functionality. The methods that are capable of providing information about the layer-thickness distribution of single particles help in gaining understanding of the process. Recently, measurement technologies, such as confocal-laser-scanning microscopy (CLSM) [16,17], optical-coherence tomography (OCT) [18–20], and micro-computed tomography (μCT) [21], have been used to investigate these key quality characteristics. In particular, μCT offers the possibility of a detailed, high-resolution, and non-destructive analysis of the layer's characteristics [22]. The principle behind μCT is to create radiographs from different angles and reconstruct the subject's inner morphology; the result is a three-dimensional image comprising an array of gray values representing local absorption. If the local absorption significantly differs, different materials can be separated. This procedure can be used in particle technology for diverse purposes, such as determining surface, volume, morphology [23–25], post-breakage changes in particle properties [26], fractal dimensions of pore spaces in rocks [27], inner structures of materials, such as limestone [28], or even estimating the mass transfer rate and primary drying times during freeze-drying of frozen maltodextrin solutions [29]. μCT can be used to determine the properties of a coating layer in three dimensions. Perfetti et al. used X-ray tomography for morphological characterization and coating thickness measurements of solvent-based coating [30]. Different definitions of the coating thickness were evaluated, such as the 2D cross-sectional thickness [31] and 3D structure thickness [32]. Perfetti et al. based their 3D image evaluation on the definition of Hildebrand and Ruegsegger [32], which is also known as “sphere fitting.” Here, the 3D structure thickness is defined as the diameter of the largest sphere, which completely fits inside the coating layer. Since hot-melt coatings lead to less uniform layers with more pores and inclusions, the evaluation of the 3D structure thickness of Perfetti et al. can be prone to errors as the pores would provide excessively small measurement results [30]. Sondej et al. also investigated the coating layer morphology of solvent-based coating using μCT. They compared the evaluation results of 2D images obtained by X-ray tomography using single X-ray images [21]. However, it has not been determined whether the methods are suitable for investigating the influence of different operating conditions. Moreover, Sondej et al. compared tomographic images of solvent-based coating using confocal-laser scanning (CLSM) to determine the coating thickness [17].

In contrast to the above presented papers on μCT analysis, in this study, we present a new method for analyzing the coating thickness distribution (distributing equidistant rays) to obtain the 3D image of a particle using the Gorski method [33]. Instead of solvent-based coating, this study investigated hot-melt coating, which is specifically prone to non-uniform coating due to their complex crystallization behavior, and material properties [7]. The new presented 3D image evaluation method offers the possibility of determining the coating layer-thickness, coating uniformity, and non-covered surface proportion on a single sphere, which were not accessible using previous evaluation methods. The novel evaluation method and its analysis are demonstrated on the basis of individual hot-melt coating experiments and compared with common methods.

2. Materials and methods

2.1. Materials

All experiments were performed using highly spherical (sphericity >0.93) microcrystalline-cellulose particles *Cellets® 1000* (HARKE Pharma GmbH, Germany). The particles have a relatively narrow size distribution with a mean particle size of $d_{50,0} = 1197$ μm, standard deviation of $\sigma = 113$ μm, and particle density of 1.4 g/cm^3. Stearin and hydrogenated palm oil were used as coating materials. Stearin is a mixture of stearic acid (approximately 54%) and palmitic acid (Hamohr 1815, Mohrmann & Co GmbH, Buchholz, Netherlands). The crystallization and melting ranges of stearin is 42 °C–53 °C and 55 °C–66 °C, respectively. At room temperature, the density of stearin is 1.0016 g/cm^3 in solid state. The hydrogenated palm oil, which was obtained from Raps GmbH & Co. KG (Kulmbach, Germany), has a density of 1.0008 g/cm^3 at room temperature. The crystallization and melting ranges of hydrogenated palm oil is 37 °C–44 °C and 45 °C–58 °C. All differential scanning calorimetry measurements were performed using DSC 214 Polyma (Netzsch Holding, Germany) with heating and cooling rates of 10 K/min. The densities of the coating materials were determined using the AccuPyc 1330 helium pycnometer (Micromeritics GmbH, Germany) at a room temperature of 25 °C.

2.2. Experimental setup of the Wurster fluidized bed

A lab-scale fluidized bed WFP Mini (DMR Prozesstechnologie GmbH, Switzerland) was used for hot-melt coating experiments. The experimental setup is schematically shown in Fig. 1.

The hydrogenated palm oil or stearin was melted in a container. To avoid thermal degradation of the melts, the temperature was increased to a maximum temperature of 100 °C. The nozzle was fed using a micro-annular gear pump (mzr-4605 HNP Mikrosysteme GmbH, Germany) through a heated hose. A three-component nozzle of DMR with an orifice size of 1 mm was installed in a bottom-spray Wurster coating configuration. The nozzle was externally heated to prevent solidification of the melt prior to atomization. Moreover, externally heated compressed air was injected to prevent contact of the particles with the nozzle's center (flushing air) and supply the required energy for atomizing fine, melt droplets (atomization air).

2.3. Operating conditions

Herein, the hot-melt coating experiment consists of four steps [3]. First, the equipment must be warmed. For this purpose, the operating conditions listed in Table 1 were established and the air flow was started. In addition to the plant, the lipids were melted and heated to the coating temperature. As soon as the process conditions reached a steady state, the process was started and hot-melt coating was sprayed onto the particles. To ensure constant process conditions, all relevant process parameters, such as gas flow, differential pressure, particle bed temperature, and gas inlet and outlet temperatures, were monitored and controlled by the operators. Moreover, all values were recorded for further data processing. In the final step of the coating experiment, the plant and coated particles were cooled to approximately 25 °C to allow congealing of all melt droplets and avoid subsequent agglomeration of the particles. After the end of the experiment, all samples were weighed and packed in airtight bags. Thereafter, the samples were analyzed using an image-analysis device QICPIC/R (Sympatec GmbH, Germany) and μCT (type: CT-1600HR, Matrix Technologies, Germany). All analysis methods are described below. Owing to the complexity of the hot-melt coating process, all process parameters were selected based on the experience of the operators and findings of previous studies. To ensure the atomization of liquid droplets into the fluidized bed of stearin and hydrogenated palm oil, the coating materials were heated above their melting range, i.e., 90 °C. Conversely, the product temperature was retained below the

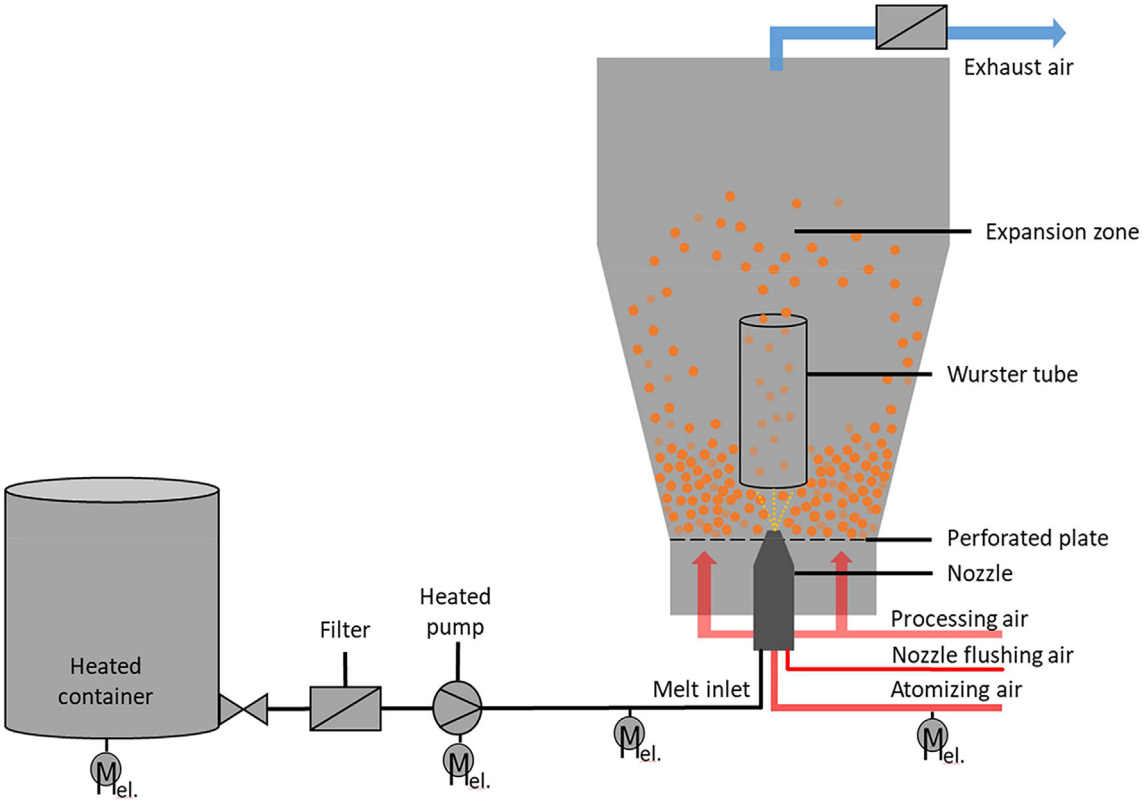

Fig. 1. Schematic of the experimental setup.

Table 1
Process conditions for the hot-melt coating experiments.

Parameter/setting	WFP mini
Coating technique	Wurster fluidized bed
Wurster tube air gab [mm]	20
Particle amount [g]	200
Coating amount [g]	4–20
Product temperature [°C]	29
Coating temperature [°C]	90
Gas volume flow rate [m^3/s]	19
Spray rate [g/min]	1
Nozzle atomizing pressure [bar]	1
Nozzle-flushing air pressure [bar]	1.5

crystallization range of the coating materials to ensure crystallization and layer formation., i.e., 29 °C for all experiments. A Wurster tube with a 20-mm gap was introduced between the perforated gas distribution plate and the Wurster tube. To determine the minimum coating amount for a complete coating, the coating amount was varied between 4 and 20 g. The spray rate was selected as 1 g/min because low spray rates facilitate a more uniform coating layer and less agglomeration [6]. Additionally, the nozzle settings, nozzle-flushing air pressure, and nozzle atomizing pressure were adjusted to ensure that no particles blocked the nozzle and sufficient atomizing of the liquid melts. Since the aim of this study is to present a new method for the analysis of hot-melt coating, all process parameters were retained constant, except for the coating amount and material. Table 1 provides an overview of the selected process conditions for all coating experiments.

2.4. Coating characterization

Four different approaches were used to analyze the coating layer. In the first approach, the coating layer was evaluated using a new 3D image-analysis method, which provides parameters, including the mean layer-thickness, layer-thickness uniformity, and non-covered surface proportion of a single particle. Next, 2D images were evaluated, and their results were compared with those of 3D image evaluation to estimate the suitability of the 2D method for non-uniform coating layers, such as hot-melt coating. Moreover, the 3D method was completed using particle-size measurements obtained by the image-analysis device QICPIC/R (Sympatec GmbH, Germany) and theoretical calculations, providing information about the mean layer-thickness of the batch and estimating overspray.

2.4.1. Micro-computed X-ray tomography

The μCT device is a custom-made μCT system (type: CT-1600HR, Matrix Technologies, Germany). The voltage was 60 kV, and the current was 60 μA at an exposure time of 2184 ms. Generally, for high image quality and accurate analysis, high resolution is preferred over a low resolution. However, the amount of data and measuring time significantly increase. For this reason, the samples were analyzed in preliminary tests at different resolutions. A resolution of 2 μm was determined to be suitable because fine differences in the layer thickness were also recorded compared with lower resolutions. A resolution of 1 μm was not considered reasonable as the possible sample size became excessively small with this high resolution. Due to better image quality, higher reproducibility of the measurements, and limitations due to sample size, a resolution of 2 μm was selected. However, the presented method can be easily adapted to higher or lower resolution. The chosen resolution of the μCT measurement corresponds to the accuracy of the measurement. To investigate the coating layer-thickness, a random sample of each coating run was fixed using superglue (UHU Sofortfest 2-K-Epoxidkleber; UHU GmbH & Co. KG; Germany) onto a sample holder between the detector and the X-ray source of the μCT. For the desired resolution, the measurement of a single particle required approximately 4 h.

2.4.1.1. Image processing and evaluation. A commercial tool (VG Studio Max 3.2.3, Volume Graphics GmbH, Germany) was used for the segmentation and smoothing of the coating layer. The resulting layer was binarized, exported, and processed using a custom MATLAB program (MathWorks, Inc., USA), MATLAB R2019b, Bresenham line-sampling algorithm [34], and marching-cubes rendering algorithm [35]. The steps from the original image (A), segmented coating layer (B), binarized coating layer (C), and measurement vectors (D) are shown in Fig. 2.

The procedure comprised the following steps: (1) importing the μCT data, (2) cutting the coating layer, (3) extracting the coating layer using the region-growing function, (4) smoothing the layer using the erosion/dilatation functions, (5) binarization of the extracted coating layer, (6) determination of the sphere's center, and (7) spherical pixelation.

Steps 1–4 were performed using the functions in VG Studio Max 3.2.3. Pratt et al. showed and described the theory behind the basic processing steps in Ref. [36]. A total of $N_{directions} = 2400$ ($N_{side} = 20$) equally distributed lines from the center were determined, as explained in Section 2.4.1.2. In each direction, the closest voxels along that direction were determined using the Bresenham line-sampling method [34]. The number of consecutive voxels of the coating was determined to be the coating layer-thickness. Hence, the accuracy was obviously limited by the resolution of the tomograph, which was 2 μm in this case. The thickness of the layer is provided as the cumulative probability distribution, as shown in Fig. 4. The mean layer-thickness was calculated by considering only the layer-thickness values of more than 0 μm.

2.4.1.2. Spherical pixelation. To evaluate coating uniformity, the coating thickness must be sampled on several points on the sphere. The representative sampling of points from a sphere is not trivial. One may just use random sampling points in a Monte Carlo manner. However, this will only lead to reasonable results if a large number of points are sampled. Here, we adopt a method that has been established in astronomy to determine the anisotropy of cosmic microwave background, which constructs a spherical pixelation using the so-called HEALPix algorithm [33]. The pixelation produces a subdivision of a spherical surface in which each pixel covers the same surface area as every other pixel. This method was originally developed to process astronomical spherical data, and it is suitable for creating equally distributed lines on a spherical particle. This method was used to create homogeneously distributed lines on a sphere, which were subsequently used to determine the coating thickness distribution after isolation. In this case, the resolution was based on 12 pixels in three rings around the poles and equator. The locations of the pixel centers are provided by the colatitude in radians, as measured from the North Pole, $\theta \in [0,\pi]$, and the longitude in radians, as measured eastward, $\Phi \in [0,2\pi]$, is provided using ($cos\theta$, Φ). The resolution in the HEALPix algorithm is set by a parameter, N_{side}, yielding a total of

$$N_{directions} = 6\,N_{side}^2 \tag{1}$$

directions. Hence, the pixel centers are located on the rings of the constant latitude. A complete description is provided in the original paper [33].

Fig. 3 shows the orthographic view of the HEALPix partition of the sphere. The octahedral symmetry of HEALPix is illustrated by the overplot of the equator and meridians. The dark-blue shade represents one of the identical equatorial base-resolution pixels. The light-blue shade denotes one of the eight (four north and four south) identical polar base-resolution pixels. The grid is hierarchically subdivided using the grid resolution parameter equivalent to $N_{side} = 4$ and a total number of pixels equivalent to $N_{pixel} = 192$. Within each panel, the areas of all pixels are identical [37].

2.4.1.3. 2D analysis. The 2D evaluation of the coating layer-thickness distribution was based on recent publications [11,17,38]. For comparison of the 2D and 3D methods, the same μCT data obtained from identical particles were used. An image of each particle's center was selected and automatically evaluated via a custom MATLAB code. Starting from the center of the particle, the layer-thickness was determined on discrete points, separated by 5° angles, resulting in 72 thickness values in each case. Only thickness values of more than 0 μm were considered for calculating the mean coating layer-thickness and standard deviation.

2.4.2. Theoretical layer-thickness estimation

The theoretical coating layer-thickness was predicted using a theoretical calculation analogous to that of Markl et al. [19]. To simplify the theoretical calculations of the layer-thickness, only the mean particle diameter, $d_{50,0}$, of the Cellets® 1000 was considered, i.e., 1197 μm. Due to overspray of the liquid melts, the full coating amount is never applied to particles in an actual process. Therefore, the loss due to overspray must be considered and was assumed to be constant among all batches. The overspray rate was estimated from the mass balances of several stearin-coating experiments and was set to 8% (*w*/w). This loss was accounted for by fraction *q*. The total coating material was assumed to be equally distributed upon the spheres. The layer-thickness estimation also assumed that the layer was perfectly uniform without pore structures or inclusions. Moreover, Eq. 2 shows the time-dependent coating thickness, $d_c(t)$:

$$d_c(t) = \frac{d_{50,0}}{2}\left(\left(q\frac{\dot{m}_{coating}\,t}{m_{p,0}^{bed}}\frac{\rho_{core}}{\rho_{coating}} + 1\right)^{\frac{1}{3}} - 1\right). \tag{2}$$

The mass of the initial particle bed, $m_{p,0}^{bed}$, and the mass flow of the hot melt, $\dot{m}_{coating}$, must be considered in the calculation. For the coating density, $\rho_{coating}$, the room temperature value was used.

2.4.3. QICPIC/R

The particle size measurements were performed using a high-speed image-analysis device QICPIC/R (Sympatec GmbH, Germany) with a Rodos dispersing system, Vibri dosing unit, and M8 lens with a

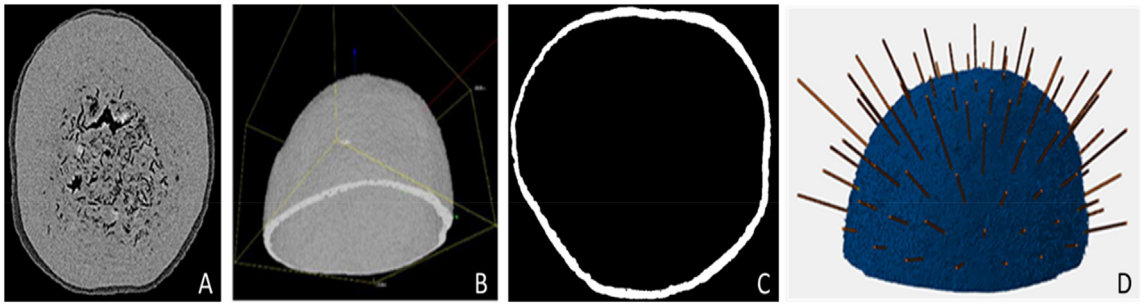

Fig. 2. Different steps in the measurement of the particle–shell thickness.

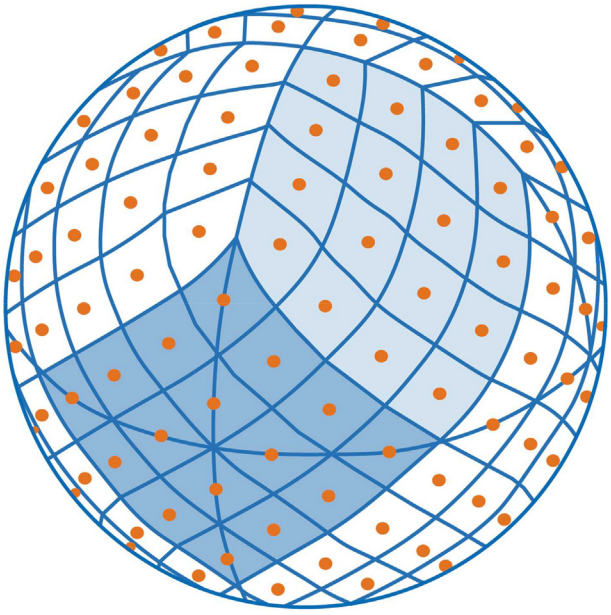

Fig. 3. Othographic view of the HEALPix partition of the sphere.

resolution of 20–6280 μm. A frame rate of 150 Hz over 40 s was used to measure a 100-g sample. The coating layer-thickness was calculated based on the particle-size distribution of uncoated and coated particles. The layer-thickness can be calculated by subtracting the two measured diameters, $d_{50,0}$, and dividing the difference by a factor of 2. The resulting coating layer is the mean layer-thickness of the batch. To determine the coating layer-thickness using the particle size measurements three assumptions were made: all particles of one size of glass grow at the same rate; all particles can be found in the same larger size class after the coating process; and all particles are spheres.

3. Results and discussion

This study presents a new analytical method that offers the possibility of analyzing and evaluating a 3D image of a coated particle. First, the information content of a single but fully 3D-analyzed hot-melt-coated particle is shown, followed by the first-process parameter and coating material variation. Then, a comparison of the proposed method with other common methods is provided. The main advantage of the proposed method is the high amount of information obtained about the coating layer. A disadvantage is the high time consumption owing to measurement and post processing. In recent studies, only 2D images of the coated particles have been evaluated [11,38].

3.1. Coating layer analysis using micro-computed tomography

A challenge of the μCT measurement was the density difference, resulting in low contrast between the coating and core particle. X-ray absorption depends on the nuclear mass and packing density. The best results are achieved for coatings that show a significantly higher absorption than the core material. In the case of diminishing contrast between the two regions, tomographic analysis is impossible. Fig. 4 presents a portion of the μCT image. In the figure, varying thicknesses of the coating and delamination are clearly visible.

The image of a wax-coated particle in Fig. 4 clearly shows that μCT measurements allow the investigation of the probability of delamination between the core particle and coating material. In addition to delamination, small pores and fractions of the coating layer area visible. The pore structures and delamination can be attributed to several variables, such as spreading mechanism, temperature fluctuations, viscosity, or drop size. Thus, μCT can be a useful tool to assess the quality of the final product and facilitate the selection of an appropriate combination of core particles and coating material.

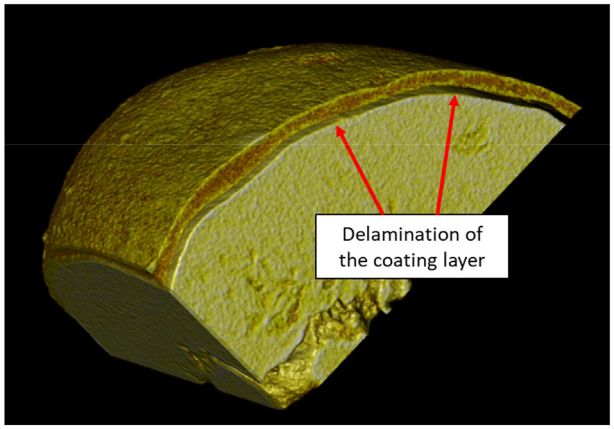

Fig. 4. Portion of a micro-computed-tomography image of a wax-coated particle showing varying coating thicknesses and delamination of the coating.

In addition to the obvious quality, the 3D method shows the respective layer-thicknesses of all measuring points. Based on these data, the thickness distribution, cumulative curve, and non-covered surface proportion were calculated. Fig. 5 (left) shows the relative frequency of three different particles from the same batch processed using 5% (*w*/w) stearin at a spraying rate of 1 g/min. Fig. 5 (right) shows the cumulative curves of the particles.

As shown in Fig. 5, the three analyzed particles from the same batch were coated in the same manner. The mean layer-thickness of each particle was calculated using 2400 individual measuring points and were as follows: particle I: 15.5 μm, particle II: 12.4 μm, and particle III: 15.6 μm. The method is limited to the selected resolution of 2 μm. Furthermore, this method is limited to analyzing batch uniformity many measurements would be required to provide a high statistical significance, which would be disproportionate to the measurement effort. Variations in the coating thickness of the batch and single particles are expected to have a significant impact on product performance and are important when using time-dependent modified-release coating. The coating layer-thickness uniformity for a single particle is more critical because it is relevant for coating functionality [19]. For this reason, the focus of this study was on the coating uniformity of single particles.

3.1.1. Qualitative comparison of coating uniformity

Using the geometric positions of the individual measuring points, visualizing the layer-thickness distribution in the form of a heat map is possible. Fig. 6 shows two heat maps representing the relative coating layer uniformity of two layer hemispheres with different coating amounts. Fig. 6 (left) shows the relative uniformity of a 2% stearin-coated particle, and Fig. 6 (right) shows the relative coating layer of a 10% stearin-coated particle.

As shown in Fig. 6 (right), most of the coating layer of a 10%-coated particle is in a similar layer-thickness range and only a few areas are uncoated, whereas the over-coated proportion is considerably larger. The 2% stearin-coated particle in Fig. 6 (left) is different in comparison. The 2% coating was insufficient for complete coating because most of the surface was still non-covered or patchily coated. The relative uniformity of the coating increased with the coating amount. The heat map shows differently coated parts of the particle and allows us to draw conclusions on the spreading process. Therefore, the visualization of the coating layer-thickness in the form of a heat map can help us to better understand the spreading process and layer formation. Moreover, it is suitable for a simple qualitative comparison of the relative uniformity of different particles.

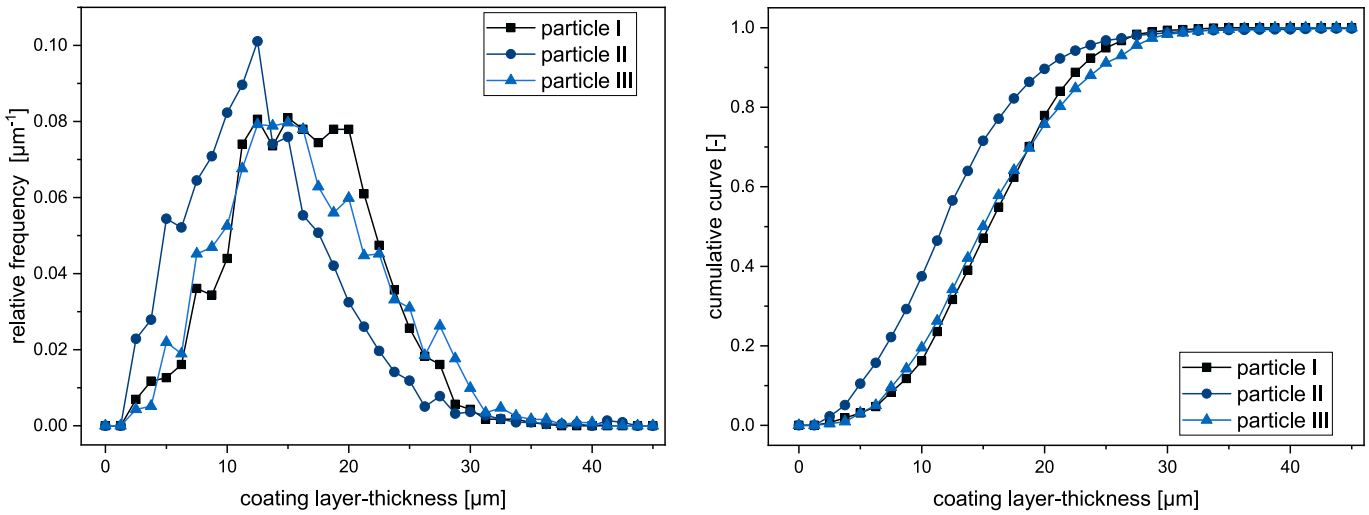

Fig. 5. Left: Relative frequency of the coating layer-thickness of three particle shells; right: cumulative curves of the layer-thickness distributions.

3.1.2. Determination of the minimum coating amount

Obviously, depending on the coating amount, the layer-thickness increases and the uncoated-surface proportion decreases. To quantify the coating uniformity, the coefficient of variation can be used, which is a relative measure of scatter. The coefficient of variation is the ratio of the empirical standard deviation and arithmetic mean. Fig. 7 (left) shows the increase in the coating layer-thickness with the coating amount, as determined by a representative and independent sample of the respected batch. Fig. 7 (right) shows the influence of the coating amount on the mean layer-thickness of the non-covered-surface proportion and variation coefficient.

Different amounts were used at a constant feed rate of 1 g/min. Hence, the mean layer-thickness increases linearly, while the norm of the distribution of this thickness decreases for coating that covers most of the particle's surface. Thus, the coating layer becomes more even with an increase in the coating amount, although in absolute terms, the distribution becomes wider. As shown in Fig. 7 (right), the non-covered-surface proportion rapidly decreased with increasing coating amounts for the first 5%, followed by a small decrease. Obviously, the 2% coating was insufficient to completely coat the surface of the particle in this case. Approximately 50% of the surface could be covered using a 2% stearin coating amount. To achieve complete coating, a coating amount of at least 10% is required, although the non-covered surface proportion for a 5% coating amount with the non-covered surface proportion of approximately 2.3% is already low. Furthermore, the possibility of determining the non-covered surface proportion offers a decisive advantage over other methods, particularly with respect to analyzing the functional coating.

3.1.3. Coating behavior of different coating materials

In addition to examining the influences of various process parameters on the thickness distribution, different coating materials were analyzed and compared. Fig. 8 shows a comparison of the stearin and hydrogenated palm oil coatings.

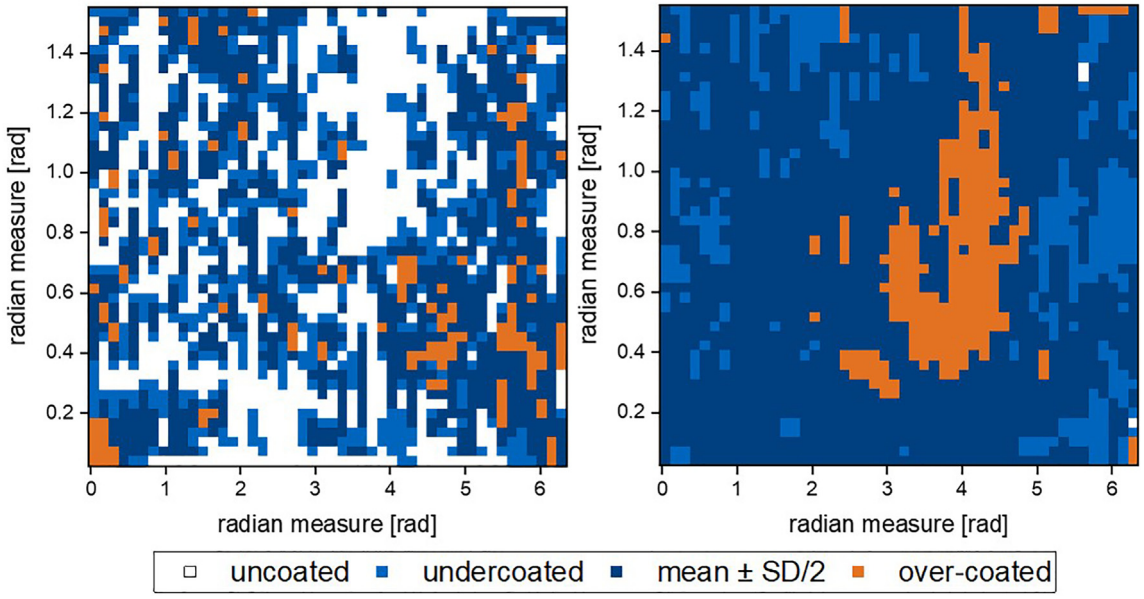

Fig. 6. left: Relative coating uniformity of a 2% stearin-coated particle; right: relative coating uniformity of a 10% stearin-coated particle. The layer-thickness distribution is divided into four classes. The layer-thickness is considered to be uniformly coated if the thickness value is within the range of $[\bar{x} \pm \frac{1}{2}\sigma]$ (dark blue). If the layer-thickness is above this range, the area is considered to be over-coated (orange). If the thickness is smaller than $[x<\bar{x}-\frac{1}{2}\sigma]$, the spot is considered to be undercoated (blue) or uncoated (white) if the thickness is 0 µm.

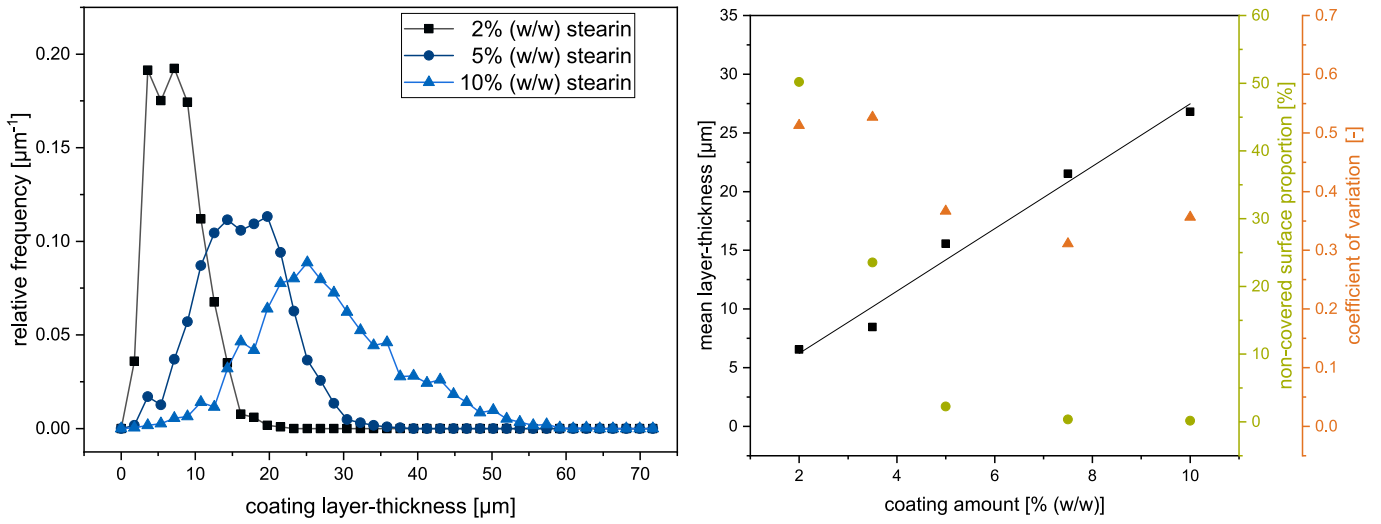

Fig. 7. Left: Increase in the coating layer-thickness with the coating amount; right: influence of the stearin-coating amount on the non-covered surface proportion and variation coefficient.

Fig. 8 shows the mean layer-thickness and non-covered-surface proportion for palm fat and stearin. In these tests, the process showed better results for stearin than palm fat. Fig. 8 shows the differences between palm fat and stearin in terms of mean layer-thickness and non-covered surface proportion, particularly at high coating amounts. The mean layer-thickness and covered surface proportion were lower for palm fat coating than stearin coating. One reason for the difference between the achieved coating qualities can be attributed to the difference in the properties governing the melting and crystallization behaviors, viscosities, or spreading behavior of the two materials. The palm fat coating crystallized before touching the particles and thus could not adhere. This also explains the increased dust formation observed after the coating experiments. Hence, the overspray amount for palm fat is expected to be higher than that for stearin. Based on the selected process temperature of 29 °C and measured crystallization range of the coating materials, palm fat was expected to show better process performance though due to its lower crystallization temperature. A reason for better processability of stearin can be attributed to the wider crystallization range, which may have provided more time for the distribution of stearin melt on the particle surface. Nevertheless, using the selected process parameter settings, uniform coating can be achieved for stearin and hydrogenated palm oil. For both coating materials, no agglomeration was observed after the coating process, which indicates insufficient fluidization or excessively high process temperature. In addition, no indications of temporary agglomeration were detected because the 3D µCT coating layer analysis did not reveal any break lines on the coating layers, which would have led to a poorer coating uniformity. A different parameter setting for palm fat based on a higher spraying or process temperature might significantly improve the process.

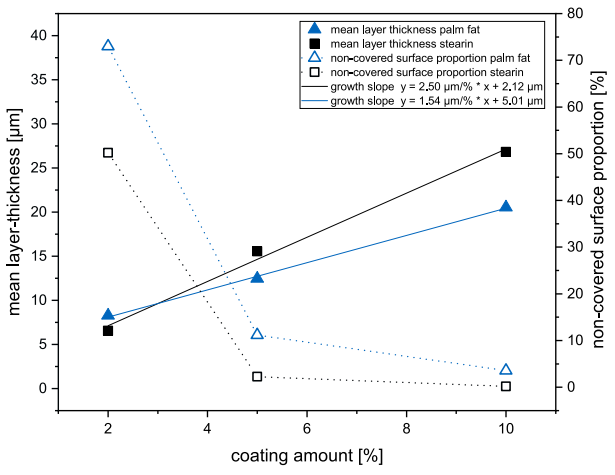

Fig. 8. Difference between palm fat and stearin in terms of mean layer-thickness and non-covered surface proportion.

3.2. Complementary methods

3.2.1. QICPIC/R

Complementary to the 3D µCT method, particles were measured using the image-analysis device QICPIC/R to determine their diameters before and after coating. The layer-thickness was determined based on the difference in the diameter between the uncoated and coated particles. The uncoated particle diameter, $d_{50,0}$, is 1196.7 µm. The coated particle sizes are 1207.6 (2% w/w), 1222.2 (5% w/w), and 1239.5 µm (10% w/w) on average. A comparison of the thicknesses of the coating layer determined using µCT with those obtained from the optical measurements showed good agreement (Fig. 10). Fig. 10 supports the µCT results. The layer-thickness from QICPIC/R represents the mean layer-thickness of approximately 10,000 particles and is a representative of the overall batch. However, the µCT obviously provides considerably additional information on single particles, allowing the computation of the mean layer-thickness and distribution of the coating material. However, the QICPIC/R measurements provide a considerably higher statistical significance than 3D analysis. Overall, QICPIC/R and µCT provide complementary information rather than one being superior to the other, and they provided consistent information regarding the mean values.

3.2.2. 2D Analysis

To demonstrate the relevance of the full 3D analysis, identical particles were additionally evaluated in 2D. Fig. 9 compares the 2D and 3D image analyses of the same three particles with different coating amounts. The boxes of the respective µCT data represent the standard deviation of the determined layer-thickness distribution of the respective spheres.

The 2D method also shows similar thickness values as the 3D image evaluation data. Fig. 9 shows a difference in the 2D image data, particularly observed in inhomogeneous coatings such as hot-melt coating. Due to the high information content, the 3D method is particularly advantageous in these cases; this is particularly evident in the case of the particle with a 10% coating amount. Specifically for hot-melt coating,

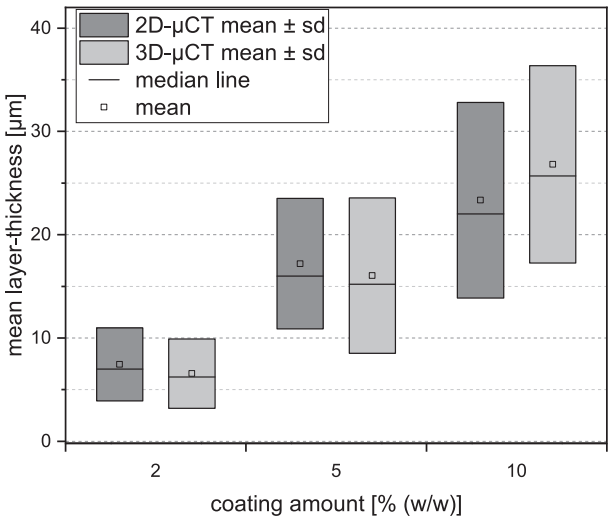

Fig. 9. Comparison of 2D and 3D image analyses.

the results from the 2D evaluation can be prone to errors because the coating layers are rarely uniform. Nevertheless, the data from the 2D method for the same single sphere are suitable for homogenous coatings because the measurement, reconstruction, and image evaluation times are significantly shorter, particularly when investigating batch homogeneity [11,17,21,38].

3.2.3. Theoretical coating layer-thickness estimation

The theoretical coating layer-thickness was calculated using Eq. 2. The layer-thickness estimation allows the prediction of layer-thickness for different coating amounts. Fig. 10 shows an overview of the mean layer-thicknesses measured using different methods for the stearin coating.

The theoretical thickness estimation with an overspray rate of 8% (*w*/w) shows good agreement with other methods for all coating amounts. Differences result from the fact that the theoretical thickness estimation assumes a perfect uniform layer for the mean particle size of the batch. The experiments showed a non-uniform layer with different thicknesses, pore structures, and inclusions for hot-melt coatings. Nevertheless, the theoretical thickness estimation for different coating amounts agrees well with the experiments. Similar results for different layer-thicknesses from the µCT measurements of individual particles, optical measurements, and theoretical layer-thickness estimation

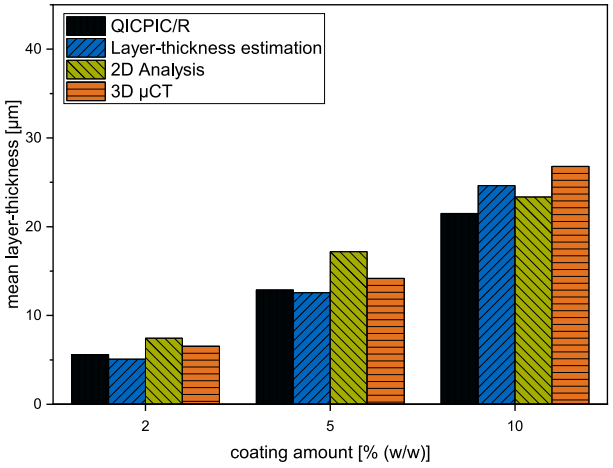

Fig. 10. Overview of the mean layer-thicknesses measured using different methods.

using the mass balance allowed different conclusions to be drawn. First, it showed that the sampling of the particles analyzed in the µCT was representative; second, it showed that the batch uniformity of the single experiments was balanced. Therefore, in case of similar results, the required effort for µCT measurements can be reduced when they are complemented by other methods that further consider the batch uniformity.

4. Conclusion

This study provides a new method for analyzing the quality of hot-melt coated particles using µCT-based 3D image analysis. The proposed method was compared with other established techniques. Generally, the information regarding mean layer-thickness was consistent for all different methods. This finding shows the general suitability of the µCT-based 3D evaluation process. In addition to this consistency test, the proposed method provides a considerably more detailed extraction, particularly regarding coating uniformity. Thus, the proposed method provides additional information regarding the coating quality compared with other common methods, such as particle-size measurements, optical coherence tomography, or 2D analysis of an X-ray image. The proposed method can identify and quantify new factors affecting the layer-thickness distribution and uniformity. The relative uniformity of the coating increases with the coating amount. The coating behaviors of different materials can be identified and compared. For instance, in our experiments, complete and uniform coating was achieved using 10% (*w*/w) stearin.

Declaration of Competing Interest

The authors declare that they have no known competing financial interests or personal relationships that could have appeared to influence the work reported in this paper.

Acknowledgements

This research was supported by the Ministry of Economics and Energy (BMWi) via AiF and the FEI (Forschungskreis der Ernährungsindustrie e. V., Bonn). Project AiF 19970 N. This study made use of equipment that was funded by the Deutsche Forschungsgemeinschaft (DFG, German Research Foundation)–198187031.

References

[1] H. Arnon-Rips, E. Poverenov, Improving food products' quality and storability by using layer by layer edible coatings, Trends Food Sci. Technol. 75 (2018) 81–92.
[2] L.S. Jackson, K. Lee, Microencapsulation and the food industry, Lebensm.-Wiss. u.-Technol. (1991) 289–297.
[3] S. Bose, R.H. Bogner, Solventless pharmaceutical coating processes: a review, Pharm. Dev. Technol. 12 (2007) 115–131.
[4] V. Jannin, Y. Cuppok, Hot-melt coating with lipid excipients, Int. J. Pharm. 457 (2013) 480–487.
[5] A. van Kampen, B. Hitzmann, R. Kohlus, Assessment of coating quality by use of dissolution kinetics, Powder Technol. 286 (2015) 325–331.
[6] M.J. Jozwiakowski, D.M. Jones, R.M. Franz, Characterization of a hot-melt fluid bed coating process for fine granules, Pharm. Res. 7 (1990) 1119–1126.
[7] M.G. Müller, J.A. Lindner, H. Briesen, K. Sommer, P. Foerst, On the properties and application of beeswax, carnauba wax and palm fat mixtures for hot melt coating in fluidized beds, Adv. Powder Technol. 29 (2018) 781–788.
[8] D.M. Jones, P.J. Percel, Coating of multiparticulates using molten materials, Multiparticulate Oral Drug Delivery 1994, pp. 113–142.
[9] A. Milanovic, I. Aleksic, S. Ibric, J. Parojcic, S. Cvijic, Hot-melt coating with Precirol ATO 5 in a fluidized-bed apparatus: application of experimental design in the optimization of process parameters, Journal of Drug Delivery Science and Technology 46 (2018) 274–284.
[10] B. Guignon, A. Duquenoy, E.D. Dumoulin, Fluid bed encapsulation of particles: principles and practiCE, Dry. Technol. 20 (2002) 419–447.
[11] P. Bachmann, K. Chen, A. Bück, E. Tsotsas, Prediction of particle size and layer-thickness distributions in a continuous horizontal fluidized-bed coating process, Particuology 50 (2019) 1–12.

[12] G. Heinicke, J.B. Schwartz, Particle size distributions of inert spheres and pelletized pharmaceutical products by image analysis, Pharm. Dev. Technol. 9 (2004) 359–367.
[13] M. Mozina, D. Tomazevic, S. Leben, F. Pernus, B. Likar, Digital imaging as a process analytical technology tool for fluid-bed pellet coating process, Eur. J. Pharm. Sci. 41 (2010) 156–162.
[14] C.C. Larsen, J.M. Sonnergaard, P. Bertelsen, P. Holm, Validation of an image analysis method for estimating coating thickness on pellets, Eur. J. Pharm. Sci. 18 (2003) 191–196.
[15] A. Bogomolov, M. Engler, M. Melichar, A. Wigmore, In-line analysis of a fluid bed pellet coating process using a combination of near infrared and Raman spectroscopy, J. Chemometrics 24 (2010) 544–557.
[16] F.L. Laksmana, L.J. van Vliet, P.J.A. Hartman Kok, H. Vromans, H.W. Frijlink, K. van der Voort Maarschalk, Quantitative image analysis for evaluating the coating thickness and pore distribution in coated small particles, Pharm. Res. 26 (2009) 965–976.
[17] F. Sondej, A. Bück, E. Tsotsas, Comparative analysis of the coating thickness on single particles using X-ray micro-computed tomography and confocal laser-scanning microscopy, Powder Technol. 287 (2016) 330–340.
[18] D. Markl, G. Hannesschläger, S. Sacher, M. Leitner, J.G. Khinast, Optical coherence tomography as a novel tool for in-line monitoring of a pharmaceutical film-coating process, Eur. J. Pharm. Sci. 55 (2014) 58–67.
[19] D. Markl, M. Zettl, G. Hannesschläger, S. Sacher, M. Leitner, A. Buchsbaum, J.G. Khinast, Calibration-free in-line monitoring of pellet coating processes via optical coherence tomography, Chem. Eng. Sci. 125 (2015) 200–208.
[20] J.M.A. Mauritz, R.S. Morrisby, R.S. Hutton, C.H. Legge, C.F. Kaminski, Imaging pharmaceutical tablets with optical coherence tomography, J. Pharm. Sci. 99 (2010) 385–391.
[21] F. Sondej, A. Bück, K. Koslowsky, P. Bachmann, M. Jacob, E. Tsotsas, Investigation of coating layer morphology by micro-computed X-ray tomography, Powder Technol. 273 (2015) 165–175.
[22] L. Schoeman, P. Williams, A. Du Plessis, M. Manley, X-ray micro-computed tomography (μCT) for non-destructive characterisation of food microstructure, Trends Food Sci. Technol. 47 (2016) 10–24.
[23] M. Wang, N. Zheng, T. Zhu, J. Shang, T. Yu, X. Song, D. Zhao, Y. Guan, Y. Tian, Using X-ray computed tomography and micro-Raman spectrometry to measure individual particle surface area, volume, and morphology towards investigating atmospheric heterogeneous reactions, J. Environ. Sci. 69 (2018) 23–32.
[24] S. Schmideder, L. Barthel, T. Friedrich, M. Thalhammer, T. Kovačević, L. Niessen, V. Meyer, H. Briesen, An X-ray microtomography-based method for detailed analysis of the three-dimensional morphology of fungal pellets, Biotechnol. Bioeng. 116 (2019) 1355–1365.
[25] T. Kovačević, J. Schock, F. Pfeiffer, H. Briesen, Shape identification of primary particles in potash alum aggregates using three-dimensional tomography data, Cryst. Growth Des. 16 (2016) 2685–2699.
[26] T. Afshar, M.M. Disfani, G.A. Narsilio, A. Arulrajah, Post-breakage changes in particle properties using synchrotron tomography, Powder Technol. 325 (2018) 530–544.
[27] M. Schmitt Rahner, M. Halisch, C. Peres Fernandes, A. Weller, Viviane Sampaio Santiago dos Santos, Fractal dimensions of pore spaces in unconventional reservoir rocks using X-ray nano- and micro-computed tomography, Journal of Natural Gas Science and Engineering 55 (2018) 298–311.
[28] D. Kalasová, K. Dvořák, M. Slobodník, D. Všianský, T. Zikmund, J. Dluhoš, R. Váňa, J. Bureš, J. Kaiser, Characterization of inner structure of limestone by X-ray computed sub-micron tomography, Constr. Build. Mater. 174 (2018) 693–700.
[29] P. Foerst, T. Melo de Carvalho, M. Lechner, T. Kovacevic, S. Kim, C. Kirse, H. Briesen, Estimation of mass transfer rate and primary drying times during freeze-drying of frozen maltodextrin solutions based on x-ray μ-computed tomography measurements of pore size distributions, J. Food Eng. 260 (2019) 50–57.
[30] G. Perfetti, E. van de Casteele, B. Rieger, W.J. Wildeboer, G.M.H. Meesters, X-ray micro tomography and image analysis as complementary methods for morphological characterization and coating thickness measurement of coated particles, Adv. Powder Technol. 21 (2010) 663–675.
[31] A.M. Parfitt, M.K. Drezner, F.H. Glorieux, J.A. Kanis, H. Malluche, P.J. Meunier, S.M. Ott, R.R. Recker, Bone histomorphometry: standardization of nomenclature, symbols, and units. Report of the ASBMR Histomorphometry nomenclature committee, Journal of bone and mineral research : the official journal of the American Society for Bone and Mineral Research 2 (1987) 595–610.
[32] T. Hildebrand, P. Rüegsegger, A new method for the model-independent assessment of thickness in three-dimensional images, J. Microsc. 185 (1997) 67–75.
[33] K.M. Gorski, E. Hivon, A.J. Banday, B.D. Wandelt, F.K. Hansen, M. Reinecke, M. Bartelmann, HEALPix: a framework for high-resolution discretization and fast analysis of data distributed on the sphere, Astrophys. J. 622 (2005) 759–771.
[34] J. Shen, 3D Bresenham's line generation, MATLAB Central File Exchange, 2020.
[35] P. Hammer, Marching Cubes, https://www.mathworks.com/matlabcentral/fileexchange/32506-marching-cubes 2020.
[36] W.K. Pratt, Digital image processing, Wiley Interscience, New York, 2001.
[37] K.M. Gorski, B.D. Wandelt, E. Hivon, F.K. Hansen, A.J. Banday, The HEALPix Primer, https://healpix.sourceforge.io/pdf/intro.pdf 2019.
[38] S. Pietsch, A. Peter, P. Wahl, J. Khinast, S. Heinrich, Measurement of granule layer thickness in a spouted bed coating process via optical coherence tomography, Powder Technol. 356 (2019) 139–147.

5.2 Paper II: Delamination and wetting behavior of natural hot-melt coating materials (Woerthmann et al., 2022)

Summary

Previous studies demonstrated that delamination of the coating layer is frequently observed in hot-melt coating products (Mueller et al. 2018; Woerthmann et al. 2021). In general, however, there is little literature on the delamination of coating materials, even though it is an already-known phenomenon in coating applications. However, the fundamentals and factors that influence this phenomenon remain unclear and need to be thoroughly researched and elucidated. Delamination is hypothesized to be due to the poor wetting behavior of the coating material on the particles. A correlation between delamination and the wetting properties of the coating materials seems likely. Therefore, this study aimed to investigate and better understand natural coating materials' delamination and wetting behavior for hot-melt coating applications. Since it is further suggested that poorer wetting also leads to more non-uniform coating layer thickness distributions, thereby also affecting the effectiveness of the coating, a detailed understanding of delamination and wetting behavior is required. Therefore, this study investigated the delamination frequency in the first step by coating experiments using a Wurster fluidized bed at a laboratory scale and by micro-computed tomography measurements using different material combinations. In the second step, material properties such as wetting behavior were investigated using a drop shape analyzer. It is shown that the delamination frequency of different material combinations differs significantly, while all investigated coating materials exhibit excellent wetting properties. A correlation between delamination and wetting behavior was, however, not found.

Author contributions

M. Woerthmann came up with the idea for this work and developed the experimental and image analysis method, conducted experiments, and evaluated and interpreted all experiments. L. Totzauer conducted experiments. M. Woerthmann supervised the work of L. Totzauer. H. Briesen supervised all work, interpreted data, and worked on conceptualization. M. Woerthmann wrote the original draft. H. Briesen corrected and proofread the article.

Copyright

Powder Technology 404 (2022) 117443

Contents lists available at ScienceDirect

Powder Technology

journal homepage: www.elsevier.com/locate/powtec

Delamination and wetting behavior of natural hot-melt coating materials

B.M. Woerthmann, L. Totzauer, H. Briesen *

Chair of Process Systems Engineering, TUM School of Life Sciences Weihenstephan, Technical University of Munich, Germany

ARTICLE INFO

Article history:
Received 11 March 2022
Received in revised form 20 April 2022
Accepted 22 April 2022
Available online 27 April 2022

Keywords:
Hot-melt coating
Wetting behavior
Delamination behavior
Wurster fluidized bed
Micro-computed tomography

ABSTRACT

In order to achieve a defined product behavior, the coating of particulate solids is an often used process in the food, chemical, and pharmaceutical industries. The wetting behavior affects the coating quality associated with hot-melt coating (HMC) considerably more than the quality associated with solvent-based coating. Thus, the uniformity and the effectiveness of the coating can be severely affected by process parameters. Furthermore, previous studies showed that delamination of the coating layer occurs frequently in HMC products [Mueller et al. 2018 (https://doi.org/10.1016/j.apt.2017.12.020); Woerthmann et al. 2021 (https://doi.org/10.1016/j.powtec.2020.09.065)]. Therefore, the successful use of natural coating materials requires a detailed understanding of the delamination and wetting behavior. The delamination observed for HMC-particles has, however, rarely been investigated, and the basis for and factors affecting this process remain unclear. However, a correlation between delamination and the wetting properties of the materials seems likely, since wetting properties provide information about the interaction between the coating and carrier material. In this work, the delamination frequency was investigated via laboratory coating experiments and via micro-computed tomographic measurements with different material combinations. In addition, the wetting behavior was investigated using a drop shape analyzer. No correlation between delamination and wetting behavior was found. All investigated coating agents exhibited excellent wetting properties with contact angles in a range of 10° to 18°, while palm fat coatings were more prone to delamination (>65%) than the rice bran (<10%) and carnauba wax coatings (<17%).

1. Introduction

The coating of particulate solids is often used in the food and pharmaceutical industries in order to create functional products with a defined product behavior [3,4]. Applying a coating layer to a product allows surface-property modification of the product and the realization of desired properties. These modifications may include changes in the appearance of the product, odor and taste masking, improvement of flow behavior as well as targeted and controlled release or protection against environmental factors (e.g., light, oxygen or moisture). In general, coating methods are classified as dry, wet, hot-melt coating (HMC), and encapsulation processes [5]. In recent years, HMC technology has become more important than other coating processes such as solvent-based coating. This results from the fact that the melts solidify during the process and energy-intensive drying steps are unnecessary. Through HMC, these cost-intensive drying steps and the use of solvents can be avoided. Furthermore, HMC with natural coating agents allows an environmentally friendly process. Waxes (e.g., carnauba wax), hydrogenated vegetable oils (e.g., hydrogenated palm oil), or animal fats (e.g., cow ghee) provide good barrier properties against moisture [6,7] and are therefore commonly used natural lipid excipients for HMC. However, previous studies have shown that, for melt-based coatings, the generation of a uniform and homogeneous coating is considerably more difficult than for solvent-based coatings. This difficulty stems from multiple dependencies on material properties (e.g., crystallization behavior, viscosity, chemical composition or wettability) [1–3,5,6,8].

Lopes et al. [8], Windbergs et al. [9], and Chansanroj et al. [10] reported that the chemical composition and the polymorphic properties of coating materials play a crucial role in process design. For example, triglycerides are prone to lipid blooming after the use of high cooling rates. Rapid cooling during the HMC process favors the formation of unstable hexagonal α-crystals. During storage, these α-crystals tend to recrystallize to more stable β or β'-crystal forms with triclinic-parallel packing, leading to structural changes in the coating layer [8–14].

Chansanroj et al. [10], Windbergs et al. [15], and Lopes et al. [8] showed that lipid blooming influences storage stability and the layer structure, as confirmed by an altered protective effect and release kinetics. According to Lopes et al. [11] and Becker et al. [16], the structural change induced by lipid blooming and recrystallization can be influenced by increasing the process temperatures, tempering after the coating process, or including additives in the coating agent.

* Corresponding author at: Chair of Process Systems Engineering, Gregor-Mendel-Str. 4, 85354 Freising, Germany.
E-mail address: heiko.briesen@tum.de (H. Briesen).

https://doi.org/10.1016/j.powtec.2022.117443
0032-5910/

Regarding (especially) the HMC process, Saleh and Guigon [5] reported that wetting of the coating material is the most important physico-chemical property to be considered. Wetting refers to the ability of a liquid to spread on a surface. Among other things, wetting depends on the state variables (temperature, pressure, and the chemical phase composition) of the materials. Surface tension measurements and contact angle measurements of the coating and carrier material are required for a complete description of the wetting behavior [17]. This description will include wetting parameters such as the surface free energy, polar and disperse fractions, and interfacial tension or work of adhesion (WoA). A high adhesion force between the phases is desirable for high coating quality [5,18]. Wetting parameters govern the particle coating mechanisms and are thus crucial for the layer formation and morphology of a coating [5]. For example, a fundamental requirement for good wetting is that the surface tension of the coating material must be lower than the surface energy of the solid. Incomplete wetting generates interfacial defects, thereby reducing the adhesive bond strength [19]. The adhesion force, which indicates the strength of the tendency for the coating and substrate to remain in contact, is considered an essential parameter in the assessment of coatings. This force can be assessed via the work of adhesion (WoA), which indicates how strongly the layer and the carrier particle are bonded, or how easily a layer detaches from a surface [17,19,20].

Müller et al. [1] and Woerthmann et al. [2] observed the delamination of coating layers on HMC using micro-computed tomography measurements (μCT). Delamination is defined as the debonding of a coating layer from a carrier particle. The delamination of coating layers from HMC products has rarely been studied. Quantification of this process is difficult and hence the extent of delamination in HMC products remains unknown. Delamination is not visible from the exterior of the product and is therefore hard to detect. However, μCT measurements allow three-dimensional imaging and non-destructive structural analyses of regions delaminated from coated particles. Structural integrity is essential for generating and maintaining the functional properties of HMC products. Nevertheless, a fundamental knowledge that can be applied to the process for minimizing delamination and structural changes of the coating remains elusive. Consequently, the expectation is that delamination of the coating layer will have a major impact on the functionality (e.g., protective effect or release behavior) and durability of a product.

The aim of the present study is to elucidate the occurrence of coating delamination from HMC products and evaluate the wetting behavior of common coating and carrier materials. Poor wetting results in weak bonding between the wetting phase and the phase to be wetted. The WoA indicates how well two phases come into contact, and can therefore be used to predict the delamination probability of the coating layer on HMC products. For this reason, as a first step, the occurrence of delamination will be systematically analyzed via laboratory tests in a fluidized bed using μCT measurements. The hypothesis is that subsequent wetting analyses of the coating and carrier materials will reveal a correlation between delamination behavior and wetting behavior.

2. Materials and methods

2.1. Materials

Materials from the pharmaceutical and food processing industries were used as carriers with particle sizes ranging from 1000 μm to 2000 μm. The selection of the core materials was based on their suitability as a carrier material for the coating and their compressibility as pure materials. In this work, the wettability and fluidized bed coating of citric acid ($\rho_{25°C} = 1654$ kg/m^3) (Jungbunzlauer GmbH, Austria), glucon-δ-lactone ($\rho_{25°C} = 1622$ kg/m^3) (Jungbunzlauer GmbH, Austria), sucrose ($\rho_{25°C} = 1587$ kg/m^3) (Südzucker AG, Germany), microcrystalline-cellulose particles Cellets® 1000 ($\rho_{25°C} = 1528$ kg/m^3) (HARKE Pharma GmbH, Germany), and sugar spheres ($\rho_{25°C} = 1541$ kg/m^3) (Pharm-a-Spheres GmbH, Germany) were investigated.

For the wettability analysis, polydimethyl-siloxane gel (PDMS) traded as SYLGARD™ 184 Silicone Elastomer (The Dow Chemical Company, USA) served as the nonpolar carrier material. Diiodomethane (Sigma-Aldrich Corp., USA) and ethylene glycol (AppliChem GmbH, Germany) were used as the nonpolar liquid and bipolar reference liquid, respectively.

Besides the core particles, only biologically benign natural coating materials (such as hydrogenated palm oil, carnauba wax, and rice bran wax) were selected for the study. All three coating materials were provided by Kahl GmbH & Co. KG (Germany). Table 1 lists the physical and chemical properties of the selected coating materials.

2.2. Methods

2.2.1. Experimental setup of the Wurster fluidized bed

The hot-melt coating (HMC) experiments were performed in a lab-scale fluidized bed WFP Mini (DMR Prozesstechnologie GmbH, Switzerland). A three-component nozzle of DMR with an orifice size of 1 mm was installed in a bottom-spray Wurster coating configuration. To prevent solidification of the melt prior to atomization, the nozzle was additionally heated. Externally heated compressed air was injected to prevent contact of the particles with the nozzle center (flushing air) and to supply the required energy for the atomization of the melt (atomization air). Using a micro-annular gear pump (mzr-4605 HNP Mikrosysteme GmbH, Germany), the nozzle was fed through a heated hose. All process parameters were selected based on experience from previous studies [2] and preliminary, non-reported studies. To ensure the atomization of i.e., liquid droplets into the fluidized bed, the coating materials were heated at 100 °C, i.e., above their melting range. Conversely, the product temperature was kept below the crystallization range of each coating material to ensure crystallization and layer formation. Complete coatings were obtained by setting the coating amount to 15% (*w*/w) for all experiments [2]. A spray rate of 3 g/min was employed because low spray rates yield a more uniform coating layer and less agglomeration than high spray rates [26]. The aim of this study is to investigate the wetting and delamination behavior of the different coating materials, and hence all process parameters were kept constant except for the process temperature. Table 2 provides an overview of the selected process conditions for all coating experiments.

Owing to the different crystallization ranges of the used coating materials, the product temperature was adapted to the material properties in each case. For hydrogenated palm oil, a product temperature of 35 °C was selected, while for rice bran wax and carnauba wax, a product temperature of 50 and 60 °C, respectively, was chosen. At the end of each coating experiment, the plant and coated particles were cooled to ~25 °C, thereby allowing solidification of all melt droplets and avoiding subsequent agglomeration of the particles. All samples were weighed and packed in airtight bags and a representative number of approximately 250–300 particles were analyzed for delamination in a μCT (type: CT-1600HR, Matrix Technologies, Germany).

2.2.2. Delamination analysis using micro-computed X-ray tomography

Regarding the coated particles, delamination of the coating layer was investigated using a custom-made μCT system (type: CT-1600HR, Matrix Technologies, Germany). μCT measurements allow non-destructive three-dimensional (3D) structural analysis of the sample, thereby providing detailed insight into the sample structure. Therefore, the sample was placed between an X-ray source and a detector. Starting from the source, the sample was irradiated with X-rays, and two-dimensional (2D) radiographs of the sample were generated. Numerous radiographs can be generated when the sample is rotated and these can then be assembled into a 3D image via mathematical reconstruction. This allows, for example, the determination of coating structure properties such as coating thickness distribution, porosity, uncoated surface

Table 1
Physical and chemical properties of the lipids.

	Hydrogenated palm oil	Rice bran wax	Carnauba wax
Product name	Kahlwax 6377	Kahlwax 2811	Kahlwax 2442 L
Chemical composition	Trisaturated triglycerids (POP POO) mainly with the fatty acids palmitic and oleic acid [21,22]	Esters, wax acids, higher alcohol esters, free fatty acids, squalene and phospholipids [23]	Aliphatic and aromatic esters (84–85%), free fatty acids (3%–3.5%), alcohols (2%–3%), lactides (2%–3%), hydrocabons (1%–3%), resins (4%–6%) [24,25]
Crystallization range [°C]	38.5–44.0	52.0–75.7	63.1–79.6
Melting range [°C]	46.1–60.3	54.0–84.8	71.8–88.3

proportion or delamination of the coating layer. A resolution of 4 μm was sufficient for the delamination analysis (a higher resolution would have resulted in a smaller sample size and was therefore considered undesirable). The voltage was 60 kV, and the current was 69 μA at an exposure time of 2184 ms. To investigate the coating layer structure of as many particles as possible, a custom-made cylindrical sample holder was used to keep approximately 40–50 particles in place. At least 250–300 particles per sample were analyzed by visual inspection of the 3D images for delaminated areas of the coating shell using the VGStudio-Max 3.1 imaging software (Volume Graphics GmbH, Germany). A particle was considered delaminated if one part of the coating layer is detached or chipped off from the carrier particle. Fig. 1 shows a coated sugar sphere with a partially chipped off and delaminated region of the coating layer.

2.2.3. Density measurement

The density of the melts was determined using a DMS 4200 M (Anton Paar Germany GmbH, Germany) density meter. The density was determined for hydrogenated palm oil (60 °C–130 °C), carnauba wax (90 °C–130 °C), and rice bran wax (85 °C–130 °C). The samples were heated to 130 °C and then placed in the measurement device. Using a temperature scan, the density was measured from the highest temperature to the lowest temperature in intervals of 5 K.

2.2.4. Melting and crystallization behavior

The melting and crystallization behavior of the melts was analyzed via differential scanning calorimetry (DSC). All measurements were performed using DSC 214 Polyma (Netzsch-Gerätebau GmbH, Germany) equipment with liquid nitrogen cooling. For each coating material, a 4 mg sample was placed in an aluminum pan, which was sealed with an aluminum lid and then placed in the DSC along with an empty reference pan. A nitrogen flow of 40 mL/min was used to avoid oxidation during the measurements. At the beginning of the measurement, the preparation steps (1–2) served to distribute the sample evenly in the crucible and to remove any crystal structure. Therefore, the sample was heated to 120 °C at a heating rate of 10 K/min. The temperature was kept constant for 3 min and then lowered to 20 °C at a cooling rate of 10 K/min. These first sample preparation steps were excluded from the evaluation. After another isothermal holding time of 3 min, the measurement started with another heating (3), isothermal, and cooling (5) step. Three runs were performed until the program ended with the final step (9). The Proteus 7.0 program (Netzsch-Gerätebau GmbH, Germany) was used to evaluate the analysis steps. Each analysis was performed in triplicate.

Table 2
Process conditions for the hot-melt coating experiments.

Parameter/setting	WFP mini
Coating technique	Wurster fluidized bed
Wurster tube air gab [mm]	20
Fluidized bed diameter range [mm]	80–210
Height cone [mm]	220
Particle amount [g]	300
Coating amount [g]	45
Coating material temperature [°C]	100
Gas volume flow rate [m^3/s]	20
Spray rate [g/min]	3
Nozzle atomizing pressure [bar]	1
Nozzle-flushing air pressure [bar]	0.5

2.2.5. Drop shape analysis

A Drop Shape Analyzer DSA25E (Krüss GmbH, Germany) was used to study the wetting behavior of solids and liquids. Drop shape analysis is an image evaluation method for determining the contact angle of a liquid on a solid surface using a shadow image of a sessile drop. The analysis can also be used to determine the surface tension or interfacial tension of liquids through evaluation of a pendant drop. Using contact angle and surface tension data, polar and disperse fractions of the surface tension can then be calculated using the method developed by Owens, Wendt, Rabel, and Kaelble (OWRK) [27–29]. The surface free energy of solids can also be calculated from the contact angle data. The drop shape analysis reveals various wetting parameters, and therefore the wetting behavior of liquids and solids can be estimated.

To investigate the temperature-dependent wetting behavior of the natural melts, the device is equipped with a temperature control unit for syringe dosing units (TC3213) and a temperature control chamber for rapid temperature changes (TC40). For the relevant measurements, the melts were placed in a glass syringe with a Luer-Lock connection (SY20). The syringe was connected to a steel needle with a PTFE coating to ensure a symmetrical drop shape by preventing external wetting of the needle. Depending on the melting range of the coating materials, a temperature range of 60 °C–120 °C could be investigated. The ADVANCE analysis software (Krüss GmbH, Germany) was used to control the measurement conditions and to evaluate the gray scale images

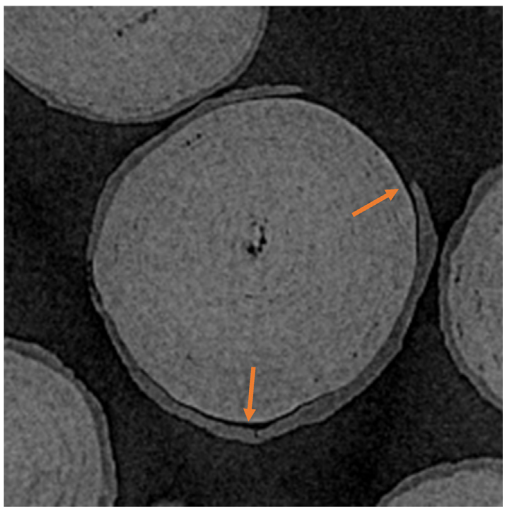

Fig. 1. Section of a raw μCT-construction showing a palm-fat-coated sugar sphere with delaminated areas.

of sessile or pendant droplets for the determination and calculation of the wetting parameters.

2.2.5.1. Surface tension measurements. In accordance with [30], the surface tension was determined as a function of temperature using the pendant drop method. A Teflon-coated needle with a diameter of 2.133 mm was used to generate each drop of melt. The maximum drop volume possible was generated by manual dosing to ensure sufficient deviation of the droplet shape from a spherical shape. The volume of the pending melt droplets ranged from 15.5 μL to 17 μL. After a constant drop shape was reached, the drop contour was recorded for 25 s (frame rate: 5 fps). The surface tension of at least five droplets comprising each coating material was determined in 5 K intervals of the respective temperature range. Using the ADVANCE software (Krüss GmbH, Germany), the radius of curvature of the droplet contour was detected via a gray scale analysis. The relevant temperature-dependent density values of the liquids were previously entered into database of the software.

2.2.5.2. Contact angle measurements. The wetting behavior of the coating materials was investigated via contact angle measurements. Moreover, the measurement results were used in the calculation of wetting parameters (the surface free energies of the carrier materials, WoA, and the polar and disperse fractions associated with the surface tension of the melts). All contact angle measurements were performed using the sessile drop protocol described in [31]. To facilitate the detection of the three-phase points, a camera viewing angle of +2° was employed. The drops were generated by a Teflon-coated stainless steel cannula with a diameter of 0.572 mm. After reaching the target temperature, a drop volume of 2 μL was generated with an automatic dosing unit. Each drop was always deposited on an unwetted solid surface. To avoid a strong spreading effect of a falling drop, the generated droplet was picked up from the needle by raising the measuring stage slowly until the droplet was deposited on the sample surface. Image analysis was performed using the numerical method of the analysis software with the best fit. In general, compared with other methods, the ellipse fitting method provided better recognition of the droplet contour and was therefore considered the best option. A circular fitting method was employed for contact angles of <20°. For each acquired image, the left and right contact angles of the drop were determined, and the mean contact angle was calculated from these values. For each test liquid, at least five independent droplets were generated and subsequently analyzed.

2.2.5.3. Calculation of the surface free energy of solids. The surface free energy (SFE) of the solid carrier materials was determined using the standard method developed by Owens, Wendt, Rabel, and Kaelble (OWRK) and performed in accordance with DIN EN ISO 19403-2 [27–29]. Through Young's eq. [32], the SFE σ_s of the solid can be expressed in terms of the contact angle θ, the interfacial tension between the solid and the liquid σ_{sl}, and the surface tension of the liquid σ_l:

$$\sigma_s = \sigma_{sl} + \sigma_l \cdot \cos\theta \tag{1}$$

This equation describes the forces acting on a sessile drop at the three-phase point in the state of equilibrium. The assumption is that the SFEs of the solid and liquid are composed of polar and disperse components (see Eq. 2 and 3). According to the OWRK method, the interfacial tension σ_{sl} between a solid and a liquid can be calculated as the sum of the surface tensions of the two phases ($\sigma_l + \sigma_s$) minus the disperse and polar interactions at the phase boundary. The interfacial tension σ_{sl} is therefore given as follows:

$$\sigma_l = \sigma_l^p + \sigma_l^d \tag{2}$$

$$\sigma_s = \sigma_s^p + \sigma_s^d \tag{3}$$

$$\sigma_{sl} = \sigma_s + \sigma_l - 2\cdot\left(\sqrt{\sigma_s^D\cdot\sigma_l^D} + \sqrt{\sigma_s^P\cdot\sigma_l^P}\right) \tag{4}$$

Inserting Young's equation (i.e., Eq. 1) into Eq. 4 yields Eq. 5, which can be fitted to the general equation of a straight line.

$$\frac{(1+\cos\theta)\cdot\sigma_l}{2\sqrt{\sigma_l^d}} = \sqrt{\sigma_s^p}\cdot\sqrt{\frac{\sigma_l^p}{\sigma_l^d}} + \sqrt{\sigma_s^d} \tag{5}$$

The polar fraction of the SFE of the solid σ_s^p is determined from the square of the slope. The dispersive fraction σ_s^d can be determined from the square of the ordinate intercept. The total SFE of the solid σ_s is calculated as the sum of the two fractions (see Eq. 3).

To determine the polar and dispersive components of the SFE via the OWRK method, contact angle measurements are required for at least two reference liquids with known polar and disperse fractions of the surface tension. Typically, one liquid is nonpolar and the other is bipolar. Diiodomethane (Sigma-Aldrich Corp., USA) and ethylene glycol (AppliChem GmbH, Germany) were used as the nonpolar liquid and the bipolar reference liquid, respectively, in the present study. Flat and smooth solid surfaces are required for the contact angle measurements, and hence all solids were previously pressed into solid tablets (although tableting may affect the SFE of the solid).

2.2.5.4. Determination of the polar and disperse fractions associated with the surface tension of the coating materials. The disperse and polar fractions of the surface tension as well as the WoA between the melts and the respective solid surface can be calculated from the results of the wetting measurements. For the wetting material, these fractions were calculated using the OWRK model for reference surfaces with SFE of >20 mJ m^{-2}, in accordance with [33]. Based on Eq. 5, the polar interactions were neglected due to the non-polarity of the PDMS surface. Rearrangement of Eq. 4 yielded Eq. 6. Young's equation was inserted into this equation and the disperse fraction σ_l^d of the surface tension was determined from the resulting relation (see Eq. 7).

$$\sigma_{sl} = \sigma_s + \sigma_l - 2 * \sqrt{\sigma_s * \sigma_l^d} \tag{6}$$

$$\sigma_l^d = \frac{\sigma_l^2}{4 * \sigma_s} * (1 + \cos(\theta))^2 \tag{7}$$

The polar fraction of the surface tension σ_l^p was obtained by rearranging Eq. 3 and was therefore taken as the difference between the total surface tension of the liquid σ_l and the disperse fraction σ_l^d.

2.2.5.5. Calculation of the WoA. The WoA is a measure of the adhesion between the melt and the respective solid surface. If the polar and disperse fractions of the surface tension or energy are known for both phases, the WoA can be calculated in accordance with Dupré's theory where,

$$W_{AD} = 2 * \left[\left(\sigma_l^d * \sigma_s^d\right)^{0,5} + \left(\sigma_l^p * \sigma_s^p\right)^{0,5}\right] \tag{8}$$

The larger the calculated value of the work of adhesion, the stronger the adhesion between the two phases [29]. In other words, the WoA is the work required to separate unit area of two phases in contact.

2.2.6. Fabrication of tablets

A flat solid surface of the core materials is required for the material-related analysis of the wetting behavior exhibited by the melts. Therefore, tablets were pressed from the carrier materials using a 15 ton hydraulic press (KBr, Perkin-Elmer Inc., USA). In order to increase compressibility, the carriers were ground in two stages using a laboratory disk mill (DLFU-230/50, Bühler GmbH, Germany) prior to tableting. A coarse grinding stage was followed by a fine grinding stage. After

placing 2.5 g of the ground core particles in the tablet mold, the particles were compressed into a tablet under a pressure of ~230 MPa. The diameter and height of each tablet were 22 mm and 4.5 mm, respectively. The roughness of the surface can influence the contact angle, and hence the roughness and the SFEs of the respective tablets were determined.

2.2.7. Surface roughness

The surface roughness of the pressed tablets was measured with a 3D laser scanning confocal microscope (VK-X1000 series, Keyence, Japan). A magnification of 10× was employed during the measurements. For each carrier material, the surface of five tablets was measured and evaluated using the VK Analysis Module 4000 software. The roughness parameter *Sa*, which was determined from the complete image area (5.7 mm^2) of each 3D microscope image, is defined as follows:

$$Sa = \frac{1}{A}\iint_A^a |Z(x,y)|dxdy \tag{9}$$

Sa denotes the arithmetic average value determined for height Z of the measured area.

3. Results and discussion

3.1. Delamination of the coating layer

As reported in previous studies [1,2], delaminated coating layers can occur with hot-melt coated particles. In the present work, the dependence of the delamination frequency on the wetting behavior or the materials combination is investigated via coating experiments. The delamination of a coating layer is illustrated in Fig. 2, where a rendered μCT-reconstruction of a Cellet® coated with 15% (*w*/w) hydrogenated palm oil is presented.

As from Fig. 1, the coating layers are relatively uniform and compact, consistent with sufficient spreading of the droplets on the carrier particles. The delamination in Fig. 2 is indicative of insufficiently strong adhesive forces between the lipid layer and the carrier material. The percentage of delaminated particles obtained via visual inspection of the μCT images directly after processing is shown in Fig. 3.

The delamination tendency differs among the coating materials. This tendency seems to be more dependent on the properties of the coating material than on the properties of the carrier materials. The highest percentage of delaminated particles occurs in the hydrogenated palm oil. The highest value (i.e., a delamination percentage of more than 99%) is obtained for Cellets® coated with this fat. The delamination tendency of sugar spheres with a palm fat coating (delamination percentage: >90%, almost all particles exhibit delamination) is similar to that of the Cellets®. In contrast, the delamination values obtained for rice bran wax and carnauba wax differ significantly from those of the palm fat. The values of all material combinations with carnauba wax are <16% and the values of all combinations with rice bran wax are <10%. The combination of Cellets® and carnauba wax yield the fewest particles with delamination. The results shown in Fig. 3 suggest that rice bran wax and carnauba wax form stable layers. However, palm fat forms layers with strong delamination tendency and (compared with those of the other materials) weaker adhesion to the surface of the carrier particles. Furthermore, the varying results suggest that the delamination behavior may be related to the wetting behavior. The delamination tendency varies among the material combinations. The batch homogeneity and consequently the functionality of the coating are directly dependent on the delamination behavior, and hence an understanding of the different delamination tendencies is important. The difference in the delamination behavior may have resulted from the difference in the wetting properties of the coating materials and carrier materials. Therefore, the wetting properties of the materials will be thoroughly analyzed.

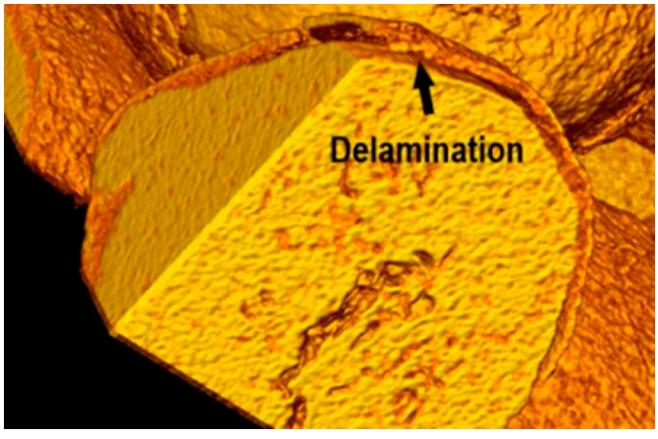

Fig. 2. Rendered μCT-reconstruction of a Cellet® coated with 15% (w/w) hydrogenated palm oil showing delamination of the coating layer.

3.2. Wetting properties of the coating and carrier materials

3.2.1. Surface tension of the coating materials

The surface tension of each coating material was determined as a function of temperature (range: 60 °C to 120 °C) depending on the crystallization temperature of the lipid. The results are shown in Fig. 4.

As expected, the surface tension decreases almost linearly with increasing temperature. Regarding the coating materials, carnauba wax exhibits the highest surface tension, followed by rice bran wax with an almost parallel shift of approx. $\Delta = -0.7$ mN/m. The lowest surface tension is obtained for hydrogenated palm oil (shift of approx. $\Delta = -1.2$ mN/m). The approximately linear dependence of the surface tension on temperature is consistent with the findings reported for cacao butter (surface tension of 26.9 mN/m at 70 °C) [34]. The surface tension values of the coating materials are similar to that of cacao butter, but are considerably lower than the surface tension of water, 64.47 mN/m at 70 °C [35]. However, these results provide no information about the wettability of the material. Consider the wettability of a liquid on a solid surface. The surface tension of the liquid and the properties of the solid (in particular the SFE) are crucial for analysis of the wetting behavior.

3.2.2. Polar and disperse fractions of the coating materials

Contact angle measurements on nonpolar PDMS-gel are useful for further characterization of the coating material, as they allow the determination of polar and disperse fractions associated with the surface tension of the melts. This characterization can then be used to assess the wetting behavior of the melts.

As expected, the contact angle measurements of all three coating materials indicate a good wetting behavior on the hydrophobic PDMS (see Fig. 5 left). Compared with the other waxes, the hydrogenated palm oil (contact angle: 46.5°–49°) exhibits the best wetting behavior on PDMS for temperatures ranging from 60 °C to 120 °C. The highest contact angles (55°–56°) are obtained for the carnauba wax. The results indicate that the contact angles at higher temperatures are slightly larger than those at lower temperatures. The surface tension of PDMS is completely hydrophobic, and hence the contact angles of carnauba wax indicate a more polar behavior compared with that of the rice bran wax and hydrogenated palm oil. The polar fraction σ_l^p and disperse fraction σ_l^d of the surface tension can be determined by inserting the contact angle measurement results of the melts on PDMS into Eq. 2 and Eq. 7. Fig. 5 right shows the polar fractions at different temperatures. With increasing temperature, the surface tensions of the melts decrease, whereas the polar fractions increase. The polar fraction of palm fat, for example, increases from ~10% to 25% when the

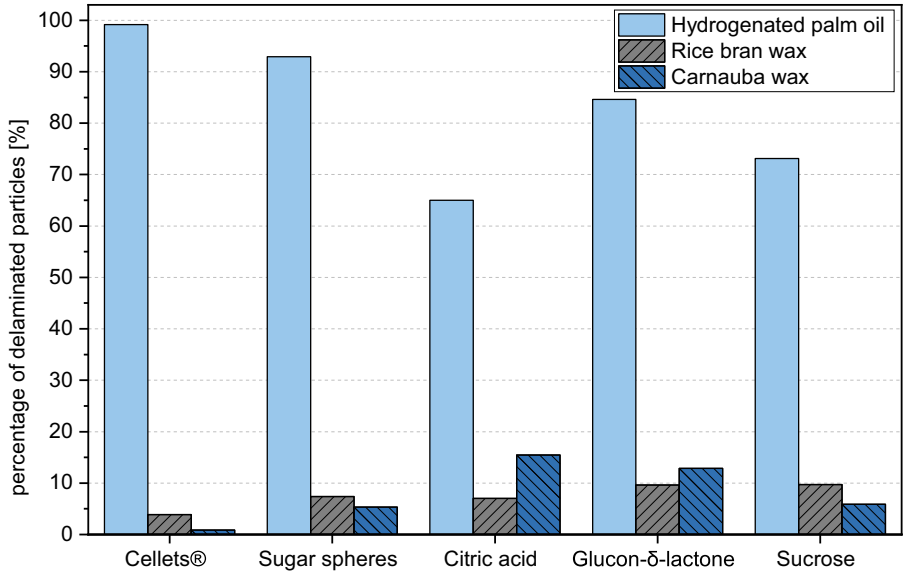

Fig. 3. Percentage of delaminated particles for Palm fat-, Rice bran wax- and Carnauba wax coatings on different carrier materials.

temperature increases from 60 °C to 120 °C. Furthermore, the fractions corresponding to rice bran wax and carnauba wax increase rapidly with rising temperature. The polar fractions are all lower than 30%, and hence the materials exhibit the expected hydrophobic properties. The largest increase in the fraction (from ~20.25% at 90 °C to 27.38% at 120 °C) occurs for the carnauba wax (see Fig. 5 right). The polar fractions of rice bran wax and palm fat are slightly lower than those of the carnauba wax. However, the polar fraction differs only slightly among the three coating materials.

3.2.3. Polar and disperse fractions associated with the SFE of the carrier materials

To determine the surface energy of the carrier materials and the corresponding polar and disperse fractions, contact angle measurements were performed with ethylene glycol and diiodmehtane on pressed tablets.

Fig. 6 shows the SFEs and the respective disperse and polar fractions of the carrier materials. The SFEs of the materials are all slightly higher than 51 mN/m and differ only modestly among the materials. This also applies to the respective polar and disperse fractions of the materials. For all carrier materials, the polar fraction is <10 mN/m and the disperse fraction is >45 mN/m, suggsesting that the dispersive properties of the materials outweigh the polar ones. Based on the minor differences in the SFEs, the expectation is that a coating material will exhibit similar wetting behavior on all substrates. A commonly used rule of thumb for assessing wetting behavior states, “If the SFE of a substrate is equal to or greater than the surface tension of the coating material, then good wetting is achieved.” [17]. Furthermore, a similar ratio of polar to dispersed proportions of coating material and substrate favors wetting. Reviewing Figs. 4, 5 (right), and 6 reveals that the wetting behavior of all coating materials should result in good wetting on all

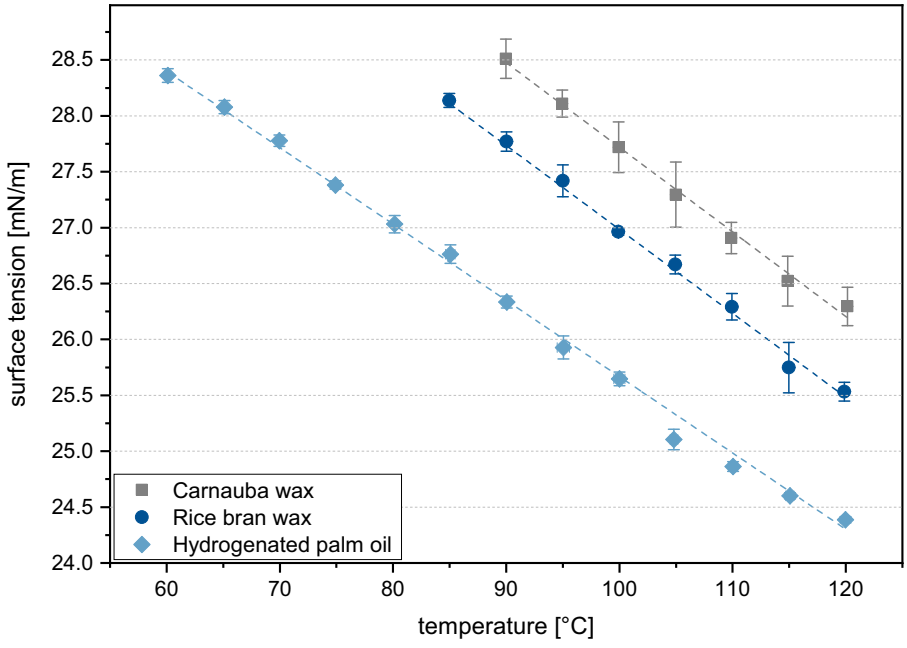

Fig. 4. Results of the surface tension measurements with respective confidence interval of the Carnauba, Rice bran, and Hydrogenated palm oil coating materials.

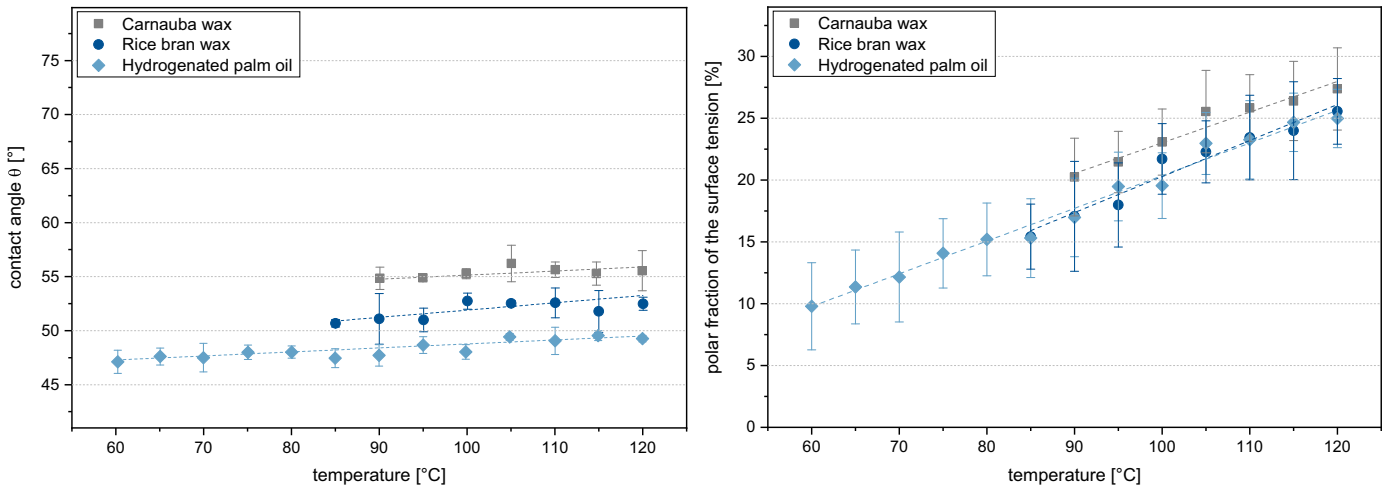

Fig. 5. Characterization of the coating materials via contact angle measurements on nonpolar PDMS-Gel. The temperature dependence of the contact angle (left plot) and the polar fraction (right plot) determined for the melts are shown.

carrier materials. This results, on the one hand, from the fact that the surface energies of the solids are greater than the surface tension of the melts and, on the other hand, from the relatively similar ratios of polar to disperse fractions.

3.2.4. Contact angle measurements on core materials

For a thorough assessment of the coating performance exhibited by the natural melts, contact angle measurements were performed on tablets of the carrier materials. Fig. 7 shows the contact angles of the coating materials on the carrier materials at 100 °C.

Contact angles of <18° occur for all material combinations, and thus good wetting can be assumed (see Fig. 7). Accordingly, all materials seemed to be well suited for coating of the carrier substances. This is particularly true of the rice bran wax, which exhibits good wetting properties, especially compared with those of the other coating materials. The contact angle measurements of the melts on the different core materials complement the previously determined wetting parameters and confirm the good wetting behavior of the material combinations.

3.2.5. Work of adhesion (WoA)

The WoA, a commonly used value for predicting the coating performance in general, indicates the likelihood of coating delamination from a solid surface [17]. Thus, an adhesion assessment focuses on the tendency of the coating and the carrier substrate to remain in contact (the WoA between the coating and substrate is typically taken as a measure of this tendency). Fig. 8 shows the values calculated for the WoA between the coating and core material.

The highest WoA and lowest WoA are obtained for all carnauba wax coatings and palm fat coatings, respectively. However, the calculated WoA values (72 mJ/m^2–75 mJ/m^2) differ only modestly among the materials. Based on the wetting properties, the phases at the interface exhibit similar levels of resistance to delamination, suggesting that the probability of delamination occurrence should differ only modestly among the coating materials. In general, high WoA values indicate a low probability of delamination at an interface. The WoA value is typically a good indicator of delamination probability. However, in the present work, this approach failed in the prediction of the probability as the wetting behavior contradicts the actually observed strong variations in delamination frequency determined via μCT measurements.

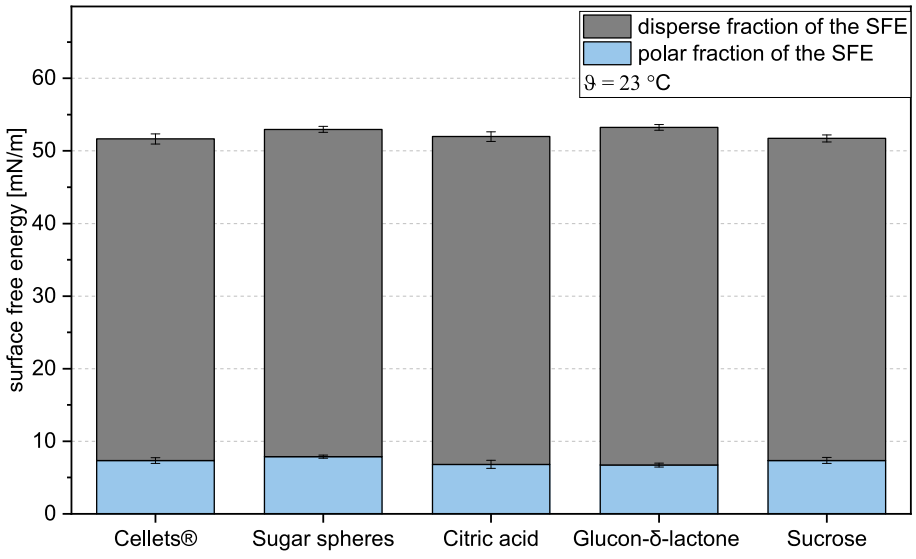

Fig. 6. Surface free energies, polar fractions, and disperse fractions of the carrier materials.

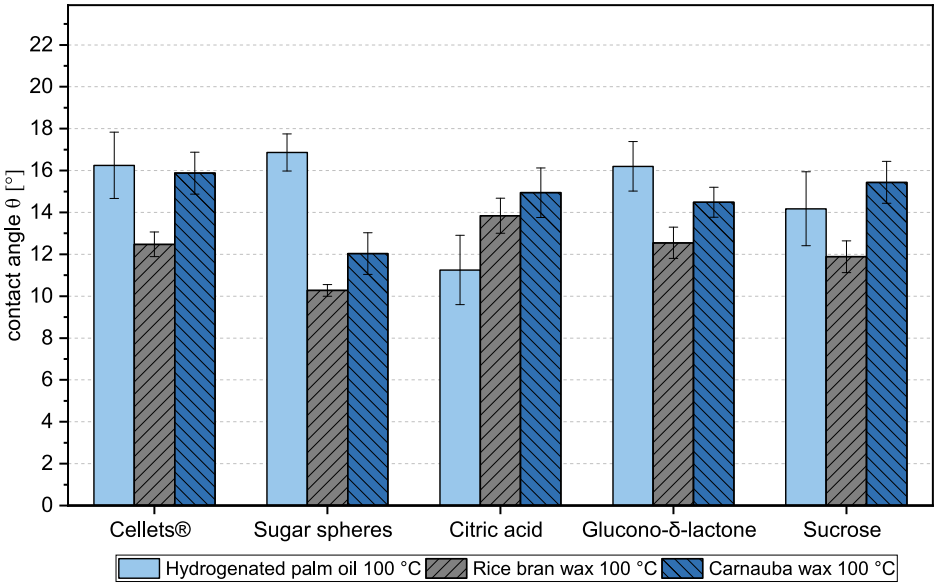

Fig. 7. Contact angles of the melts on different core materials at 100 °C.

3.2.6. Surface roughness

The surface roughness values of the pressed tablets are listed in Table 3.

Busscher et al. [36] investigated the influence of roughness on the wetting of water on polymer surfaces. According to Busscher et al. [36], the influence of roughness on contact angle measurements can only be neglected if the roughness *Ra* is <0.1 μm. For contact angles above 86°, Busscher et al. found an increase in the contact angle with increasing roughness. In contrast, for contact angles below 60°, a decrease in the contact angle with increasing roughness was found [36]. Although the surface roughness as an influencing factor must be taken into consideration, measured values ranging from 2.95 μm to 7.49 μm are obtained for all samples. Furthermore, the calculated confidence intervals of the contact angle mesasurements are all lower than 3° and lie within the acceptable range specified in [33] for the calculation of disperse and polar fractions associated with the surface tension and SFE. The low confidence intervals of the roughness measurements suggest that the tablet-production process yielded a sufficiently reproducible solid surface. Therefore, the effect of roughness on the contact angle measurements is expected to be similar for all samples. In this case, only a low discrepancy between the measured apparent contact angles and the ideal Young contact angle must be assumed. For this reason, roughness is not expected to influence the conclusions of the wetting analysis.

4. Discussion and conclusion

This study provides new insights into the wetting and delamination behavior of natural lipids during the HMC process. The delamination tendency of the coating layer on HMC products was investigated. Three coating materials were tested, each on six common substrates for industrial applications. μCT measurements revealed that delamination

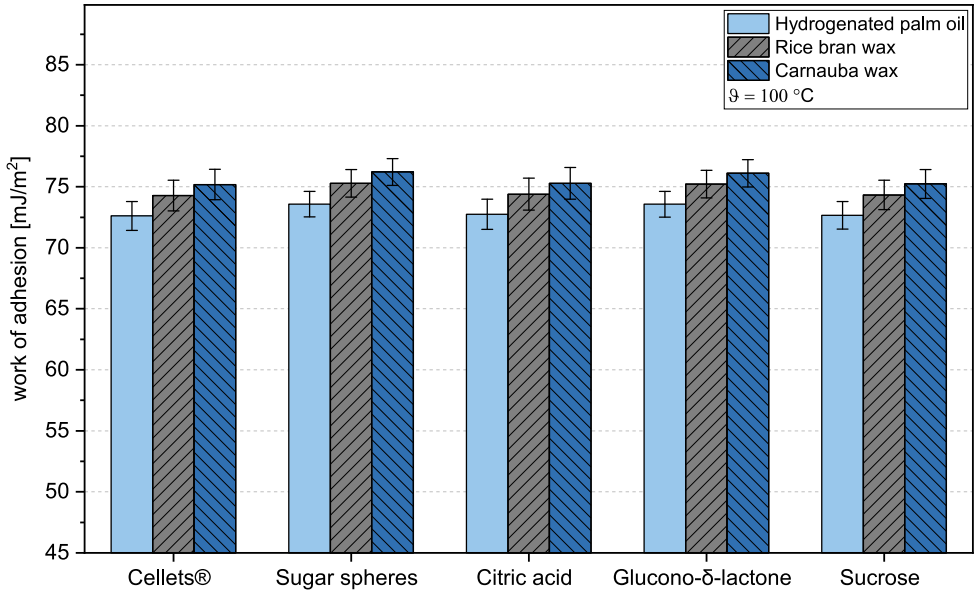

Fig. 8. WoA between the coating materials and core materials at 100 °C.

Table 3
Surface roughness and corresponding confidence interval of the pressed tablets.

	Sa [µm]
Cellets	7.49 ± 0.46
Sugar spheres	4.14 ± 0.60
Citric acid	3.94 ± 0.59
Glucon-δ-lactone	3.53 ± 0.23
Sucrose	2.95 ± 0.17

occurs frequently in the HMC process with natural coating substances, and can have a significant influence on the quality and protective effect of the coating layer. Delamination was considerably more severe in the palm fat coatings than in the rice bran wax and carnauba wax coatings. The temperature-dependent surface tension of the melts is lower than the determined surface energies of the carrier substances. However, the ratios of the polar and disperse fractions of the materials are similar. Good wetting of the melts could therefore be assumed, as confirmed by contact angle measurements of the coating materials on the respective carrier substances. In addition, similar WoA (a wetting parameter that is a measure of the bonding between the materials) values were obtained for all material combinations. Although the contact angles of the hydrogenated palm oil were slightly higher than those of the other coating materials, all three materials exhibited similar and adequate wetting behavior. A hypothesized correlation between wetting behavior and delamination frequency was falsified. Therefore, the results (rather than providing a complete explanation of the observed delamination phenomena) allow the proposal of various hypotheses.

Delamination may have resulted from the different thermal expansion coefficients of the carrier particle and the coating material [19]. A change in temperature may have led to thermal stresses and may have promoted spalling or delamination. Subsequent swelling of a hygroscopic carrier material due to moisture could also lead to structural changes in the coating structure and might cause delamination. However, increased cracking rather than delamination of the coating layer would be expected. Another possible explanation for the occurrence of delamination could be the inherent crystalline behavior and recrystallization of the coating materials.

As previously mentioned, several studies have shown that rapid cooling of triglycerids leads to the formation of thermodynamically unstable α-crystals, which tend to recrystallize to more stable β or β'-crystal forms [8–14]. The studies thus support the assumption that recrystallization can have a significant influence on the coating layer structure and possibly the occurrence of delamination. Of the coating substances, hydrogenated palm oil, which exhibits the highest tendency for delamination, has the highest content of triglycerides (see Table 1). A connection between the chemical composition of the coating material or between the complex crystallization behavior and the occurrence of delamination remains elusive. However, one or both of these connections may explain the occurrence of delamination in the coatings.

In future studies, the complexity of the delamination process occurring in natural melt coatings will be further investigated. The thermal expansion coefficients of the materials and (especially) the crystallization behavior of the coating materials will be investigated in further detail. Furthermore, the durability of the coating layer as a function of environmental conditions will be analyzed. The work will help to elucidate the complexity of delamination occurrence in HMC products. This will contribute to a more systematic materials selection (than those currently employed) and further optimization of the process strategy in order to produce high-quality coatings that resist delamination.

Author statement

B.M. Woerthmann: Data curation, Execution of experiments, Writing-original draft, Conceptualization, Methodology, Formal analysis, Data interpretation, Project administration.

L. Totzauer: Execution of experiments.

H. Briesen: Writing – review and editing, Conceptualization, Data interpretation, Project administration.

Declaration of Competing Interest

The authors declare that they have no known competing financial interests or personal relationships that could have appeared to influence the work reported in this paper.

Acknowledgments

This research was supported by the Ministry of Economics and Climate (BMWK) via AiF and the FEI (Forschungskreis der Ernährungsindustrie e.V., Bonn) Project AiF 19970 N. Equipment funded by the Deutsche Forschungsgemeinschaft (DFG, German Research Foundation)–198187031 was used in this study.

Appendix A. Appendix

Table 4
Surface tension measurement results and corresponding density values.

	Hydrogenated palm oil		Rice bran wax		Carnauba wax	
Temperature [°C]	Density [g/cm^3]	Surface tension [mN/m]	Density [g/cm^3]	Surface tension [mN/m]	Density [g/cm^3]	Surface tension [mN/m]
25	0.9995	–	0.9767	–	1.0015	–
60	0.8785	28.36	–	–	–	–
65	0.8752	28.08	–	–	–	–
70	0.8718	27.78	–	–	–	–
75	0.8684	27.38	–	–	–	–
80	0.8651	27.03	–	–	–	–
85	0.8618	26.76	0.8277	28.14	–	–
90	0.8584	26.34	0.8245	27.77	0.8449	28.51
95	0.8551	25.93	0.8214	27.42	0.8418	28.11
100	0.8518	25.65	0.8183	26.96	0.8387	27.72
105	0.8485	25.11	0.8152	26.67	0.8356	27.30
110	0.8452	24.86	0.8120	26.29	0.8324	26.91
115	0.8419	24.60	0.8089	25.75	0.8293	26.52
120	0.8386	24.39	0.8058	25.53	0.8262	26.30

References

[1] M.G. Müller, J.A. Lindner, H. Briesen, K. Sommer, P. Foerst, On the properties and application of beeswax, carnauba wax and palm fat mixtures for hot melt coating in fluidized beds, Adv. Powder Technol. 29 (3) (2018) 781–788.

[2] B.M. Woerthmann, J.A. Lindner, T. Kovacevic, P. Pergam, F. Schmid, H. Briesen, A novel method for assessing the coating uniformity of hot-melt coated particles using micro-computed tomography, Powder Technol. 378 (2021) 51–59.

[3] A.S. Achanta, P.S. Adusumilli, K.W. James, C.T. Rhodes, Development of hot melt coating methods, Drug Dev. Ind. Pharm. 23 (2008) 441–449.

[4] S. Gupta, S. Khan, M. Muzafar, M. Kushwaha, A.K. Yadav, A.P. Gupta, Encapsulation: Entrapping Essential Oil/Flavors/Aromas in Food, 2016 229–268.

[5] K. Saleh, P. Guigon, Chapter 7 Coating and Encapsulation Processes in Powder Technology, 11, 2007 323–375.

[6] V. Jannin, Y. Cuppok, Hot-melt coating with lipid excipients, Int. J. Pharm. 457 (2013) 480–487.

[7] N. Gontard, S. Marchesseau, J.-L. Cuq, S. Guilbert, Water vapour permeability of edible bilayer films of wheat gluten and lipids, Int. J. Food Sci. Technol. 30 (1995) 49–56.

[8] D.G. Lopes, K. Becker, M. Stehr, D. Lochmann, D. Haack, A. Zimmer, S. Salar-Behzadi, Role of lipid blooming and crystallite size in the performance of highly soluble drug-loaded microcapsules, J. Pharm. Sci. 104 (2015) 4257–4265.

[9] M. Windbergs, C.J. Strachan, P. Kleinebudde, Investigating the principles of recrystallization from glyceride melts, AAPS PharmSciTech 10 (2009) 1224–1233.

[10] K. Chansanroj, G. Betz, H. Leuenberger, A. Mitrevej, N. Sinchaipanid, Polymorphic change of a triglyceride base in hot melt coating process and stability acceleration by tempering process, J. Drug Deliv. Sci. Technol. 17 (2007) 347–352.

[11] D.G. Lopes, S. Salar-Behzadi, A. Zimmer, Designing optimal formulations for hot-melt coating, Int. J. Pharm. 533 (2017) 357–363.

[12] J.B. Brubach, M. Ollivon, V. Jannin, B. Mahler, C. Bourgaux, P. Lesieur, P. Roy, Structural and thermal characterization of mono- and diacyl polyoxyethylene glycol by infrared spectroscopy and X-ray diffraction coupled to differential calorimetry, J. Phys. Chem. B 108 (2004) 17721–17729.

[13] J.B. Brubach, V. Jannin, B. Mahler, C. Bourgaux, P. Lessieur, P. Roy, M. Ollivon, Structural and thermal characterization of glyceryl behenate by X-ray diffraction coupled to differential calorimetry and infrared spectroscopy, Int. J. Pharm. 336 (2007) 248–256.

[14] C.D. Doan, I. Tavernier, P.K. Okuro, K. Dewettinck, Internal and external factors affecting the crystallization, gelation and applicability of wax-based oleogels in food industry, Innovative Food Sci. Emerg. Technol. 45 (2018) 42–52.

[15] M. Windbergs, C.J. Strachan, P. Kleinebudde, Understanding the solid-state behaviour of triglyceride solid lipid extrudates and its influence on dissolution, Eur. J. Pharm. Biopharm. 71 (2009) 80–87.

[16] K. Becker, S. Salar-Behzadi, A. Zimmer, Solvent-free melting techniques for the preparation of lipid-based solid oral formulations, Pharm. Res. 32 (2015) 1519–1545.

[17] A. Mellor, P. Della Valentina, Predicting Coatability: Contact Angle and Surface Tension Results as a Basis for Targeted Development of Coating AR296, https://www.kruss-scientific.com/en/know-how/application-reports/ar296-predicting-coatability 2021.

[18] M. Sapper, M. Bonet, A. Chiralt, Wettability of starch-gellan coatings on fruits, as affected by the incorporation of essential oil and/or surfactants, Food Sci Technol-Leb 116 (2019), 108574.

[19] S. Ebnesajjad, A.H. Landrock, Introduction and adhesion theories, Adhesives Technology Handbook, 38, Elsevier 2015, pp. 1–18.

[20] S. Ebnesajjad, A.H. Landrock, Durability of adhesive bonds, Adhesives Technology Handbook, 21, Elsevier 2015, pp. 297–338.

[21] S.W. Lin, Palm oil, in: F.D. Gunstone (Ed.), Vegetable Oils in Food Technology, Wiley-Blackwell, vol. 63, Oxford, UK 2011, pp. 25–58.

[22] R.E. Timms, Phase behaviour of fats and their mixtures, Prog. Lipid Res. 23 (1984) 1–38.

[23] S.R. Vali, Y.-H. Ju, T.N.B. Kaimal, Y.-T. Chern, A process for the preparation of food-grade rice bran wax and the determination of its composition, J. Am. Oil Chem. Soc. 82 (2005) 57–64.

[24] L.E. Vandenburg, E.A. Wilder, The structural constituents of carnauba wax, J. Am. Oil Chem. Soc. 47 (1970) 514–518.

[25] L.S.K. Dassanayake, D.R. Kodali, S. Ueno, K. Sato, Physical properties of rice bran wax in bulk and organogels, J. Am. Oil Chem. Soc. 86 (2009) 1163–1173.

[26] M.J. Jozwiakowski, D.M. Jones, R.M. Franz, Characterization of a hot-melt fluid bed coating process for fine granules, Pharm. Res. 7 (1990) 1119–1126.

[27] D.K. Owens, R.C. Wendt, Estimation of the surface free energy of polymers, J. Appl. Polym. Sci. 13 (1969) 1741–1747.

[28] W. Rabel, Einige Aspekte der Benetzungstheorie und ihre Anwendung auf die Untersuchung und Veränderung der Oberflächeneigenschaften von Polymeren, Farbe und Lack 77 (1971) 997–1005.

[29] D.H. Kaelble, Dispersion-polar surface tension properties of organic solids, J. Adhes. 2 (1970) 66–81.

[30] DIN Deutsches Institut für Normung e. V, Beschichtungsstoffe – Benetzbarkeit: Teil 3: Bestimmung der Oberflächenspannung von Flüssigkeiten mit der Methode des hängenden Tropfens, 87, Beuth Verlag GmbH, 2020 040.

[31] DIN Deutsches Institut für Normung e. V, Beschichtungsstoffe – Benetzbarkeit: Teil 1: Begriffe und allgemeine Grundlagen (ISO 19403-1:2017), Beuth Verlag GmbH, 2020 01.040.87; 87.040.

[32] T. Young III, An essay on the cohesion of fluids, Phil. Trans. R. Soc. A 95 (1805) 65–87.

[33] DIN Deutsches Institut für Normung e. V., Beschichtungsstoffe – Benetzbarkeit: Teil 5: Bestimmung des polaren und dispersen Anteils der, Beuth Verlag GmbH 87 (2020) 040.

[34] H.K. Cammenga, K. Hopp, K. Gehrich, G. Ziegleder, Relevant fürs Aroma, Benetzungsverhalten von Kakaobestandteilen auf unterschiedlichen Zuckern, Lebensmitteltechnik 40 (2008) 54–57.

[35] N.B. Vargaftik, B.N. Volkov, L.D. Voljak, International tables of the surface tension of water, J. Phys. Chem. Ref. Data 12 (1983) 817–820.

[36] H.J. Busscher, A.W.J. van Pelt, P. de Boer, H.P. de Jong, J. Arends, The effect of surface roughening of polymers on measured contact angles of liquids, Colloids Surf. A Physicochem. Eng. Asp. 9 (1984) 319–331.

5.3 Paper III: Analyzing batch homogeneity of natural hot-melt coating materials (Woerthmann et al., 2023)

Summary

In previous investigations and studies, the need for an analytical method to study the interparticle batch homogeneity of hot-melt coatings became apparent. µCT measurements are suitable for analyzing the uniformity of the coating layer thickness of a particle but are severely limited for analyzing a large number of particles. Therefore, they allow only limited conclusions on interparticle batch homogeneity. At the same time, it became clear that delamination is a common phenomenon in natural hot-melt coating and can negatively affect the interparticle batch homogeneity. To ensure the requirements and functionalities of coated products, a high degree of uniformity of coating of the single particles and a high interparticle batch homogeneity are required. To investigate further influencing factors and relationships, an analytical method based on fluorescence spectroscopy was established to quantify the batch homogeneity. In the study, an emphasis was also placed on comparing the results with standard optical methods for complementary data interpretation. These included the determination of the layer thickness distributions via µCT and particle size measurements. The study's results confirm the process temperature as a primary influencing factor for HMC in a fluidized bed. For hydrogenated palm oil coatings, a process temperature of 40°C proved to have the preferable effect on interparticle batch homogeneity. At the same time, the spray rate factor showed only a minor influence on the interparticle batch homogeneity.

Author contributions

M. Woerthmann came up with the idea for this work and developed the experimental and analysis methods, did the conceptualization, conducted experiments, evaluated all experiments, and wrote the original draft. T. Wittkamp and J. Gerber helped developing the analysis method and conducted experiments. A. Hoffmann conducted experiments. M. Woerthmann supervised the work of T. Wittkamp, A. Hoffmann, and J. Gerber. H. Briesen supervised all work, corrected and proofread the article, and worked on the conceptualization and data interpretation.

Copyright

Powder Technology 426 (2023) 118626

Contents lists available at ScienceDirect

Powder Technology

journal homepage: www.journals.elsevier.com/powder-technology

Analyzing the interparticle batch homogeneity of natural hot-melt coatings

B.M. Woerthmann, A. Hoffmann, J. Gerber, T. Wittkamp, H. Briesen *

Chair of Process Systems Engineering, TUM School of Life Sciences Weihenstephan, Technical University of Munich, Germany

HIGHLIGHTS

- Using fluorescent spectroscopy for batch homogeneity analysis.
- micro-computed tomography of hot-melt coated particles.
- coating layer structure independent interparticle batch homogeneity analysis.

GRAPHICAL ABSTRACT

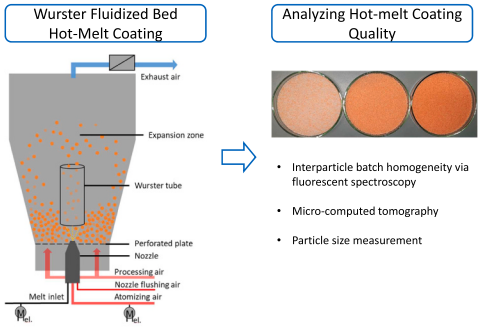

ARTICLE INFO

Keywords:
Natural hot-melt coating
Wurster fluidized bed
Interparticle batch homogeneity analysis
Micro-computed tomography
Interparticle coating variability

ABSTRACT

The hot-melt coating process is widely used in the food and pharmaceutical industries. Its purpose of use is very diverse and includes, among other things, changing the functional properties of the particle surfaces, forming a protective layer or influencing the release rate of the encapsulated substance. To achieve such purposes for each product particle, a high degree of uniformity of coating of the single particles and a high interparticle batch homogeneity are required. However, such requirements are affected by multiple factors throughout the hot-melt coating process.

The main focus of this research is to evaluate the interparticle batch homogeneity, and to compare the results with alternative methods for coating quality analysis.

As a testing system, sugar spheres are coated with hydrogenated palm oil in a lab-scale Wurster fluidized bed. The coatings are investigated under various process conditions using particle size measurement and micro-computed tomography analysis. Additionally, a new method based on fluorescence spectroscopy is proposed to quantify interparticle batch homogeneity unaffected by structural phenomena such as delamination.

For the investigated test system, the results of this study show that a process temperature of 40 °C has the most favorable effect on the interparticle batch homogeneity, while spray rates between 3 and 20 g/min have only a minor influence.

* Corresponding author at: Chair of Process Systems Engineering, Gregor-Mendel-Str. 4, D-85354 Freising, Germany.
E-mail address: heiko.briesen@tum.de (H. Briesen).

https://doi.org/10.1016/j.powtec.2023.118626
Received 27 March 2023; Received in revised form 28 April 2023; Accepted 4 May 2023
Available online 5 May 2023

1. Introduction

The coating process in a fluidized bed is widely used in the agricultural, chemical, food and pharmaceutical industries. The application objectives are wide-ranging, as the coating process can be used to influence surface properties or to protect sensitive ingredients from reactive environmental factors such as moisture, light or oxygen. In the food and pharmaceutical industries, for example, it is used for controlled release, taste masking, coloring or to improve handling by modifying flowability and dust prevention [1,2]. Due to the increasing demand for solids with functional properties and the growing quality requirements, the coating process is becoming increasingly important. In particular, the so-called hot-melt coating (HMC) with natural coating materials is increasingly coming into focus, as it meets the growing requirements for environmental sustainability and energy efficiency. Major coating materials for industrial HMC applications are hydrogenated vegetable oils (e.g. hydrogenated palm oil) and waxes, such as beeswax, carnauba wax or rice bran wax, due to their good moisture barrier [3,4]. The use of environmentally friendly and cost-effective raw materials gives a high innovation potential [1,5]. In HMC, the coating material is melted, sprayed onto and crystallized on the carrier particle. Compared to solvent-based coating, an energy-intensive drying step is not needed, allowing high spray rates with a fast coating build-up and a short process time. This, however, also limits the wetting and spreading process, which can lead to non-uniform layer structures. The coating provides the particle with a special functionality. The degree of functionality depends crucially on the quality of the coating layer. In particular, the benchmarks of intraparticle coating uniformity and interparticle batch homogeneity govern the quality and functionality of coatings. The coating structure should always be of uniform thickness, free of pores and cracks, and thus uniform [6]. Furthermore, to ensure consistent quality over all particles i.e. a high interparticle batch homogeneity with a low level of variation is desired [7]. Compliance with high quality requirements is very challenging in HMC and requires a high degree of knowledge about the process parameters and the coating material properties, especially for HMC of fine particles (> 100 μm). Consequently, understanding the influence of various parameters on the quality of the coated products is essential. Although the HMC process can be used for many applications, its potential use is still limited. The main reason for this is a lack of the fundamental understanding of the complex relationships between material properties and process parameters on the final product. Recent scientific studies are therefore following different directions in order to better understand this complex interplay.

Several studies have focused on the characterization of coating material properties that can affect final quality. Goslinka and Heinrich investigated the coating properties of natural waxes by determining their material properties such as water vapor permeability, thermal properties such as minimum film formation temperature, or surface roughness [8]. Especially beeswax and rice bran wax proved to be favorable as natural coating agents [8]. Lopes et al. studied the crystallization behavior as a function of the process temperature guidance of triacylglycerides, more specifically tristearin [9]. It was shown that the crystal form can be especially influenced by the process temperature control. Low process temperatures lead to unstable α-crystals, which in turn tend to recrystallize, resulting in a structural change of the coating layer morphology, which can subsequently decrease the interparticle batch homogeneity [9]. Post-coating tempering or the addition of additives to the coating material can help to promote polymorphic stabilization at lower temperatures [9–11]. Müller et al. influenced the complex thermal behavior of natural fats and waxes by specific blending without adding additives to achieve uniform coatings [12]. Meanwhile, Woerthmann et al. (2022) investigated the thermal wetting and delamination behavior of natural coating materials. Good wetting properties were shown, while differences in delamination behavior could be observed. Hydrogenated palm oil showed a higher tendency to delamination than waxes such as carnauba wax or rice bran wax [13]. A correlation between the choice of coating material and the resulting interparticle batch homogeneity in HMC was demonstrated [13,14].

Other studies, however, have focused specifically on process-influencing parameters or on novel analytical methods for analyzing the coating layer structure to better understand the complex relationships between coating quality and process conditions. The main process influencing factors are atomization pressure, fluidization velocity, spray rate, type of nozzle, plant geometry, process temperature, inlet air and hot-melt temperature [1,3,15]. The crucial quality characteristics of the coating layer can be the dissolution kinetics, mean layer thickness, non-coated surface proportion, the layer thickness distribution of a single particle, coating structures, and the interparticle batch homogeneity. For highly functional coatings, interparticle batch homogeneity together with intraparticle coating uniformity (i.e. uniform coating of a single particle) are of particular importance. Recently, studies have strongly focused on the systematic process understanding of the coating process. This can be achieved, for example, by experimental studies or by modeling and numerical simulations. The potential of numerical simulations for improving the understanding of the coating process is enormous. However, prediction accuracy depends on the accuracy of the experimental input data [16,17]. Dissolution tests and particle size analyses are popular and frequently used methods for evaluating coating success and quality. Release kinetics are particularly suitable for determining the protective effect of the coated product. However, no direct conclusions on interparticle batch homogeneity can be drawn from release kinetics of a particle collective, since the functionality and the protective effect in each case depend on both the uniformity of the coating within a particle and on the homogeneity of the particles among themselves [7,16]. Particle size analysis is also a standard method for proving coating success and calculating the mean coating layer thickness. However, particle size analyses are also limited in their validity and information content. For example, it is assumed that each particle is spherical, each size class grows uniformly, and an ideally uniform layer is formed on each particle without inclusions or delamination. Consequently, a comparison of the initial and coated particle size distribution allows only limited conclusions about the coating success and uniformity [18,19]. The method is therefore not suitable for the determination of interparticle batch homogeneity due to the numerous assumptions and dependency to structural phenomena such as delamination of the coating layer. Methods for determining coating thickness and interparticle batch homogeneity include confocal laser scanning microscopy (CLSM) [20,21], optical coherence tomography (OCT) [6,22,23], terahertz pulsed imaging (TPI) [24] or micro-computed tomography (μCT) measurements [25,26]. These methods allow the study of key characteristics providing information about the layer thickness distribution of single particles for a better systematic understanding of the process. Especially μCT measurements allow a detailed, high-resolution, non-destructive analysis of the surface, volume, or internal structures of materials in the field of particle technology [13,27–29]. For HMC, Woerthmann et al. (2021) developed a method to characterize the layer thickness uniformity and determine the uncoated surface fraction of single particles [26]. In another study, Woerthmann et al. (2022) used μCT measurements to show that material- and process-dependent delamination behavior in HMC can have a negative effect on interparticle batch homogeneity [13]. However, in addition to the large information density provided by μCT measurements of HMC particles, the disadvantages also became apparent. For example, the long measurement times, the large amount of data, and the costly and complicated measurement and analysis procedures are severely limiting. A significant number of samples for the investigation of interparticle batch homogeneity by means of μCT is therefore very difficult to implement or only with limited information content. Although there are many methods for characterizing coatings, there is still a lack of practical and cost-effective methods for investigating and identifying process parameters that influence the interparticle batch homogeneity of HMC. In

contrast, an efficient, easy-to-perform measurement method with a high information content could be the investigation of batch homogeneity using an ancillary dye. Šibanc et al. investigated the interparticle batch homogeneity of solvent-based coatings by determining the amount of coating per particle via the measured tetrazine concentration in a UV/Vis spectrometer [30]. Following the method of Šibanc et al., the coating layer is dyed with a heat-stable fluorescent dye in order to quantify the coating amounts per particle via a fluorescence spectrophotometric measurement. By measuring the dye concentration per particle, the coating variability and the interparticle batch homogeneity will be determined afterwards.

The major motivation for this work is to better understand the coating variability of natural HMCs in a Wurster coater. This work is intended to enable a rapid non-hazardous and accurate analytical method to study the interparticle batch homogeneity of fine hot-melt coated particles, allowing conclusive interpretation of the data. Due to the frequent occurrence of delamination in natural hot-melt coated products, an additional objective is to obtain experimental data independent from structural phenomena. Furthermore, it will be shown that process-influencing variables on interparticle batch homogeneity can be identified. For an interpretation and discussion of the data, the experiments will be compared with common high-precision measurement methods and interpreted in a supplementary way. The process understanding will be extended by new knowledge about influencing variables of the coating variability in HMC, which will allow the data to be used for numerical simulations and modeling.

2. Materials and methods

2.1. Materials

The experiments were performed using highly spherical (sphericity >0.93) sugar spheres ($\rho_{25°C}$ = 1541 kg/m^3) (Pharm-a-Spheres GmbH, Germany). The particles have a relatively narrow size distribution with a mean particle size of $d_{50,3}$ = 1140 μm with a standard deviation of σ = 75 μm. Hydrogenated palm oil (Kahlwax 6377) was used as natural coating material obtained from Kahl GmbH & Co. KG (Germany). The crystallization and melting ranges of the lipid is 38.5–44 °C and 46.1–60.3 °C. Before the coating process, the hydrogenated palm oil was dyed with a fluorescent marker. For the interparticle batch homogeneity analysis, the heat-stable fluorescent dye ARANGEN-103 Orange (ARALON Color GmbH, Germany) was used. Commercially available sunflower oil (Bellasan®, Brökelmann & Co. Oelmühle GmbH, Germany) was used as dilution fluid for the analysis of the batch homogeneity using fluorescent dye. Sunflower oil is not only inexpensive and readily available, but also has the advantage that its excitation wavelength range does not overlap with that of the fluorescent dye, thus allowing precise measurements.

2.2. Methods

2.2.1. Particle coating process

All particles investigated in this study were coated in a lab-scale fluidized bed WFP Mini (DMR Prozesstechnologie GmbH, Switzerland). The experiments were carried out batchwise in a bottom-spray Wurster coating configuration with an externally heated three component nozzle of DMR with an orifice size of 1 mm. All feeders and plant components were externally heated to prevent solidification of the melt prior to atomization. To ensure a constant volume flow of the melt without a pulsating atomization, a micro-annular gear pump (mzr-4605 HNP Mikrosysteme GmbH, Germany) was used. At the end of each coating experiment, the plant and coated particles were cooled to ~25°C to allow solidification of the coating layer and to prevent the particles from subsequent agglomeration. All samples were weighed to determine the yield of each batch. The samples were then packed in airtight bags for further analysis.

Fig. 1 shows the hot-melt coating setup schematically.

All process parameters were selected and adjusted on the basis of experience from previous studies [13,14,26] and by continuously considering new findings. Table 1 provides an overview of the selected process conditions of the coating experiments.

Since the aim of this study is to find a simple and fast method to identify and investigate the process influencing parameters on the batch homogeneity of HMC, the two parameters, i.e., process temperature and spray rate, were varied. By varying the spray rate, but keeping the coating amount constant, the coating time varies between 2.25and 15 min. Each experiment was performed in duplicate or triplicate. Table 4 in the appendix provides an overview of all coating experiments performed.

2.2.2. Coating characterization

2.2.2.1. QICPIC/R. The particle size measurements were performed with a high-speed image analysis device QicPic (Sympatec GmbH; Germany). For particle dispersion, a Vibri was used in combination with a Gradis free-fall shaft. Imaging was performed with an M6 lens with a resolution of 5–1705 μm, and a frame rate of 150 Hz. A triplicate determination was made per batch, each with 50 g sample size. In addition to the coated samples, uncoated particles were analyzed, allowing the mean layer-thickness $\overline{d}$ of a batch to be calculated using Eq. (1).

$$\overline{d} = \frac{x_{coated\ 50,0} - x_{uncoated\ 50,0}}{2} \quad (1)$$

The calculation of the mean coating layer thickness by particle size analysis is a standard method, which is, however, limited in its validity by the following assumptions: all particles are spheres; all particles of the one-size class grow at the same rate; the coating layer is ideal without inclusions, pores or delamination; and all particles can be found in the same larger size class after the coating process.

2.2.2.2. Micro-computed X-ray tomography for layer thickness distribution measurements. So a statement on the layer thickness distribution of palm fat coatings can be provided, single spheres were analyzed in a custom-made μCT system (type: CT-1600HR, Matrix Technologies, Germany). The measurement and analysis method was analogous to the method published by 26 [26].

For the analysis method, a coated sugar sphere was first fixed on the measuring rod with a double-sided adhesive pad. Thereafter, 2000 projections with a resolution of 2 μm were recorded. The voltage was 60 kV, and the current was 60 μA at an exposure time of 2184 ms. For segmentation and smoothing of the coating layer, the commercial tool VGStudio Max 3.2.3 (VolumeGraphics GmbH, Germany) was used. The resulting layer was exported and binarized using the MAVI program (Fraunhofer Institute IWTM, Germany). For the layer thickness analysis, a custom MATLAB program (The MathWorks, Inc., USA) MATLAB R2019b, the Bresenham's line-sampling algorithm [31], and the marching cubes rendering algorithm [32] were used. A total of 2400 uniformly distributed lines were determined from the particle center before the closest voxels along that direction were determined. The resulting layer thickness distribution of a single particle is therefore based on 2400 measured thickness values. Due to the time-consuming and cost-intensive method, three randomly selected spheres from each experiment (Batch 3, Batch 5 and Batch 8) were analyzed for their layer thickness distribution.

2.2.2.3. Batch homogeneity analysis by fluorescent spectroscopy. The HMC interparticle batch homogeneity analysis is based on a fluorescence spectrometric measurement, in which the coating amount is determined via a fluorescent dye concentration. Before the particles get hot-melt coated in a fluidized bed, the coating material is dyed with a specific concentration of fluorescent dye. By melting off the coating

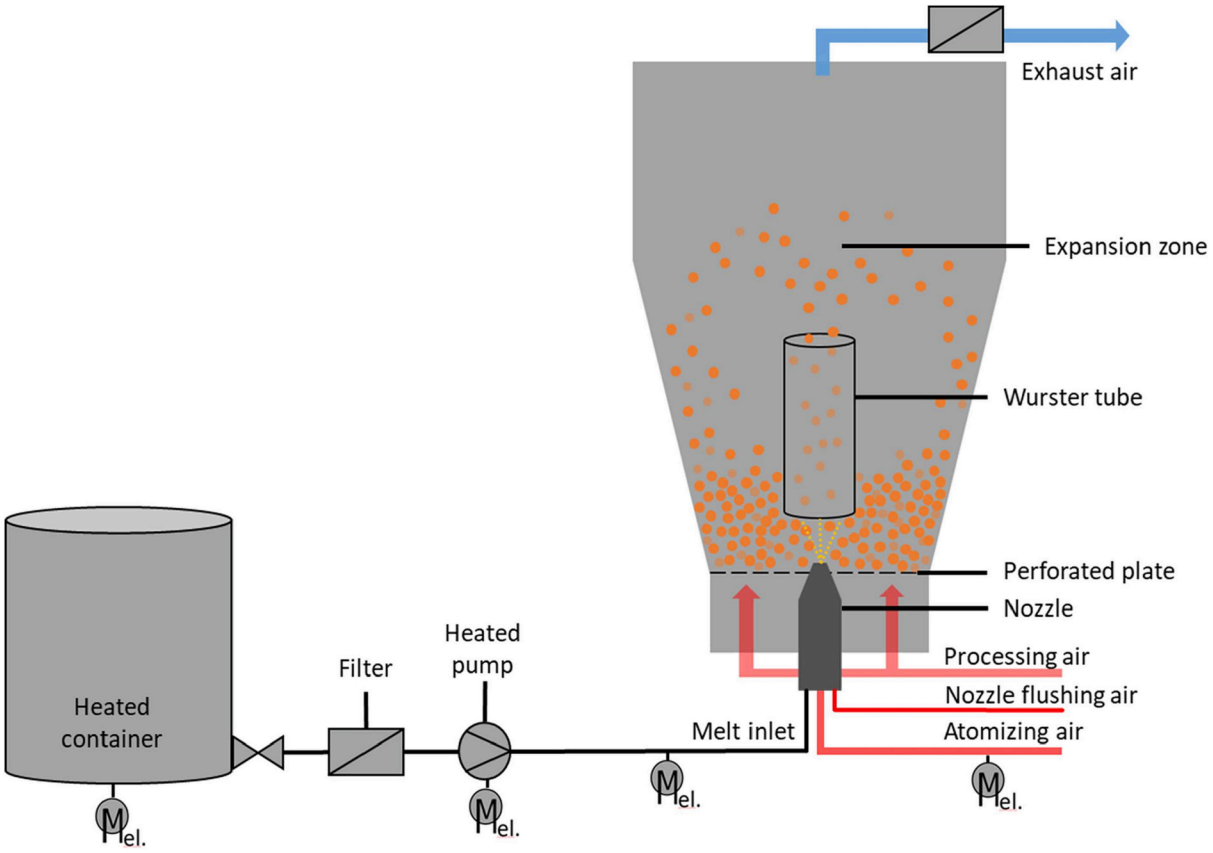

Fig. 1. Schematic setup of the hot-melt coating experiments [26].

Table 1
Process conditions for the hot-melt coating experiments.

Parameter/setting	WFP mini
Coating technique	Wurster fluidized bed
Wurster tube air gap [mm]	20
Particle amount [g]	300
Coating amounts [g]	45
Coating material temperature [°C]	100
Gas volume flow rate [m^3/h]	20
Nozzle atomizing pressure [bar]	1
Nozzle-flushing air pressure [bar]	0.5
Product temperatures [°C]	30; 35; 40
Spray rates [g/min]	3; 5; 10; 20

layer in a defined amount of sunflower oil, the emission of the solution can be measured in a fluorescence spectrometer. Since the emission of the solution correlates with the amount of fluorescent dye, the coating amount per coated particle can be calculated. Fig. 2 shows an abstract illustration of the method procedure.

For the method, the fluorescent dye ARAGEN-103 Orange (Aralon COLOR GmbH, Germany) is used as it is fat soluble, heat resistant and, in addition, there is no overlap of the excitation wavelength ranges between dye, palm fat or the solvent sunflower oil. The dye concentration is adjusted to a concentration of about 25 *mg per g* of coating material to ensure light emission in the linear analysis range of the fluorescence spectrometer (Cary Eclipse Fluorescence Spectrometer, Agilent Technologies, Inc., USA). Before and after each coating batch, the actual dye concentration is measured and used for further calculation. For screening many samples a microplate reader (Agilent Technologies Inc., USA) is additionally used. To ensure a significant sample size, 384 coated spheres per batch are analyzed. For this purpose, each of the spheres is placed in a single vial and heated up to 80 °C (15 min) with 500 µl sunflower oil to melt the coating layer off and dilute the fluorescent dye. Each solution of a particle is then transferred and measured in the microplate. Using the Cary Eclipse Advanced Reads analysis software, each sample was measured in triplicate. The exact

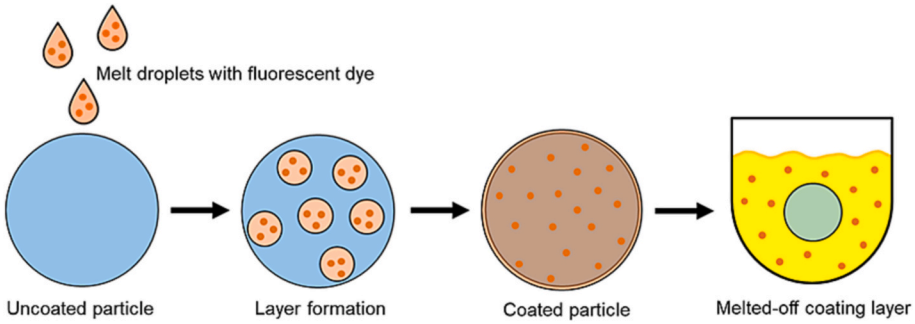

Fig. 2. Schematic illustration of the fluorescent coating batch homogeneity analysis.

measurement settings are listed in Table 2.

Further, based on the dye concentration, the coating material density, mean particle size, the coating amount per particle, the mean coating thickness per particle and the coefficients of variation as a measure of interparticle batch homogeneity are calculated.

2.2.2.4. Calculations of the palm fat amount and layer thickness per particle. The coating amount $m_{Coating,\ F}$ was determined for each particle with the fluorescent measured value F using the previously determined calibration (see Eq. (2)). Since the coating was dissolved in 0.4514 g sunflower oil, a dilution factor m_{oil} needs to be taken into account. Together with the known dye concentration c_{dye}, Eq. (3) is obtained.

$$F = m_{cal} \bullet x + t_{cal} \tag{2}$$

$$m_{Coating,F} = \frac{\frac{F - t_{cal}}{m_{cal}} \bullet m_{oil}}{c_{dye}} \tag{3}$$

The mean coating thickness $d_{Coating,\ F}$ of a particle can be calculated according to Eq. (4). Converting the amount of coating into a mean coating thickness per particle is intended to simplify the comparison with other methods and the interpretation of the experimental data. For this, the density of the palm fat coating ($\rho_{palm\ fat;25°C} = 1.0008 \frac{g}{cm^3}$) as well as the radius of an uncoated sugar sphere r_{SS} are additionally taken into account.

$$d_{Coating,F} = \left(\frac{3 \bullet m_{Coating,F}}{4\pi \bullet \rho_{palm\ fat}} + r_{SS}^3 \right)^{\frac{1}{3}} - r_{SS} \tag{4}$$

As can be derived from Eq. (4), the assumption is made that the particles are ideally spherical. To quantify the interparticle batch homogeneity, the coefficient of variation is used, which is a relative measure of scatter. The coefficient of variation is the ratio of the empirical standard deviation and arithmetic mean. To compare the measured distributions, they are presented as boxplots. The size of the box corresponds to the area where the middle 50% of the data is located while the whiskers show the ends of the fifth and ninety-fifth percentiles.

3. Results and discussion

3.1. Influence of the process temperature

3.1.1. Optical assessment

Coloring of the coating material with a fluorescent dye enables a quantitative determination of the coating amount on single particles. At the same time, optical differences of the coated particles can be more easily perceived due to the coloring. Fig. 3 shows three samples, which differ from each other only in the applied process temperature.

Sample Batch 3, which was prepared at a temperature of 30 °C (Fig. 3 left), appears significantly brighter and not homogeneous. Individual sugar spheres are colored orange, while others have hardly received any coating material and are still white. Furthermore, a large amount of dust was observed on the container wall after the process (see Fig. 3 bottom left). Comparing the sample with the other two samples, which were coated at higher product temperatures (Fig. 3 middle and right), it can be seen that the color intensity of the spheres increases, as does the batch homogeneity. Sample Batch 8 (40 °C) shows the most intense orange color (see Fig. 3 top right) and at the same time the lowest dust content on the container wall (see Fig. 3 bottom right).

It seems that the selected process temperatures that are too low lead to a crystallization effect and less coating amount is applied to the particles. This has already been observed in other studies [12]. For palm fat coatings, for example, we showed that a process temperature of 40 °C in a fluidized bed is advantageous over cooler temperatures [13]. For 30 °C process temperature, the mean yield was 85.8%, for 35 °C 93.9%, and for 40 °C, 95.9% for a spray rate of 3 g/min (see Table 4 in the Appendix). Accordingly, the optical assessment already gives a good first impression, but cannot provide an accurate and quantitative statement regarding the interparticle batch homogeneity.

Table 2
Measurement parameters of the fluorescent spectroscopy.

Parameter	Value
Excitation wavelength [nm]	543
Emission wavelength [nm]	585
Excitation slit [nm]	5
Emission slit [nm]	5
Average measuring time [s]	2
PMT voltage [V]	650
Excitation filter	Auto
Emission filter	Open
Software	Cary Eclipse Advanced Reads
96 microplate white	Nunc A/S, Denmark

3.1.2. QICPIC/R

A common technique for the characterization of encapsulated particles is particle size analysis. For this purpose, the particle size distribution of coated and uncoated particles is measured. The change in particle size distribution can subsequently provide information about the coating layer thickness but also about the batch homogeneity. Fig. 4 shows the sum curves of uncoated and coated particles as a function of process temperature.

Fig. 4 shows that the particle size distributions have shifted and the particles have become larger as a result of the process. At the same time, the curves have not changed significantly, indicating that the individual particle size classes have grown uniformly and that no particle breakage or excessive agglomeration has occurred during the process. In this case, the average particle layer thickness can be determined by the difference in the diameters of uncoated and coated particles. On average, the mean particle layer thicknesses of 13.8 µm (30 °C), 26.7 µm (35 °C) and 28.6 µm (40 °C) were determined for the trails with a varied process temperature. The results thus support the first visual impression after the process. Particles coated at a higher process temperature but with the same coating amount grew more and exhibited greater film thickness. The average particle layer thickness from QICPIC/R is based in each case on a particle count of 10,000 particles and thus has a high statistical significance. Nevertheless, it bears the risk of misinterpretation and cannot provide complete information about the layer structure. Since it is an optical 2-dimensional method that does not examine the three-dimensional nature of the particle, no information about the coating uniformity of a single particle is provided. In addition, common HMC phenomena such as delamination, pores or inclusions in the coating layer can make the analyzed particles appear larger and lead to misinterpretation [13].

3.1.3. Micro-computed X-ray tomography for layer thickness distribution measurements

In addition to the particle size measurements, µCT is a suitable method for examining the coating structure of individual particles to provide more information about the coating layer thickness uniformity [25,26,33]. µCT measurements enable a non-destructive investigation of a sample with a high information density. For coated particles, for example, the coating layer structure can be examined in great detail. In addition to the mean layer thickness, the layer thickness uniformity, the delamination tendency, the non-covered surface proportion [13,26] or the layer porosity [33] of a particle can be determined. Fig. 5 shows the cumulative curves of the determined layer thickness distributions of three randomly selected particles in each of the process temperatures of 30 °C (Batch 3), 35 °C (Batch 5) and 40 °C (Batch 8).

Each of the cumulative curves shown in Fig. 5 is based on 2400 coating thickness values and shows, besides the coating layer thickness distribution, the non-covered surface proportion on a single particle too. As shown in Fig. 5, the cumulative curves of the coating layer thickness

Fig. 3. Coated product and fluidized bed reactor after the 30 °C (left, Batch 3), 35 °C (middle, Batch 5) and 40 °C (right, Batch 8) coating processes.

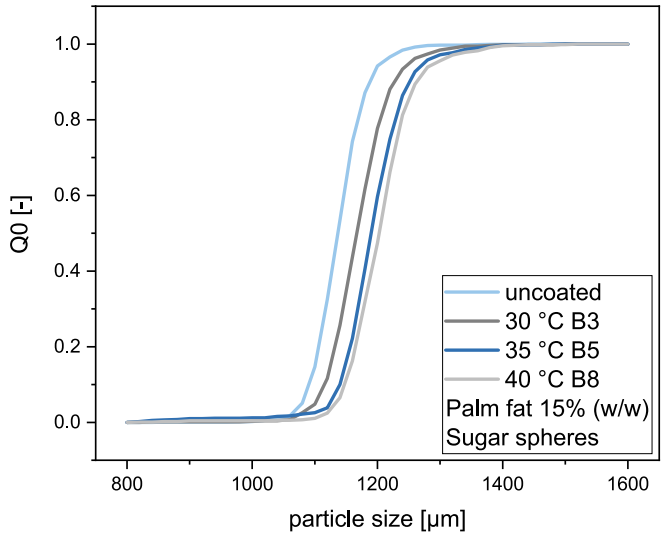

Fig. 4. Particle size distributions of uncoated and coated particles depending on the process temperature.

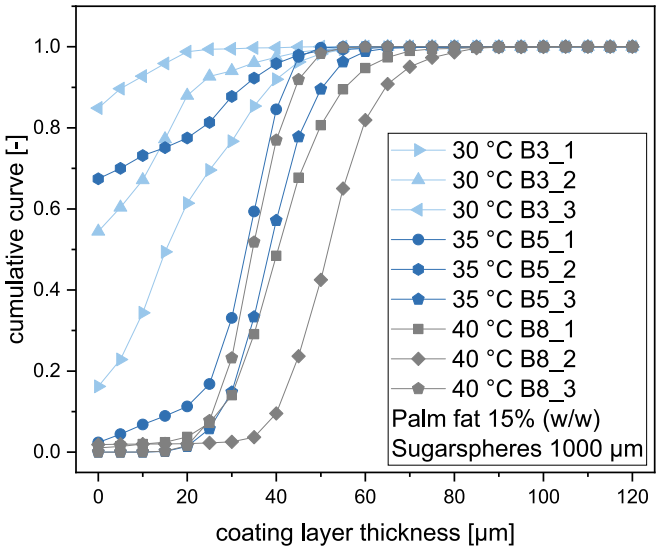

Fig. 5. Cumulative curves of the layer thickness distribution of single particles as a function of the process temperature.

values on a single particle differ significantly from each other in some cases, although all nine particles were coated with the same coating amount. Table 3 summarizes the results of the µCT evaluation of the nine particles investigated. The three particles coated at 30 °C were not fully coated and also differed from each other in their layer thickness distribution. However, higher process temperatures of 35 and 40 °C resulted in thicker coating layers and in less non-covered surface. In addition, the steeper curves of the 40 °C samples show that the particle coating is more uniformly applied, which is especially important for the functionality of a coating [6]. The coefficient of variation, which is the ratio of the empirical standard deviation and the arithmetic mean layer thickness, allows the uniformity of the coating to be captured. The values between 0.2 and 0.3 show that the particles coated at 40 °C are more uniformly coated (see Table 3).

A comparison of the mean layer thicknesses of the particles also indicates that the interparticle batch homogeneity is more even at higher process temperatures. However, the method is limited to statements on interparticle batch homogeneity. For conclusions on the interparticle batch homogeneity, a significantly larger sample size is necessary, which, however, would be disproportionate to the measurement effort and costs. In addition, the method is limited in its resolution - in this case 2 µm - and by the material properties of the core particle and the coating material. X-ray absorption depends on the nuclear mass and packing density. If the carrier and coating material do not differ significantly in these material properties, tomographic analysis is not possible. µCT measurements are therefore not applicable for every sample type. For the coating of sugar spheres with hydrogenated palm oil, the method

Table 3
µCT evaluation results.

	Mean particle layer thickness	Mean layer thickness	Non-covered surface proportion	Coefficient of variation
	[µm]	[µm]	[%]	[–]
30 °C B3_1	17.8	21.3	16.21	0.67
30 °C B3_2	7.6	16.7	54.47	0.67
30 °C B3_3	1.6	10.6	84.89	0.46
35 °C B5_1	31.4	32.1	2.38	0.32
35 °C B5_2	8.4	25.9	67.45	0.56
35 °C B5_3	38.8	38.8	0.00	0.23
40 °C B8_1	40.6	41.1	1.06	0.30
40 °C B8_2	51.4	52.4	1.87	0.23
40 °C B8_3	34.9	34.9	0.00	0.20

works well, though. In this case, µCT measurements are a very useful tool for assessing quality, especially for analyzing the coating layer structure. However, besides the layer structure of single particles, the interparticle batch homogeneity is also decisive for the final product performance. Therefore, a new, simple and statistically robust method is used to provide a supplementary statement on the interparticle batch homogeneity of HMC.

3.1.4. *Fluorescent batch homogeneity analysis*

To investigate the interparticle batch homogeneity, 384 individual particles per batch were analyzed for their dye concentration in a fluorescence spectrometer. For each measured emission value, a melt quantity can be calculated via a previously created dilution series. Fig. 6 shows an example of the resulting distribution of the coating amount values of batch 5 as a histogram.

The coating amount distribution resembles a normally distributed curve and shows that different amounts have been applied to the particles. For further evaluation and interpretation of the data, the respective coating amount on a particle is converted into an ideal layer thickness. Fig. 7 shows the layer thicknesses of Batches 1–9 determined from fluorescence spectrometry as a function of temperature and in the form of boxplots.

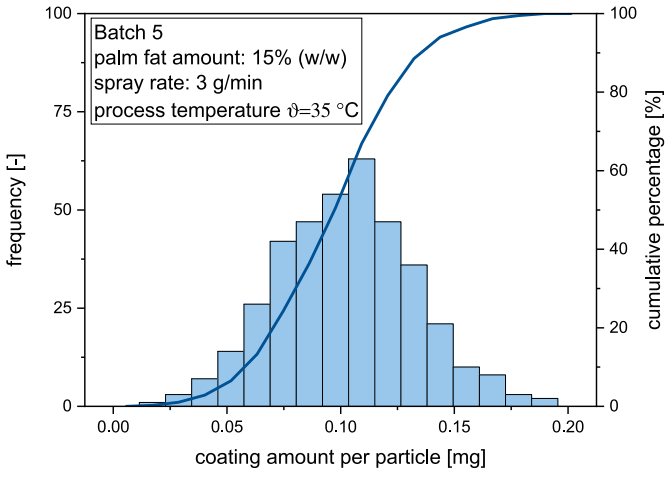

Fig. 6. Distribution of the coating amount of Batch 5.

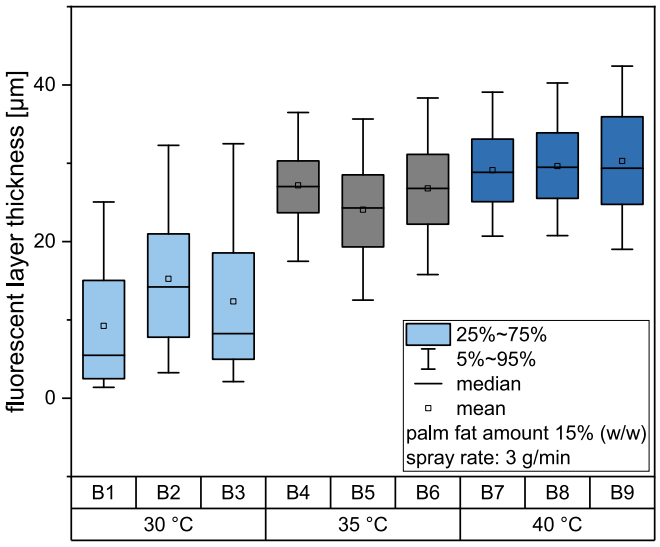

Fig. 7. Fluorescence layer thickness results as a function of the process temperature.

The fluorescence layer thicknesses show a trend as a function of the process temperature. The higher the process temperature, the more coating amount could be applied to the sugar spheres. As already suggested by the optical evaluation, the yields, particle size analyses and µCT measurements and results in Fig. 7 also indicate that low process temperatures lead to less applied palm fat on the particles. One explanation for this is overspray, more specifically the crystallization effect. Low temperatures lead to crystallization, where the melt crystallizes before particle contact and thus cannot adhere to the core particle.

Furthermore, several studies have shown that delamination of the coating layer can be a typical structural phenomenon for hot-melt coating [12,13,26]. Delamination is defined as the detachment of a coating layer from the carrier particle. In previous studies, we found an increased delamination tendency for a process temperature of 35 °C compared to 40 °C for palm fat hot-melt coatings [14]. A process temperature of 35 °C resulted in 92.9% of the particles having delaminated domains. An increase in temperature to 40 °C reduced the proportion of delaminated particles to 50.3% [14]. A correlation between delamination tendency and process temperature and material properties could be shown [13,14]). Both overspray and delamination lead to less applied coating amount. Broad distributions at a lower temperature were therefore to be expected. At the same time, the multiple determinations also indicate an increasing process reproducibility at higher process temperatures, which can be taken from Fig. 7 and Fig. 8. One advantage of the fluorescence measurement method is the method's independence against delamination, since the coating amount is determined. Moreover, the method is robust against any volume-changing phenomena of the coating layer. However, this does not apply to particle size measurements, where delamination leads to a false image of the particle size and makes it appear larger, thus suggesting a larger coating thickness. Fig. 8 shows the mean film thicknesses from the particle size measurements as well as the calculated film thicknesses and coefficients of variation from the fluorescence method as a function of process temperature. Values that are above each other on the vertical axis refer to the same batch.

It is notable that the coating thickness results of the methods differ less as process temperature increases. At the same time, Fig. 8 shows that the values of the fluorescence method for 30 and 35 °C tend to be slightly lower than those of the particle size analysis. However, this can be explained by the temperature-dependent delamination tendency of palm fat, which is higher at lower temperatures.

The coefficient of variation, which is a measure of scattering, is lower

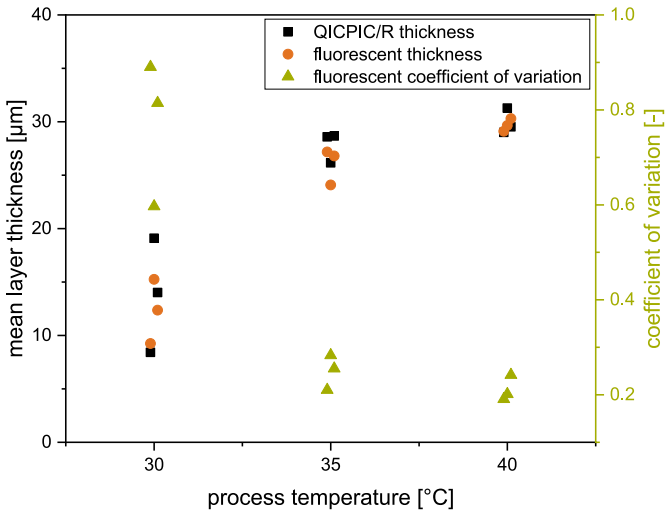

Fig. 8. Comparison of the results from particle size measurement and the fluorescence coating amount determination.

for higher process temperatures, i.e. the interparticle batch homogeneity is higher, since the coating amounts differ less from each other. This observation also fits with the studied delamination behavior of Woerthmann et al. (2022) and the coefficients of variation of the µCT values (see Table 3) [13]. Accordingly, a higher process temperature leads to less delamination, increases the intraparticle coating thickness uniformity, the process reproducibility and also improves the interparticle batch homogeneity. Van Kampen's observations from statistical models support these conclusions. Less overspray increases the yield and leads to higher interparticle batch homogeneity and coating quality [16].

3.2. *Influence of the spray rate on the interparticle batch homogeneity*

In addition to the process temperature, other process parameters such as the spray rate can also be investigated by the fluorescence method. To investigate the influence of the spray rate on the interparticle batch homogeneity, the parameters of process temperature (40 °C), fluidization, and coating amount (15% *w*/w) were kept constant. The spray rate, in contrast, was varied between 3 g/min and 20 g/min. Fig. 9 shows the calculated film thickness distributions of the fluorescence

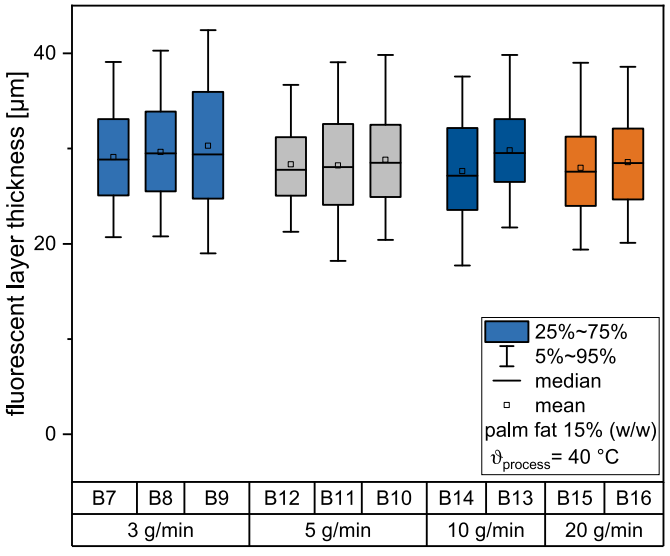

Fig. 9. Influence of the spray rate on the interparticle Batch homogeneity.

measurements in the form of boxplots.

As shown in Fig. 9, the distributions do not differ significantly from each other. Consequently, the spray rate does not seem to be a major influence factor on the interparticle batch homogeneity. This is also confirmed by the related coefficients of variation, which are listed in Table 4 in the Appendix.

However, at a spray rate of 20 g/min, the beginning of agglomeration of individual particles could be observed. High spray rates add more heat to the process, which can affect the crystallization of the coating material. At the same time, the tendency for agglomeration is also increased by larger droplet sizes. Since the atomization pressure was kept constant, less kinetic energy is available for atomizing the coating material, resulting in larger droplets. Therefore, high spray rates are not advisable without an additional adaption of the atomization pressure and fluidization. Spray rates of <3 g/min can be set, but this unnecessarily extends process time and increases the risk of a crystallization effect and increased overspray.

In total, the results are surprising, since an influence of the spray rate on the batch homogeneity was expected. In theory, low spray rates lead to smaller droplet sizes and a longer process time. This is expected to result in a uniform coating layer and a high batch homogeneity. In contrast, larger droplets crystallize more slowly, resulting in longer wetting and spreading of the droplets, which can, however, also lead to a uniform coating layer. At the same time, slow crystallization can conceivably lead to an exchange of coating material among particles, which would possibly improve the interparticle batch homogeneity but also drastically increase the agglomeration tendency. The results show that for a good process parameter setting for high batch homogeneity of hot-melt coatings, the combination of process temperature and spray rate should be considered. Overall, however, the coating quality is not only affected by the process parameters spray rate and process temperature, but results from a complex interaction of all process parameters and the respective material properties. Therefore, detailed knowledge of the material properties as well as of the complex relationships between the different process parameters is necessary for the production of high-quality coatings. As the results show, the three methods presented complement each other in their respective informative content, allowing them to contribute to a better understanding of the complexity of the hot-melt coating application.

4. Conclusion

In this study, three different methods for assessing the interparticle batch homogeneity were tested and evaluated. A common method for studying coating quality are particle size measurements where a large number of particles can be analyzed in a short period of time. However, its validity is limited to spherical particles with an ideal coating structure, i.e. without pores, delaminations or inclusions. Thus, for coatings with layer structure phenomena such as delamination, there is a high risk of misinterpretation. Especially for hot-melt coatings, delamination can occur and coated particles might seem to be larger than they really are, thereby affecting data interpretation. µCT was confirmed to be an excellent method for analyzing the coating layer structure of a single particle. It is suitable to provide complementary and detailed insights about the layer structure, such as non-covered surface proportion, layer thickness distribution, and layer porosity. Furthermore, µCT measurements allow the analysis of layer structure phenomena such as inclusions or delamination. Consequently, µCT analyses enable the prevention of misinterpretation of experimental data, making conclusions drawn less prone to error. However, it is limited for the investigation of interparticle batch homogeneity due to the time-consuming and costly measurement procedure and is therefore not suitable to investigate a large number of particles. Fluorescence spectroscopy, in contrast, is suitable for analyzing a large number of particles. Further, fluorescence spectroscopy is particularly suitable for products with such structural phenomena, since the applied coating amount per particle is

analyzed using a fluorescent dye. The method presented is thus robust against all layer structure phenomena such as pores, inclusions or delamination and is particularly suitable for the investigation of process parameters influencing the batch homogeneity of hot-melt coatings. Although the fluorescent method is based on a destructive analysis, it can nonetheless provide valuable information for a systematic process understanding of HMC.

Overall, the results of the different methods were consistent and complementary in their respective information content for data interpretation and drawing conclusions for improving interparticle batch homogeneity and systematic process understanding.

Author statement

B.M. Woerthmann: Conceptualization, Methodology, Formal analysis, Data curation, Execution of experiments, Data interpretation, Writing - original draft, Project administration.

J. Gerber: Execution of experiments, Methodology.

A. Hoffmann: Execution of experiments.

T. Wittkamp: Execution of experiments, Methodology.

H. Briesen: Writing – review and editing, Conceptualization, Data interpretation, Project administration.

Declaration of Competing Interest

The authors declare that they have no known competing financial interests or personal relationships that could have appeared to influence the work reported in this paper.

Data availability

The data that has been used is confidential.

Acknowledgments

This research was supported by the Ministry of Economics and Climate (BMWK) via AiF and the FEI (Forschungskreis der Ernährungsindustrie e.V., Bonn) Project AiF 19970 N. Equipment funded by the Deutsche Forschungsgemeinschaft (DFG, German Research Foundation)–198187031 was used in this study.

Appendix A

Table 4
Overview of the experiments and results.

Batch number [−]	Coating material [−]	Coating amount [%]	Process temperature [°C]	Spray rate [g/min]	Process time [s]	Yield [%]	QICPIC/R mean layer thickness [μm]	Fluorescent mean layer thickness [μm]	Fluorescent coefficient of variation [−]
B 1	palm fat	15	30	3	900	87.16	8.42	9.24	0.89
B 2	palm fat	15	30	3	900	84.52	19.09	15.25	0.60
B 3	palm fat	15	30	3	900	85.90	14.01	12.36	0.81
B 4	palm fat	15	35	3	900	94.43	28.58	27.18	0.21
B 5	palm fat	15	35	3	900	92.89	26.16	24.08	0.28
B 6	palm fat	15	35	3	900	94.54	28.66	26.79	0.26
B 7	palm fat	15	40	3	900	96.08	29.00	29.11	0.19
B 8	palm fat	15	40	3	900	96.07	31.28	29.64	0.20
B 9	palm fat	15	40	3	900	95.50	29.53	30.30	0.24
B 10	palm fat	15	40	5	540	97.04	28.27	28.33	0.17
B 11	palm fat	15	40	5	540	96.75	26.23	28.22	0.23
B 12	palm fat	15	40	5	540	96.82	26.18	28.82	0.21
B 13	palm fat	15	40	10	270	97.32	27.19	27.63	0.22
B 14	palm fat	15	40	10	270	96.85	25.98	29.81	0.19
B 15	palm fat	15	40	20	135	96.55	25.52	27.95	0.21
B 16	palm fat	15	40	20	135	96.49	26.46	28.55	0.20

References

[1] A.S. Achanta, P.S. Adusumilli, K.W. James, C.T. Rhodes, Development of hot melt coating methods, Drug Dev. Ind. Pharm. 23 (2008) 441–449.
[2] L. Mörl, S. Heinrich, M. Peglow, Fluidized bed spray granulation, in: A. Salman, M. Hounslow, J.P.K. Seville (Eds.), Granulation vol. 11, Elsevier Science, Amsterdam, The Netherlands, 2007, p. 1402.
[3] V. Jannin, Y. Cuppok, Hot-melt coating with lipid excipients, Int. J. Pharm. 457 (2013) 480–487.
[4] N. Gontard, S. Marchesseau, J.-L. Cuq, S. Guilbert, Water vapour permeability of edible bilayer films of wheat gluten and lipids, Int. J. Food Sci. Technol. 30 (1995) 49–56.
[5] M. Kumpugdee-Vollrath, J.-P. Krause, Easy Coating, 2011.
[6] D. Markl, M. Zettl, G. Hannesschläger, S. Sacher, M. Leitner, A. Buchsbaum, J. G. Khinast, Calibration-free in-line monitoring of pellet coating processes via optical coherence tomography, Chem. Eng. Sci. 125 (2015) 200–208.
[7] Y. Dong, H. Lin, V. Abolghasemi, L. Gan, J.A. Zeitler, Y.-C. Shen, Investigating intra-tablet coating uniformity with spectral-domain optical coherence tomography, J. Pharm. Sci. 106 (2017) 546–553.
[8] M. Goslinska, S. Heinrich, Characterization of waxes as possible coating material for organic aerogels, Powder Technol. 357 (2019) 223–231.
[9] D.G. Lopes, K. Becker, M. Stehr, D. Lochmann, D. Haack, A. Zimmer, S. Salar-Behzadi, Role of lipid blooming and crystallite size in the performance of highly soluble drug-loaded microcapsules, J. Pharm. Sci. 104 (2015) 4257–4265.
[10] K. Chansanroj, G. Betz, H. Leuenberger, A. Mitrevej, N. Sinchaipanid, Polymorphic change of a triglyceride base in hot melt coating process and stability acceleration by tempering process, J. Drug Deliv. Sci. Technol. 17 (2007) 347–352.
[11] K. Becker, S. Salar-Behzadi, A. Zimmer, Solvent-free melting techniques for the preparation of lipid-based solid oral formulations, Pharm. Res. 32 (2015) 1519–1545.
[12] M.G. Müller, J.A. Lindner, H. Briesen, K. Sommer, P. Foerst, On the properties and application of beeswax, carnauba wax and palm fat mixtures for hot melt coating in fluidized beds, Adv. Powder Technol. 29 (2018) 781–788.
[13] B.M. Woerthmann, L. Totzauer, H. Briesen, Delamination and wetting behavior of natural hot-melt coating materials, Powder Technol. 404 (2022), 117443.
[14] B.M. Woerthmann, H. Briesen, Schmelzcoating - Nutzung von μCT-Daten zur gezielten Erzeugung homogener Schichtstrukturen, Lampertheim, Der Lebensmittelbrief – ernährung aktuell, 2022, pp. 33–36.
[15] S.G. Sudke, D.M. Sakarakar, Hot-melt coating: an innovative pharmaceutical coating technique, J. Pharm. Res. Clin. Pract. 3 (2013) 16–26.
[16] A. van Kampen, R. Kohlus, Statistical modelling of coating layer thickness distributions: influence of overspray on coating quality, Powder Technol. 325 (2018) 557–567.
[17] H. Wang, G. Qiu, J. Ye, W. Yang, Experimental study and modelling on gas–solid flow in a lab-scale fluidised bed with Wurster tube, Powder Technol. 300 (2016) 14–27.
[18] G. Heinicke, J.B. Schwartz, Particle size distributions of inert spheres and pelletized pharmaceutical products by image analysis, Pharm. Dev. Technol. 9 (2004) 359–367.

[19] P. Bachmann, K. Chen, A. Bück, E. Tsotsas, Prediction of particle size and layer-thickness distributions in a continuous horizontal fluidized-bed coating process, Particuology 50 (2019) 1–12.
[20] F.L. Laksmana, L.J. van Vliet, P.J.A. Hartman Kok, H. Vromans, H.W. Frijlink, K. van der Voort Maarschalk, Quantitative image analysis for evaluating the coating thickness and pore distribution in coated small particles, Pharm. Res. 26 (2009) 965–976.
[21] F. Sondej, A. Bück, E. Tsotsas, Comparative analysis of the coating thickness on single particles using X-ray micro-computed tomography and confocal laser-scanning microscopy, Powder Technol. 287 (2016) 330–340.
[22] S. Pietsch, A. Peter, P. Wahl, J. Khinast, S. Heinrich, Measurement of granule layer thickness in a spouted bed coating process via optical coherence tomography, Powder Technol. 356 (2019) 139–147.
[23] D. Markl, G. Hannesschläger, S. Sacher, M. Leitner, J.G. Khinast, Optical coherence tomography as a novel tool for in-line monitoring of a pharmaceutical film-coating process, Eur. J. Pharm. Sci. 55 (2014) 58–67.
[24] H. Lin, R.K. May, M.J. Evans, S. Zhong, L.F. Gladden, Y. Shen, J.A. Zeitler, Impact of processing conditions on inter-tablet coating thickness variations measured by terahertz in-line sensing, J. Pharm. Sci. 104 (2015) 2513–2522.
[25] G. Perfetti, E. van de Casteele, B. Rieger, W.J. Wildeboer, G.M.H. Meesters, X-ray micro tomography and image analysis as complementary methods for morphological characterization and coating thickness measurement of coated particles, Adv. Powder Technol. 21 (2010) 663–675.
[26] B.M. Woerthmann, J.A. Lindner, T. Kovacevic, P. Pergam, F. Schmid, H. Briesen, A novel method for assessing the coating uniformity of hot-melt coated particles using micro-computed tomography, Powder Technol. 378 (2021) 51–59.
[27] S.A. Schiele, F. Antoni, R. Meinhardt, H. Briesen, Analysis of nonideal shape evolution during potash alum crystallization using microcomputed tomography and three-dimensional image analysis, Cryst. Growth Des. 21 (2021) 1751–1761.
[28] S. Schmideder, L. Barthel, T. Friedrich, M. Thalhammer, T. Kovačević, L. Niessen, V. Meyer, H. Briesen, An X-ray microtomography-based method for detailed analysis of the three-dimensional morphology of fungal pellets, Biotechnol. Bioeng. 116 (2019) 1355–1365.
[29] L. Schoeman, P. Williams, A. Du Plessis, M. Manley, X-ray micro-computed tomography (μCT) for non-destructive characterisation of food microstructure, Trends Food Sci. Technol. 47 (2016) 10–24.
[30] R. Šibanc, M. Turk, R. Dreu, An analysis of the mini-tablet fluidized bed coating process, Chem. Eng. Res. Des. 134 (2018) 15–25.
[31] J. Shen, 3D Bresenham's line generation, in: MATLAB Central File Exchange, 2020.
[32] P. Hammer, Marching Cubes. https://www.mathworks.com/matlabcentral/fileexchange/32506-marching-cubes, 2020. Accessed Retrieved 21 March 2020.
[33] F. Sondej, A. Bück, K. Koslowsky, P. Bachmann, M. Jacob, E. Tsotsas, Investigation of coating layer morphology by micro-computed X-ray tomography, Powder Technol. 273 (2015) 165–175.

Chapter 6

Discussion and concluding remarks

HMC, as a solvent-free coating technology in a fluidized bed, is a suitable technology to meet the growing industrial requirements. The increasing demand for foods with functional properties can be met with the help of coating technology. In the food industry, for example, value-giving ingredients such as flavors or herbs can be protected from oxidation or released in a controlled manner. In addition, hygroscopic substances such as icing sugar or citric acid can be protected from moisture by the hydrophobic coating layer, or unpleasant taste components can be masked. In addition to functional applications, natural HMC offers advantages over solvent-based coatings, especially regarding sustainability and environmental compatibility. The omission of water and organic solvents used in solvent-based coating avoids time-consuming and costly steps such as solvent evaporation and residue analysis and reduces microbial risk. Moreover, higher spray rates speed up the process. Another advantage is that coating in a fluidized bed allows a wide range of particle sizes, from a few microns to tablet size. Additionally, a wide range of adjustable process parameters enables controlled layer formation.

Nevertheless, there are drawbacks to natural HMC with fats and waxes. These include the complex crystallization behavior of the natural coating materials and the complex relationships with process parameters. Particularly in the case of food products, the properties of the core material need to be especially considered. These include the following properties: particle size distribution (PSD) (Atarés et al., 2012; Faham et al., 2000; Iley, 1991; J.R. Davis & Associates and ASM International, 2004; Savini, 1998), porosity (Iley, 1991; Kennedy and Niebergall, 1996; Srivastava and Mishra, 2010), density (Jannin and Cuppok, 2013), shape (Iley, 1991; Jannin and Cuppok, 2013), surface roughness (Lin and Krochata, 2006; Rajesh et al., 2012), and substrate stability (Cobb et al., 2013; Jannin and Cuppok, 2013; Prasad et al., 2013).

Producing satisfying product quality and reproducibility is challenging due to the large number of dependencies and interrelationships. Facilitating extra steps, such as granulation to improve PSD or flowability, is rarely used due to additional costs. This is why material properties and process parameters need to be even better harmonized to produce high-functional coatings.

The functionality of coatings is directly related to the uniformity of the layer structure and the interparticle batch homogeneity. Therefore, the need for analysis possibilities and methods to investigate layer structures is enormous in industry and research. The need for detailed experimentally obtained data and information on the uniformity of the layer structure and homogeneity of the batch is high (Dong et al., 2017; van Kampen et al., 2015). For example, recent studies increasingly focus on the systematic process understanding through modeling or numerical simulations. However, without high-precision experimental data, the potential of modeling and simulations cannot be fully exploited (van Kampen and Kohlus, 2018; Wang et al., 2016). New developments and improvements in measurement technologies for analyzing inner-layer structures allow us to gain even deeper insights. As a result, they can be the critical factor in meeting the increasing demand for detailed information for modeling and simulations. Confocal laser scanning microscopy (CLSM) (Laksmana et al., 2009; Sondej et al., 2016), optical coherence tomography (OCT) (Markl et al., 2014; Markl et al., 2015; Pietsch et al., 2019), terahertz pulse imaging (TPI) (Lin et al., 2015), neutron imaging (Gruber et al., 2020) or micro-computed tomography (µCT) (Müller et al., 2018; Perfetti et al., 2010) are among these modern measurement techniques.

It is important to keep in mind that the measurement data may differ significantly depending on the measurement technique. Firstly, with the CLSM, for example, the layer thickness analysis is a destructive test with a complex and error-prone sample preparation. Data collected with a CLSM are obtained from a 2D sectional plane. A statement about the entire intraparticle uniformity is, therefore, not possible.

Secondly, OCT is a contact-free and non-destructive high-resolution imaging technique based on low-coherence interferometry, which can already be used in-line for process monitoring (Markl et al., 2015). However, Markl et al. (2015) used solvent-based coatings in their study, which are only analyzed pointwise or in a measuring line when determining the coating layer thickness in-line. Although this ensures fast data processing, providing a statement on the interparticle batch homogeneity, it limits the information content since only the layer thickness can be determined. A complete 3D image layer structure analysis with statements regarding layer porosity or the occurrence of delamination cannot be offered.

Thirdly, µCT images have already been successfully acquired for HMC products by Müller et al. (2018). µCT measurements are non-destructive and high-resolution. Although µCT in-line measurements cannot yet be carried out for HMC processes at the current state of the art, the measurement technology enables complete 3D off-line image

analysis. The requirements for precise 3D analyses of the coating layer structure without loss of information about intraparticle layer thickness uniformity are thus met.

Besides further developments in the field of measurement technologies, additional developments in methods for data processing are also required.

Development of a 3D µCT analysis method to study intraparticle coating layer thickness uniformity.

3D µCT layer structure analyses can obtain data with a very high information density. Compared to 2D analyses, 3D analyses are much more complex and challenging. Within the scope of this thesis, a method was developed to investigate the coating layer of HMC particles and the intraparticle layer thickness uniformity.

Developing the published analysis method had several challenges and limitations (Woerthmann et al., 2021). One of the biggest challenges was to find the correct measurement parameters (e.g., resolution, exposure time, etc.) to achieve a satisfying image quality with proper contrast between the core and coating material. A high resolution is necessary to access detailed information about the layer structure. A resolution of 2 µm turned out to be practicable. However, a high resolution leads to long measurement times (approx. 4 hours) and massive data volumes in the mid-two-digit gigabyte range. Also, the measurement zone became relatively small, meaning only one particle per measurement could be placed on the sample holder. As a result, the number of analyzed particles was severely limited due to the measurement effort and the additional time-consuming evaluation. Statements about the interparticle batch homogeneity were impossible due to the limited number of samples.

Unfortunately, saving time by analyzing several particles at once, analogous to what Müller et al. (2023) did with fungal pellets, was impossible for several reasons. Firstly, a lower resolution would have had to be chosen for a larger measuring zone. Less accurate data would have been the result. Secondly, an automated segmentation of the particles would not have worked. Unlike fungal pellets, coated particles consist of at least two materials. However, a sharp contrast of the materials is not given because several particles in the measuring zone cause shadowing effects of the X-ray radiation, reducing image quality. Consequently, a single-particle analysis with a longer, more accurate data generation was chosen.

The novel developed method enables a high-precision, non-destructive analysis of melt-coated particles, allowing the layer thickness distribution and the non-covered surface proportion to be determined. As part of the study, Woerthmann et al. (2021)

demonstrated different intraparticle layer thickness uniformities of palm fat and stearin and underlined the importance of the individual adjustment of process parameters. The method is, therefore, suitable for the systematic investigation of various process influencing factors on intraparticle coating thickness uniformity, contributes to a better understanding of the process, and can make a significant contribution to the production of highly functional coatings.

In addition, the layer thickness information obtained with 3D-µCT analysis proved to help interpret measurement data from standard methods such as particle size analysis. The combination with other methods allows identifying process-influencing factors, enabling more systematic process optimization. Structural phenomena such as delamination have been observed sporadically.

Delamination and microstructural changes in the coating layer are known phenomena in coating applications (Müller et al., 2018; Woerthmann et al., 2021). Very little is known about influencing factors or correlations of the delamination phenomenon. No scientific literature can be found regarding the frequency of delamination in HMC applications.

First-time quantification of delamination frequency of hot-melt coatings via 3D-µCT-Analysis.

Non-destructive 3D-µCT analysis provided first-time insights into the delamination probability and its dependencies. Quantifying the delamination probability with the newly established method as a function of several coating materials indicated a correlation with material properties. A substantial influence of the coating material on the delamination probability of the coating layer was observed. Hydrogenated palm oil, in particular, showed a high susceptibility to delamination, especially compared to waxes such as rice bran wax or carnauba wax. Accordingly, a material dependency seems likely (Woerthmann et al., 2022).

Different wetting behavior of the coating materials was suspected as the main influencing factor. The wetting behavior was investigated using a drop shape analyzer to elucidate a possible relationship between delamination behavior and wetting behavior. However, the study did not confirm this. All tested materials showed good wetting properties.

Although the 3D-µCT analysis proved to be suitable for the investigation of delamination, the exact influencing factors and dependencies remain unknown to avoid delamination through controlled process control. Besides the wetting properties, different mechanical stabilities, different thermal expansion coefficients of the coating materials, or post-

process nano- and microstructural changes due to recrystallization or blooming could be responsible for the delamination and cracking of the coating layer.

In further investigations, Woerthmann and Briesen showed that the delamination probability depends not only on the coating material but also on the process temperature and, thus, the process design (Woerthmann and Briesen, 2022a, 2022b). Increasing the process temperature of a palm fat coating resulted in a reduction in delamination frequency. This suggests less of a connection with the mechanical properties of the coating material and more of a relationship with thermal expansion or crystallization behavior. Considering the differences in delamination behavior between lipids and waxes, the differences in the compositions, and findings from crystallization studies, a correlation between delamination behavior and crystallization behavior is evident.

Hydrogenated vegetable oils are mainly composed of trisaturated TAGs, whereas waxes are primarily composed of esters, such as alcohol, aliphatic and aromatic esters, wax acids, and free fatty acids (Dassanayake et al., 2009; Lin, 2011; Timms, 1984; Vali et al., 2005; Vandenburg and Wilder, 1970). The crystallization behavior of TAGs in food applications has been intensively studied in scientific literature but not in the context of HMC. Natural fats such as cocoa butter, hydrogenated vegetable oils, or milk fat have complex and varying compositions. Consequently, derivations and interpretations are challenging to transfer to the HMC process, resulting in the fact that correlations can hardly be drawn regarding the coating layer structure.

In comparison, studies from the field of pharmaceutical research indicate (Becker, 2016; Chansanroj et al., 2007; Lopes et al., 2015; Lopes et al., 2017) a correlation with the crystallization behavior of natural coating materials. For instance, scientific studies by Lopes et al. (2015) and Chansanroj et al. (2007) show an influence of crystallization behavior on the nanostructure of TAGs. Rapid cooling processes lead to thermodynamically unstable α-crystals, which tend to recrystallize towards more stable β'- or β-crystals. Different dissolution kinetics were observed and could be influenced by adapted temperature control and an additional tempering step. The influence of delamination, however, was not investigated.

Consequently, nanostructural changes during and after the coating process, such as blooming, could lead to stresses within the coating layer and promote cracking and delamination. Therefore, the different dissolution kinetics could also be caused by a different delamination frequency. Since a connection between delamination and the crystallization behavior of the coating materials seems obvious, a subsequent

occurrence of delamination, e.g., due to incorrect storage conditions due to polymorphic transition or blooming, may also be possible.

An impact on the intraparticle layer thickness uniformity, interparticle batch homogeneity, and functionality of HMCs due to recrystallization and transformation processes seem likely. At this point, however, it is up to future studies to evaluate the relationships between delamination behavior, process conditions, crystallization behavior, dissolution kinetics, and the storage stability of different coating materials in HMC applications. Since tempering is known to impact blooming and the crystallization behavior of TAGs, an additional tempering step could be an exciting subject for further studies regarding delamination prevention and contribute to more functional coatings.

Overall, delamination behavior represents a new, so far unknown main influencing factor for the coating process. Delamination behavior is to be considered, in particular, when selecting coating materials and designing process strategies since functionality can be significantly reduced.

In the past, the focus of research was predominantly on coating material properties and the performance of coatings regarding dissolution kinetics. Only recently has research been expanded by new optical measurement methods and increasingly includes coating layer structures to study influencing factors.

3D-µCT imaging has proven to be a valuable tool for detailed investigations of the coating layer thickness uniformity and layer structure analysis of HMC in the context of this thesis. The high time requirements for the measurements and data processing limited the number of samples and potential conclusions. Continued measurement technology and data processing progress will be expected in the coming years and will contribute to further understanding of processes to produce high-functional natural HMC.

High-speed synchrotron X-ray computed tomography, for example, is a further development already available in the field of µCT measurement technology. High-speed synchrotron X-ray computed tomography allows extremely short measurement times of less than one second and provides improved image quality (Zwanenburg et al., 2022). Finegan et al. (2016), for example, used the synchrotron µCT technology to quantify the bulk electrode strain and material displacement within lithium batteries. Moreover, Müller et al. (2023) could examine more samples with each measurement when studying the growth of fungal pellets using this technology. Unfortunately, such a high-end device was not available for this thesis. For future applications, in-line measurement techniques in a

fluidized bed or even a live recording of a delamination process of a coating layer are also conceivable (Zwanenburg et al., 2022).

Due to the limitations of the sample size mentioned above, a fluorescent method was developed to investigate factors influencing interparticle batch homogeneity.

Development of a fluorescent method for analyzing interparticle batch homogeneity.

The functionality of HMCs is directly related to the intraparticle layer uniformity and the interparticle batch homogeneity. Cost-effective methods for the systematic investigation of the interparticle batch homogeneity of HMCs are hardly available. In general, optical techniques such as 3D-µCT are suitable for determining both the intraparticle layer thickness uniformity and the interparticle batch homogeneity, but these are still time-consuming and cost-intensive. It is, therefore, common practice to determine the particle size before and after the coating process. Although this procedure is quick and economical, it provides no detailed information or only very limited information about batch homogeneity and coating thickness. Apart from this, the results can be strongly falsified by layer structure phenomena such as porosity, inclusions, or delamination.

For this reason, an easy-to-use and cost-effective method for analyzing HMC was applied to quantify the interparticle batch homogeneity.

Following the method of Šibanc et al. (2018), the amount of coating material per particle was determined by the fluorescent coloring of the coating material.

In an ideal coating process, all particles should have the same amount of coating material and a uniform layer thickness. The presented method is suitable for determining the interparticle batch homogeneity by determining the amount of coating material per particle due to a large sample size. Structural information is not obtained by the destructive method. It was shown that the method is suitable for investigating various influencing factors with regard to interparticle batch homogeneity. A primary advantage of the method is the independent data collection from layer structure phenomena.

Although the spray rate was not found to be the major influencing factor on interparticle batch homogeneity, a strong focus on atomization conditions is recommended for future studies. Several literature sources show that for different material systems, the droplet size distribution during atomization depends on the gas-liquid ratio. A large gas-liquid ratio generally leads to smaller droplet sizes (Chen et al., 2020; García et al., 2017; Kleinhans et al., 2016; Mlkvik et al., 2015). This could indicate a correlation between

interparticle batch homogeneity and atomization and droplet size distribution. Especially in the context of the process temperature and the individual crystallization behavior of natural coating materials, studies on atomization can elucidate further relationships and contribute to improving the functionality and more targeted process design for HMC processes.

A combination of 3D-µCT coating layer thickness analysis with interparticle batch homogeneity analysis enables conclusions about the process to be drawn more easily and reliably. One of the main drawbacks of 3D-µCT coating layer thickness analysis is the small sample size, which can, however, be compensated for by determining batch homogeneity. Since the interparticle batch homogeneity and the intraparticle layer thickness homogeneity are decisive for the functionality of HMC, the combination of the two measurement methods can be used to investigate influencing factors and dependencies on the coating layer structure, the interparticle batch homogeneity and the connection with the functionality in a targeted and detailed manner.

Natural HMC will continue to gain importance in food and pharmaceutical industries. The demand for high-functionality products is constantly increasing. At the same time, the requirements for industrial processes and products in terms of health awareness, environmental compatibility, sustainability, and energy efficiency are rising. HMC with renewable raw materials can meet these increasing requirements.

The exact interaction of influencing factors from process parameters, plant design and technology, coating material, and core material properties is, however, highly complex and still needs to be fully elucidated and requires further investigation.

In this thesis, a significant knowledge gap was identified by the delamination analysis, showing that delamination was hitherto strongly underestimated and, to this extent, an unknown phenomenon in HMC. In total, three methods for the detailed analysis of HMCs could be developed and applied. It has been shown several times that combining complementary methods helps interpret data, find new insights, and make HMCs even more uniform, homogeneous, and functional. To put it into a nutshell, producing satisfying product quality and reproducibility is challenging due to a large number of dependencies and interrelationships. Thus, it is important for the future to continue identifying and investigating interrelationships and dependencies. Existing literature still lacks systematic studies on delamination, crystallization processes, storage conditions, and their effects on coating functionality. The methods developed for investigating

coating thickness uniformity, delamination, and interparticle batch homogeneity can be used for this purpose more extensively.

One of the main challenges will be to correctly conclude and implement the complex relationships, the large amount of complex data, and the large number of dependencies. If it is possible to bring findings into direct connection with the coating functionality, it could be possible to precisely predict and generate coating functionalities.

Key elements here will be progress in in-line process monitoring, big data management, and possibly artificial intelligence. Large amounts of complex information can be quickly processed, refined, and analyzed by artificial intelligence, enabling faster insights to be gained. Proactive and targeted process control is also conceivable, which could raise quality standards to a new level.

This will give in-line sensors a significant part to play. While temperatures, pressure differences, and flow velocities are already monitored in-line and are available as process data, an in-line layer structure analysis with enormous amounts of data is still in the future. Further developments and optimizations in process engineering, especially in hot-melt coating, promise to be exciting!

Literature

Acevedo NC, Marangoni AG. Nanostructured fat crystal systems. Annual review of food science and technology 2015;6:71–96. https://doi.org10.1146/annurev-food-030713-092400.

Achanta AS, Adusumilli PS, James KW, Rhodes CT. Hot-melt coating: water sorption behavior of excipient films. Drug Dev Ind Pharm 2001a;27(3):241–50. https://doi.org10.1081/DDC-100000242.

Achanta AS, Adusumilli PS, James KW, Rhodes CT. Thermodynamic analysis of water interaction with excipient films. Drug Dev Ind Pharm 2001b;27(3):227–40. https://doi.org10.1081/DDC-100000241.

Achanta AS, Adusumilli PS, James KW, Rhodes CT. Development of Hot Melt Coating Methods. Drug Development and Industrial Pharmacy 2008;23(5):441–9. https://doi.org10.3109/03639049709148493.

Atarés L, Depypere F, Pieters JG, Dewettinck K. Coating quality as affected by core particle segregation in fluidized bed processing. Journal of Food Engineering 2012;113(3):415–21. https://doi.org10.1016/j.jfoodeng.2012.06.012.

Bachmann P, Chen K, Bück A, Tsotsas E. Prediction of particle size and layer-thickness distributions in a continuous horizontal fluidized-bed coating process. Particuology 2019. https://doi.org10.1016/j.partic.2019.06.005.

Banker GS, Peck GE. The new water-based colloidal dispersions, 1981;5:55–61.

Becker K. Hot melt coating with lipid-based excipients Development of a solvent-free technology for the coating of multiparticulate drug delivery systems, 2016.

Becker K, Salar-Behzadi S, Zimmer A. Solvent-free melting techniques for the preparation of lipid-based solid oral formulations. Pharm Res 2015;32(5):1519–45. https://doi.org10.1007/s11095-015-1661-y.

Bodmeier RA. Encyclopedia of pharmaceutical technology. New York, 2002:2988–3000.

Bold S, Boegershausen A, Rusch O, Graner O, Klein S. Hot Melt Coating with Fast Release as an Innovative Taste Masking Concept: AAPS, 2012.

Bose S, Bogner RH. Solventless pharmaceutical coating processes: a review. Pharm Dev Technol 2007;12(2):115–31. https://doi.org10.1080/10837450701212479.

Chansanroj K, Betz G, Leuenberger H, Mitrevej A, Sinchaipanid N. Polymorphic change of a triglyceride base in hot melt coating process and stability acceleration

by tempering process. Journal of Drug Delivery Science and Technology 2007;17(5):347–52. https://doi.org10.1016/S1773-2247(07)50053-5.

Chen B, Gao D, Li Y, Chen C, Yuan X, Wang Z, et al. Investigation of the droplet characteristics and size distribution during the collaborative atomization process of a twin-fluid nozzle. Int J Adv Manuf Technol 2020;107(3-4):1625–39. https://doi.org10.1007/s00170-020-05131-1.

Cobb J, Brett RJ, Ruff MD, Berry A, Epps R. Using Quality by Design (QbD) for Process Optimization of a Novel Oral Solid Dosage Form, 2013 (accessed October 21, 2023). https://www.pharmoutsourcing.com/1613-WhitePapers-ApplicationNotes/130571-Using-Quality-by-Design-QbD-for-Process-Optimization-of-a-Novel-Oral-Solid-Dosage-Form/.

Dassanayake LSK, Kodali DR, Ueno S, Sato K. Physical Properties of Rice Bran Wax in Bulk and Organogels. J Am Oil Chem Soc 2009;86(12):1163–73. https://doi.org10.1007/s11746-009-1464-6.

Dong Y, Lin H, Abolghasemi V, Gan L, Zeitler JA, Shen Y-C. Investigating Intra-Tablet Coating Uniformity With Spectral-Domain Optical Coherence Tomography. J Pharm Sci 2017;106(2):546–53. https://doi.org10.1016/j.xphs.2016.09.021.

Dredán J, Antal I, Zelkó R, Rácz I. Modification of drug release with application of pharmaceutical technological methods. Acta pharmaceutica Hungarica 1999;69(4):176–80.

Faham A, Prinderre P, Farah N, Eichler KD, Kalantzis G, Joachim J. Hot-melt coating technology. I. Influence of Compritol 888 Ato and granule size on theophylline release. Drug Dev Ind Pharm 2000;26(2):167–76. https://doi.org10.1081/DDC-100100341.

Finegan DP, Tudisco E, Scheel M, Robinson JB, Taiwo OO, Eastwood DS, et al. Quantifying Bulk Electrode Strain and Material Displacement within Lithium Batteries via High-Speed Operando Tomography and Digital Volume Correlation. Advanced science (Weinheim, Baden-Wurttemberg, Germany) 2016;3(3):1500332. https://doi.org10.1002/advs.201500332.

García JA, Lozano A, Alconchel J, Calvo E, Barreras F, Santolaya JL. Atomization of glycerin with a twin-fluid swirl nozzle. International Journal of Multiphase Flow 2017;92(1):150–60. https://doi.org10.1016/j.ijmultiphaseflow.2017.03.010.

Geldart D. Types of gas fluidization. Powder Technol 1973;7(5):285–92. https://doi.org10.1016/0032-5910(73)80037-3.

Gontard N, Marchesseau S, Cuq J-L, Guilbert S. Water vapour permeability of edible bilayer films of wheat gluten and lipids. International Journal of Food Science & Technology 1995;30(1):49–56. https://doi.org10.1111/j.1365-2621.1995.tb01945.x.

Gorski KM, Hivon E, Banday AJ, Wandelt BD, Hansen FK, Reinecke M, et al. HEALPix: A Framework for High-Resolution Discretization and Fast Analysis of Data Distributed on the Sphere. The Astrophysical Journal 2005;622(2):759–71. https://doi.org10.1086/427976.

Goslinska M, Heinrich S. Characterization of waxes as possible coating material for organic aerogels. Powder Technol 2019;357(3):223–31. https://doi.org10.1016/j.powtec.2019.08.096.

Grave A, Pöllinger N. GLATT Wirbelschichttechnologie zum Coating von Pulvern, Pellets und Mikropellets. 1st ed.: Vieweg+Teubner, 2011;4:87–119.

Gruber S, Vorhauer N, Schulz M, Hilmer M, Peters J, Tsotsas E, et al. Estimation of the local sublimation front velocities from neutron radiography and tomography of particulate matter. Chemical Engineering Science 2020;211:115268. https://doi.org10.1016/j.ces.2019.115268.

Hampel NA. Diskontinuierliches und kontinuierliches Pelletcoating im Wurster-Wirbelschichtprozess, 2015.

Handbook of thermal spray technology. Materials Park, OH: ASM International; 2004.

Heinicke G, Schwartz JB. Particle size distributions of inert spheres and pelletized pharmaceutical products by image analysis. Pharm Dev Technol 2004;9(4):359–67. https://doi.org10.1081/PDT-200032996.

Heinrich S. Einführung in die Wirbelschicht-Technologie, 2015.

Hüttlin H. Coatings mittels INNOJET®-Verfahren. In: Kumpugdee-Vollrath M, Krause J-P, editors. Easy Coating. Wiesbaden: Vieweg+Teubner; 2011. p. 120–132.

Idziak SHJ. Powder X-ray Diffraction of Triglycerides in the Study of Polymorphism. In: Structure-Function Analysis of Edible Fats. Elsevier; 2018. p. 73–99.

Iley WJ. Effect of particle size and porosity on particle film coatings. Powder Technol 1991;65(1-3):441–5. https://doi.org10.1016/0032-5910(91)80205-W.

Indiana C, Bellenoue M, Boust B. EXPERIMENTAL INVESTIGATIONS OF DROP SIZE DISTRIBUTIONS WITH IMPINGING LIQUID JETS USING PHASE DOPPLER ANEMOMETER. Int J Energetic Materials Chem Prop 2015;14(3):241–64. https://doi.org10.1615/IntJEnergeticMaterialsChemProp.2015011292.

Jannin V, Cuppok Y. Hot-melt coating with lipid excipients. Int J Pharm 2013;457(2):480–7. https://doi.org10.1016/j.ijpharm.2012.10.026.

Jones DM, Percel PJ. Coating of Multiparticulates Using Molten Materials. In: Multiparticulate Oral Drug Delivery; 1994. p. 113–142.

Jozwiakowski MJ, Jones DM, Franz RM. Characterization of a hot-melt fluid bed coating process for fine granules. Pharm Res 1990;7(11):1119–26. https://doi.org10.1023/A:1015972007342.

Karlsson S, Niklasson Björn I, Folestad S, Rasmuson A. Measurement of the particle movement in the fountain region of a Wurster type bed. Powder Technol 2006;165(1):22–9. https://doi.org10.1016/j.powtec.2006.03.014.

Kawaguchi T, Nakamura H, Watano S. Dry coating of electrode particle with model particle of sulfide solid electrolytes for all-solid-state secondary battery. Powder Technol 2018;323:581–7. https://doi.org10.1016/j.powtec.2016.03.055.

Kennedy JP, Niebergall PJ. Development and optimization of a solid dispersion hot-melt fluid bed coating method. Pharm Dev Technol 1996;1(1):51–62. https://doi.org10.3109/10837459609031418.

Kleinhans A, Georgieva K, Wagner M, Gaukel V, Schuchmann HP. On the characterization of spray unsteadiness and its influence on oil drop breakup during effervescent atomization. Chemical Engineering and Processing: Process Intensification 2016;104:212–8. https://doi.org10.1016/j.cep.2016.03.011.

Knezevic Z, Gosak D, Hraste M, Rausl D, Khan MZI. Application of hot-melt coating process for designing a lipid based controlled release drug delivery system for highly aqueous soluble drugs. Chemical & pharmaceutical bulletin 2009;57(5):464–71. https://doi.org10.1248/cpb.57.464.

Kraume M. Transportvorgänge in der Verfahrenstechnik. Berlin: Springer; 2004.

Kulah G, Kaya O. Investigation and scale-up of hot-melt coating of pharmaceuticals in fluidized beds. Powder Technol 2011;208(1):175–84. https://doi.org10.1016/j.powtec.2010.12.016.

Kumpugdee-Vollrath M, Gögebakan E, Krause J-P, Müller U, Waßmann G. Coatings in der pharmazeutischen Industrie. In: Kumpugdee-Vollrath M, Krause J-P, editors. Easy Coating. Wiesbaden: Vieweg+Teubner; 2011. p. 52–79.

Kumpugdee-Vollrath M, Krause J-P. Easy Coating 2011.

Laicher A, Fuchs WS. Die Pellet-Technologie: Retardpellets in Hartgelatine-Kapseln: eine geeignete Arzneiform für Theophyllin, 1998. Arzneimittel-Forschung:540–7.

Laksmana FL, van Vliet LJ, Hartman Kok PJA, Vromans H, Frijlink HW, van der Voort Maarschalk K. Quantitative image analysis for evaluating the coating thickness and pore distribution in coated small particles. Pharm Res 2009;26(4):965–76. https://doi.org10.1007/s11095-008-9805-y.

Lin H, May RK, Evans MJ, Zhong S, Gladden LF, Shen Y, et al. Impact of Processing Conditions on Inter-tablet Coating Thickness Variations Measured by Terahertz In-Line Sensing. J Pharm Sci 2015;104(8):2513–22. https://doi.org10.1002/jps.24503.

Lin SW. Palm Oil. In: Gunstone FD, editor. Vegetable Oils in Food Technology. Oxford, UK: Wiley-Blackwell; 2011. p. 25–58.

Lin S-Y, Krochata JM. Fluidized-bed System for Whey Protein Film Coating of Peanuts. J Food Process Engineering 2006;29(5):532–46. https://doi.org10.1111/j.1745-4530.2006.00081.x.

Lonchampt P, Hartel RW. Surface bloom on improperly tempered chocolate. Euro J Lipid Sci & Tech 2006;108(2):159–68. https://doi.org10.1002/ejlt.200500260.

Lopes DG, Becker K, Stehr M, Lochmann D, Haack D, Zimmer A, et al. Role of Lipid Blooming and Crystallite Size in the Performance of Highly Soluble Drug-Loaded Microcapsules. J Pharm Sci 2015;104(12):4257–65. https://doi.org10.1002/jps.24660.

Lopes DG, Salar-Behzadi S, Zimmer A. Designing optimal formulations for hot-melt coating. Int J Pharm 2017;533(2):357–63. https://doi.org10.1016/j.ijpharm.2017.08.086.

Louge MY, Mastorakos E, Jenkins JT. The role of particle collisions in pneumatic transport. J. Fluid Mech. 1991;231:345–59. https://doi.org10.1017/S0022112091003427.

Ludewig C, Ganzelmeier H. Phase doppler anemometry-a new measuring system to determine the droplet size of agricultural nozzles. Stuttgart: Eugen Ulmer GmbH & Co, 1993. Nachrichtenbl. Deut. Pflanzenschutzd;45:103–9.

Markl D, Hannesschläger G, Sacher S, Leitner M, Khinast JG. Optical coherence tomography as a novel tool for in-line monitoring of a pharmaceutical film-coating process. Eur J Pharm Sci 2014;55:58–67. https://doi.org10.1016/j.ejps.2014.01.011.

Markl D, Zettl M, Hannesschläger G, Sacher S, Leitner M, Buchsbaum A, et al. Calibration-free in-line monitoring of pellet coating processes via optical coherence tomography. Chemical Engineering Science 2015;125:200–8. https://doi.org10.1016/j.ces.2014.05.049.

Mayama H. Blooming theory of tristearin. Soft Matter 2009;5(4):856. https://doi.org10.1039/B815005B.

Minami T, Mayama H, Nakamura S, Yokojima S, Shen J-W, Tsujii K. Formation mechanism of fractal structures on wax surfaces with reference to their super - repellency. Soft Matter 2007;4(1):140–4. https://doi.org10.1039/B712938F.

Mittal. B., Kidney D, Sy E, Chu J. Taste masking of aspirin using hot-melt coating approach: AAPS, 2003. Pharmaceutical Science Technology;3.

Mlkvik M, Stähle P, Schuchmann HP, Gaukel V, Jedelsky J, Jicha M. Twin-fluid atomization of viscous liquids: The effect of atomizer construction on breakup process, spray stability and droplet size. International Journal of Multiphase Flow 2015;77:19–31. https://doi.org10.1016/j.ijmultiphaseflow.2015.06.010.

Mörl L, Heinrich S, Peglow M. Fluidized Bed Spray Granulation. In: Salman A, Hounslow M, Seville JPK, editors. Granulation. Amsterdam, The Netherlands: Elsevier Science; 2007. p. 1402.

Müller H, Deffur C, Schmideder S, Barthel L, Friedrich T, Mirlach L, et al. Synchrotron radiation-based microcomputed tomography for three-dimensional growth analysis of Aspergillus niger pellets. Biotechnology and bioengineering 2023. https://doi.org10.1002/bit.28506.

Müller MG, Lindner JA, Briesen H, Sommer K, Foerst P. On the properties and application of beeswax, carnauba wax and palm fat mixtures for hot melt coating in fluidized beds. Advanced Powder Technology 2018. https://doi.org10.1016/j.apt.2017.12.020.

Perfetti G, van de Casteele E, Rieger B, Wildeboer WJ, Meesters GMH. X-ray micro tomography and image analysis as complementary methods for morphological characterization and coating thickness measurement of coated particles. Advanced Powder Technology 2010;21(6):663–75. https://doi.org10.1016/j.apt.2010.08.002.

Pietsch S, Peter A, Wahl P, Khinast J, Heinrich S. Measurement of granule layer thickness in a spouted bed coating process via optical coherence tomography. Powder Technol 2019;356:139–47. https://doi.org10.1016/j.powtec.2019.08.022.

Prasad MB, Vidyadhara S, Sasidhar RLC, Balakrishna T, Trilochani P. Development and evaluation of diltiazem hydrochloride controlled-release pellets by fluid bed coating process. Journal of advanced pharmaceutical technology & research 2013;4(2):101–7. https://doi.org10.4103/2231-4040.111526.

Qiyun G. A study of factors affecting spray-congealed micropellets for drug delivery, 2008 (accessed November 03, 2023). http://scholarbank.nus.edu.sg/handle/10635/13176.

Rajesh AM, Reetika D, Sangeeta A, Ashok B, Arvind M. WURSTER COATING - PROCESS AND PRODUCT VARIABLES, 2012.

Rothrock DA, Cheetham HC. Hot-melt Coating, 1942.

Saleh K, Guigon P. Chapter 7 Coating and encapsulation processes in powder technology 2007;11:323–75. https://doi.org10.1016/s0167-3785(07)80042-x.

Sato K, Bayés-García L, Calvet T, Cuevas-Diarte MÀ, Ueno S. External factors affecting polymorphic crystallization of lipids. Euro J Lipid Sci & Tech 2013;115(11):1224–38. https://doi.org10.1002/ejlt.201300049.

Sato K, Goto M, Yano J, Honda K, Kodali DR, Small DM. Atomic resolution structure analysis of β′ polymorph crystal of a triacylglycerol: 1,2-dipalmitoyl-3-myristoyl-sn-glycerol. Journal of Lipid Research 2001;42(3):338–45. https://doi.org10.1016/S0022-2275(20)31656-4.

Sauer D, Cerea M, DiNunzio J, McGinity J. Dry powder coating of pharmaceuticals: a review. Int J Pharm 2013;457(2):488–502. https://doi.org10.1016/j.ijpharm.2013.02.032.

Savini M. On the Optimization of the Fluidized Bed Particulate Coating Process, 1998.

Schiele SA, Antoni F, Meinhardt R, Briesen H. Analysis of Nonideal Shape Evolution during Potash Alum Crystallization Using Microcomputed Tomography and Three-Dimensional Image Analysis. Crystal Growth & Design 2021;21(3):1751–61. https://doi.org10.1021/acs.cgd.0c01644.

Schmideder S, Barthel L, Friedrich T, Thalhammer M, Kovačević T, Niessen L, et al. An X-ray microtomography-based method for detailed analysis of the three-dimensional morphology of fungal pellets. Biotechnology and bioengineering 2019;116(6):1355–65. https://doi.org10.1002/bit.26956.

Schoeman L, Williams P, Du Plessis A, Manley M. X-ray micro-computed tomography (μCT) for non-destructive characterisation of food microstructure. Trends in Food Science & Technology 2016;47:10–24. https://doi.org10.1016/j.tifs.2015.10.016.

Shelukar S, Ho J, Zega J, Roland E, Yeh N, Quiram D, et al. Identification and characterization of factors controlling tablet coating uniformity in a Wurster coating process. Powder Technol 2000;110(1-2):29–36. https://doi.org10.1016/S0032-5910(99)00265-X.

Shukla P, Mandal RK, Ojha SN. Non-equilibrium solidification of undercooled droplets during atomization process. Bull Mater Sci 2001;24(5):547–54. https://doi.org10.1007/BF02706729.

Šibanc R, Turk M, Dreu R. An analysis of the mini-tablet fluidized bed coating process. Chemical Engineering Research and Design 2018;134:15–25. https://doi.org10.1016/j.cherd.2018.03.020.

Sinchaipanid N, Junyaprasert V, Mitrevej A. Application of hot-melt coating for controlled release of propranolol hydrochloride pellets. Powder Technol 2004;141(3):203–9. https://doi.org10.1016/j.powtec.2004.02.008.

Sondej F, Bück A, Tsotsas E. Comparative analysis of the coating thickness on single particles using X-ray micro-computed tomography and confocal laser-scanning microscopy. Powder Technol 2016;287:330–40. https://doi.org10.1016/j.powtec.2015.09.039.

Srivastava S, Mishra G. Fluid bed technology: overview and parameters for process selection: International Journal of Pharmaceutical Sciences and Drug Research, 2010;2:236–46.

Sudke SG, Sakarakar DM. Hot-melt coating: an innovative pharmaceutical coating technique. J Pharm Res Clin Pract. 2013;3(1):16–26.

Thies C. Granulation Technology for Bioproducts: Microencapsulated Enzymes and Live Mammalian Cells. Boca Raton FL, 1989:179–206.

Timms RE. Phase behaviour of fats and their mixtures. Progress in Lipid Research 1984;23(1):1–38. https://doi.org10.1016/0163-7827(84)90004-3.

Vali SR, Ju Y-H, Kaimal TNB, Chern Y-T. A process for the preparation of food-grade rice bran wax and the determination of its composition. J Am Oil Chem Soc 2005;82(1):57–64. https://doi.org10.1007/s11746-005-1043-z.

van Kampen A, Hitzmann B, Kohlus R. Assessment of coating quality by use of dissolution kinetics. Powder Technol 2015;286:325–31. https://doi.org10.1016/j.powtec.2015.08.024.

van Kampen A, Kohlus R. Statistical modelling of coating layer thickness distributions: Influence of overspray on coating quality. Powder Technol 2018;325(8):557–67. https://doi.org10.1016/j.powtec.2017.11.031.

Vandenburg LE, Wilder EA. The structural constituents of carnauba wax. J Am Oil Chem Soc 1970;47(12):514–8. https://doi.org10.1007/BF02639240.

Wang H, Qiu G, Ye J, Yang W. Experimental study and modelling on gas–solid flow in a lab-scale fluidised bed with Wurster tube. Powder Technol 2016;300:14–27. https://doi.org10.1016/j.powtec.2016.01.025.

Waßmann G, Kumpugdee-Vollrath M, Krause J-P. Einführung und Geschichte des Coatings. In: Kumpugdee-Vollrath M, Krause J-P, editors. Easy Coating. Wiesbaden: Vieweg+Teubner; 2011. p. 1–6.

Wen H, editor. Oral controlled release formulation design and drug delivery: Theory to practice. Hoboken, NJ: Wiley; 2010.

Woerthmann BM, Briesen H. Schmelzcoating feiner Pulver zur Erreichung einer geschlossenen homogenen Schicht. AiF-Schlussbericht IGF-Vorhaben Nr. 19970 N, 2022a.

Woerthmann BM, Briesen H. Schmelzcoating - Nutzung von µCT-Daten zur gezielten Erzeugung homogener Schichtstrukturen. Lampertheim, 2022b. Der Lebensmittelbrief – ernährung aktuell:33–6.

Woerthmann BM, Hoffmann A, Gerber J, Wittkamp T, Briesen H. Analyzing the interparticle batch homogeneity of natural hot-melt coatings. Powder Technol 2023;426:118626. https://doi.org10.1016/j.powtec.2023.118626.

Woerthmann BM, Lindner JA, Kovacevic T, Pergam P, Schmid F, Briesen H. A novel method for assessing the coating uniformity of hot-melt coated particles using micro-computed tomography. Powder Technol 2021;378:51–9. https://doi.org10.1016/j.powtec.2020.09.065.

Woerthmann BM, Totzauer L, Briesen H. Delamination and wetting behavior of natural hot-melt coating materials. Powder Technol 2022;404(3):117443. https://doi.org10.1016/j.powtec.2022.117443.

Wong PM, Chan LW, Heng PWS. Investigation on side-spray fluidized bed granulation with swirling airflow. AAPS PharmSciTech 2013;14(1):211–21. https://doi.org10.1208/s12249-012-9906-0.

Wozniak G. Zerstäubungstechnik: Prinzipien, Verfahren, Geräte. Berlin, Heidelberg, s.l.: Springer Berlin Heidelberg; 2003.

Wurster DE, 1953.

Yang W-C. Modification and re-interpretation of Geldart's classification of powders. Powder Technol 2007;171(2):69–74. https://doi.org10.1016/j.powtec.2006.08.024.

Zwanenburg EA, Williams MA, Warnett JM. Review of high-speed imaging with lab-based x-ray computed tomography. Meas Sci Technol 2022;33(1):12003. https://doi.org10.1088/1361-6501/ac354a.